UNIVERSIDAD NACIONAL AUTÓNOMA DE MÉXICO

PROGRAMA DE MAESTRÍA Y DOCTORADO EN INGENIERÍA
INGENIERIA CIVIL – INGENIERIA SISMICA

NOMBRE DE TESIS

A DISPLACEMENT-BASED SEISMIC DESIGN METHOD FOR FRAMED STRUCTURES INVOLVING SIDESWAY-COLLAPSE PREVENTION

TESIS
QUE PARA OPTAR POR EL GRADO DE:
DOCTOR EN INGENIERÍA

PRESENTA:
SAÚL ESTEBAN LÓPEZ RÍOS

TUTOR PRINCIPAL:
DR. AMADO GUSTAVO AYALA MILIÁN
INSTITUTO DE INGENIERÍA

COMITÉ TUTORIAL:

DR. LUIS ESTEVA MARABOTO
INSTITUTO DE INGENIERÍA-UNAM

DR. EDUARDO REINOSO ANGULO
INSTITUTO DE INGENIERÍA-UNAM

DR. OSCAR ALBERTO LÓPEZ BÁTIZ
CENAPRED-UNAM

DR. DARÍO RIVERA VARGAS
FES ACATLÁN-UNAM

MÉXICO, D. F. AGOSTO 2015

JURADO ASIGNADO:

Presidente: Dr. Luis Esteva Maraboto

Secretario: Dr. Eduardo Reinoso Angulo

Vocal: Dr. Amado Gustavo Ayala Milián

1er Suplente: Dr. Oscar Alberto López Bátiz

1er Suplente: Dr. Darío Rivera Vargas

Lugar o lugares donde se realizó la tesis:

Instituto de Ingeniería, UNAM

TUTOR DE TESIS:

Dr. Amado Gustavo Ayala Milián

FIRMA

INDEX

ABSTRACT.....iii

1 INTRODUCTION 4

1.1 Background 4

1.2 Objective of this investigation 5

1.3 Outline 5

2 STRUCTURAL COLLAPSE DUE TO DYNAMIC LOADING 7

2.1 Structural collapse types 7

2.1.1 Dynamic instability of unstable structural systems 8

2.1.2 Influence of cyclic degradation in dynamic instability 9

2.2 P-Delta effects in structures 10

2.2.1 Effect of gravity loads in the lateral stiffness and strength of structural systems 10

2.2.2 P-Delta effects in SDOF systems 10

2.2.3 P-Delta effects in MDOF systems 12

2.3 Assessment of sidesway collapse of structures subjected to seismic loading 14

2.3.1 Incremental dynamic analysis 14

2.3.2 Simplified assessment procedures for collapse capacity estimation 16

2.4 P-Delta effects in seismic design 17

2.4.1 Force based design approach 17

2.4.2 Displacement based design approaches 17

3 FUNDAMENTALS OF THE METHOD PROPOSED 19

3.1 Reference SDOF system 19

3.2 Elastic and “damaged” model 20

3.3 Definition of design displacement shapes 21

3.4 Definition of design demands of reference SDOF system 23

3.5 Definition of design demands of higher modes 24

3.5.1 Definition of modal force demands 25

3.6 Modal spectral analysis 25

3.7 DESIGN FOR SIDESWAY COLLAPSE DUE TO P-DELTA EFFECTS 26

3.7.1 Auxiliary SDOF system 27

3.7.2 Collapse capacity and constant ductility spectra of SDOF systems with negative post-yield stiffness branch 28

3.7.3 Design procedure 30

4 VALIDATION OF THE METHOD PROPOSED 32
4.1 Overview of the case studies considered and validation approach 32
4.2 Characteristics of example frames 33
4.3 Design demands and performance targets 33
4.4 Detailed description of design application of 16-storey frame 34
4.5 Incremental dynamic analysis of designed frames 36
4.6 Evaluation of results 37
5 CONCLUSIONS 97
5.1 RSDOF system approach 97
5.2 Special spectra for P-Delta induced instability prone systems 98
5.3 Applicability of the method proposed 98
5.4 Future studies 98
REFERENCES 100

ABSTRACT

In this thesis, a displacement-based seismic design method for framed structures involving sidesway collapse prevencion due to P-Delta effects is presented. Currently, simplified sidesway collapse assessment methods that are sufficiently accurate and relatively easy to apply are available, however, development of design oriented simplified methods is an issue that requires further research, being the motivation behind this study.

The displacement-based approach employed in the method proposed is based on the characterization of a multiple degree of freedom structure by means of an inelastic single degree of freedom system whose properties are consistent with its fundamental mode, which in the framework of this method is referred to as reference single degree of freedom system. The effect of higher modes in the response is taken into account by a simplified criterion involving modal spectral analysis.

The design approach consists on the definition of a design bilinear behaviour curve, i.e., a spectral displacement *vs* spectral pseudo-aceleration curve of the reference single degree of freedom system, which provides the stiffness and strength required by the structure to fulfil a given performance objective. From such curve and the criterion employed to account for higher mode contribution, the force demands of the structure are defined and the design of structural components is carried out.

Design applications of the method proposed aimed at control of theoretical P-Delta induced collapse and exceedance of several interstorey drift thresholds were carried out for 8-, 12- and 16- storey generic frames, regular in elevation, subjected to different levels of axial load. The design demands employed were 50% constant ductility spectra calculated for two sets of records corresponding to stiff and soft soil types. The validation of the method proposed was performed via incremental dynamic analysis of the designed frames using the corresponding sets of records. From the results obtained in this investigation, it is concluded that the method proposed allows the design of structures with P-Delta induced instability to either satisfy a given interstorey drift threshold or to prevent dynamic instability.

CHAPTER 1

INTRODUCTION

1.1 Background

The current approach for the seismic design of structures is performance oriented since it establishes that a building structure should be able to exhibit adequate behaviour when subjected to ground motions induced by seismic events that may occur during its entire lifespan. In accordance with this approach, adequate performance of a structure is deemed as the accomplishment of prescribed limit states, measured through a performance index or indices, *e.g.*, interstorey drift, plastic rotation of structural components, when subjected to seismic design intensities. The set of limit states to be satisfied for a given set of demands is known as performance objective, PO, which is defined according to the function, type and importance of a building.

For low probability seismic events that induce high intensity ground motions, the PBEE approach includes in its basic PO a collapse prevention limit state. This limit state considers that building structures should be able to maintain global stability, *i.e.*, avoid collapse, accepting the possibility of severe strength-stiffness degradation of structural components, such that substantial safety for the occupants of the building under this scenario is provided.

Structural collapse is defined as the local or global failure of a system that occurs due to severe reduction or complete loss of its vertical load carrying capacity. Two primary types of global seismic collapse may be identified: progressive and sidesway (Ibarra and Krawinkler 2005). The first may be defined as the total or disproportionate failure of the system triggered by an initial local failure. Sidesway collapse, also referred to as incremental collapse, is defined as the global failure of the system due to severe deterioration of storey lateral shear stiffness when subjected to large displacements, usually caused by the destabilizing effect of gravity loads, *i.e.*, second order or P-Delta effects, and/or in-cycle degradation. Moreover, such deterioration may be accelerated by cyclic deterioration of structural components (FEMA 2009).

Researchers such as Ibarra and Krawinkler (2005), Haselton *et al.* (2009), Lignos and Krawinkler (2008) have studied in depth the factors that intervene in the occurrence of collapse under seismic action relying on state of the art analytical and experimental resources. Due to the complexity of the factors involved, the rigorous prediction of collapse is a difficult task since the variability of the characteristics of the seismic

demands and the structural properties require elaborate structural models and extensive numerical simulations (Krawinkler *et al.* 2009). For this reason, the collapse limit state of several current national and international codes is defined as the exceedance of a prescribed interstorey drift or plastic rotation of an element section associated to near-collapse behaviour rather than actual instability of the system (Haselton *et al.* 2009).

According to Adam and Jäger (2012b), sidesway collapse is frequent in catastrophic seismic events and, for certain classes of flexible regular framed structures with high ductility capacity, is governed by P-Delta effects. Therefore, studies focusing on the development of simplified methods to assess collapse due to P-Delta effects that are sufficiently accurate and relatively easy to apply have been carried out, *e.g.*, Takizawa and Jennings (1980), Bernal (1998) and Adam and Jäger (2012b). For the case of design, Asimakopoulos *et al*. (2007) developed an implementation in the Direct Displacement Based Design method (Priestley *et al.* 2007), to account for the modification of the response due to severe P-Delta effects of inelastic steel frames valid for the EC8 (2001) design limit state that corresponds to life safety assurance.

1.2 Objective of this investigation

In general, few efforts focused on the development of performance based simplified design methods that consider explicitly design for actual collapse prevention have been developed; hence, it is a subject that requires further investigation. This circumstance has motivated the author to develop and validate a new simplified design method that can be used to design instability prone structures due to P-Delta effects, not only for deformation control corresponding to a near collapse limit state as currently established in several design codes, but also for actual sidesway collapse prevention. Although reliable collapse prediction is still a subject that requires extensive investigation, the development of simplified procedures that are consistent with the state of the art on such subject is necessary.

The displacement based seismic design method described in this work is an evolution of the original method proposed by Ayala *et al.* (2012). The design approach consists on the definition of a bilinear or trilinear behaviour curve, *i.e.*, spectral displacement, Sd, *vs.* pseudo-acceleration, Sa, of a reference SDOF system corresponding to the fundamental mode of a structure, defined in such a way that a considered performance objective, PO, is satisfied. The yield and maximum displacements of the aforementioned curve are defined in such a way that a given interstorey drift threshold and/or structural stability is achieved under the design demands corresponding to the considered limit states.

The method proposed allows the design of regular framed structures that are potentially unstable due to the effects of gravity loads, *i.e.*, P-Delta induced negative post-yield stiffness, under severe seismic demands. Even though instability due to gravity loads of a designed structure is an undesirable condition, in many cases it is not practical or economically feasible to avoid completely such condition (Fenwick *et al.* 1992). Currently, the method proposed addresses only the design of non-degrading structures with P-Delta induced instability; in-cycle degradation and cyclic deterioration of structures are not considered in this study as it is a subject of future investigations. Nonetheless, ductile structures need stringent detailing requirements, hence, moderate levels of deterioration can be expected.

1.3 Outline

The background and objectives of this investigation were given in the current chapter. In the second chapter the phenomenon of sidesway collapse due to earthquakes is reviewed, with particular emphasis on the basic

mechanics that rule P-Delta effects in SDOF and MDOF structures and its relation with static and dynamic instability. Subsequently, the assessment of sidesway collapse prone structures via Incremental Dynamic Analysis and a summary of simplified assessment procedures are presented. At the final part of the chapter, current approaches focused on the consideration of P-Delta effects in both force-based and displacement-based design procedures are discussed.

In the third chapter the design method proposed in this thesis is presented. First, the general framework is illustrated in detail focusing on the most relevant concepts and assumptions. Subsequently, the specific design approach for the design of frame structures considering P-Delta induced dynamic instability is discussed and the application of the design procedure is described step by step.

Chapter 4 presents the results of design applications of the method proposed to 8-, 12-, and 16-storey frames, each designed for four levels of axial load. A detailed description of the case studies are provided along with the discussion of the results obtained with basis on the comparison of expected performance vs. that calculated via incremental dynamic analysis. The main conclusions of this investigation are presented in Chapter 5, discussing particular issues relative to the method proposed. Moreover, recommendations for future research are suggested to provide continuity to this investigation.

CHAPTER 2

STRUCTURAL COLLAPSE DUE TO DYNAMIC LOADING

2.1 Structural collapse types

Structural collapse is defined as the local or global failure of a system that occurs due to severe reduction or complete loss of its load carrying capacity. Two primary types of global structural collapse may be identified: progressive and sidesway (Ibarra and Krawinkler 2005). The first may be defined as the total or disproportionate failure of the system due to the progressive loss of vertical load carrying component triggered by an initial local failure (Fig. 2.1.a). Under seismic loading, reinforced concrete structures can fail in this manner as a consequence of shear and axial-shear failures of columns and joints, punching of slab-column connections, inadequate splices in plastic hinge regions (Baradaran Shoraka 2013); steel structures collapse owing to buckling of columns, web panel zone failures, brittle failure of weldings or bolts, amongst others.

a) **b)**

Figure 2.1 Different types of collapse: a) Vertical collapse due to loss of vertical-load carrying capacity; b)Incipient sidesway collapse due to loss of lateral-force-resisting capacity (FEMA 2009)

Sidesway collapse, also referred to as incremental collapse, is defined as the global failure of the system due to severe deterioration of storey lateral shear stiffness when subjected to large displacements in the inelastic range, caused primarily by the destabilizing effect of gravity loads, *i.e.,* second order effects, and/or in-cycle deterioration. (Fig. 2.1.b). This type of collapse is the predominant type in ductile structures and is the subject of this investigation, as this study is oriented towards the design of new structures for which appropriate detailing is to be provided to ensure adequate performance under seismic demands.

2.1.1 Dynamic instability of unstable structural systems

Sidesway collapse is a consequence of dynamic instability, defined as a disproportionate response of a system subjected to dynamic loading for a relatively small variation of its intensity in a lapse of time (Bernal 1998). Dynamic instability occurs when a structure subjected to dynamic loading presents a static instability condition during a lapse or lapses of time throughout its response, *i.e.,* when its instantaneous stiffness matrix is not positive definite. This condition may be recognized in the load-displacement relationship of the system by the presence of a segment with negative slope, which represents a strength decay under increasing displacements in a given direction, *i.e*., in-cycle degradation (FEMA 2009).

The main factors that induce "negative stiffness", *i.e.*, instability in structural systems under static and dynamic conditions, are second order effects (P-Delta) and material strain softening of structural components. In reinforced concrete components, the latter is a result of damage due to crushing, shear failure, buckling, fracture and/or splice failures of longitudinal reinforcement. In steel components, material strain softening is a consequence of buckling of bracing element, local and flexural-torsional buckling, and fracture of bolts, welds or base material. (FEMA 2009)

Even though, static instability, is a necessary condition for the occurrence of dynamic instability; it is not sufficient since the inertial and damping forces may provide a stabilizing effect on the response (Bernal 1998), hence, the intensity and the frequency content of the input play an important role in structural stability. For this reason, non-linear dynamic analysis is required to identify sidesway collapse for a particular loading.

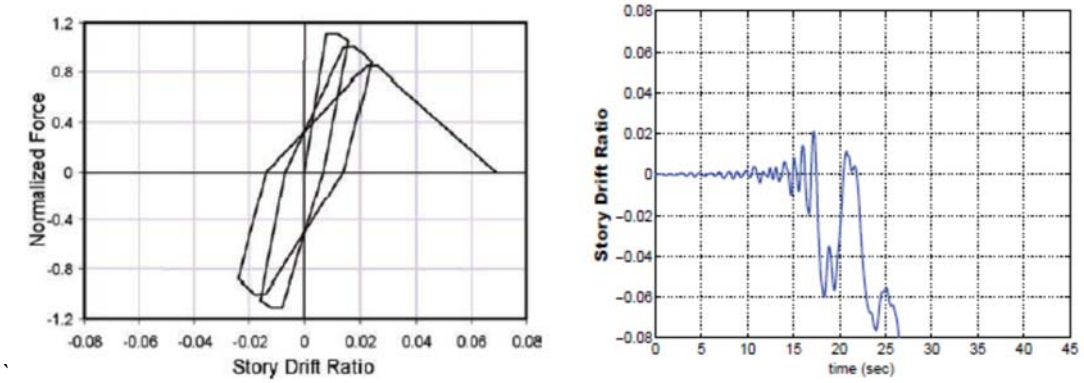

a) **b)**

Figure 2.2 Dynamic behaviour of instability prone systems: a) Hysteresis; b) Displacement time history (FEMA 2009)

The dynamic response of instability prone systems is characterized by the progressive increase of displacements in a single direction throughout successive load cycles, *i.e.,* the cyclic response tends to be non-reversible, as a consequence of the stiffness decrease within each load cycle (Fig. 2.2.a). This effect, referred to as *ratcheting* or *crawling* of structural response (Paulay 1979; Gupta and Krawinkler 2000), leads to larger residual displacements and, in the extreme case, to sidesway collapse of the system (Fig. 2.2.b). Assuming that the system is modelled appropriately, dynamic instability is considered equivalent to numerical instability, *i.e.,* disproportionate displacements, in a transient analysis.

2.1.2 Influence of cyclic degradation in dynamic instability

Cyclic degradation is the progressive loss of strength and/or stiffness throughout successive cycles of response due to damage of a system subjected to dynamic loading. It is important to highlight that cyclic degradation is fundamentally different than in-cycle degradation as, in this case, the loss of strength within a cycle of response is caused by unloading or reloading only, *i.e.,* strength decay occurs only when displacement decreases (Fig. 2.3.a). For this reason, this type of degradation does not cause an instability condition by itself.

Even though that, theoretically speaking, systems that exhibit cyclic deterioration only, without in cycle deterioration, can fail due to the depletion of its energy dissipation capacity (Ibarra and Krawinkler 2005), several studies show that, in general, their response is stable or, at least, is more stable than systems with a comparable cyclic envelope, as that shown in Fig. 2.3.b (FEMA 2009).

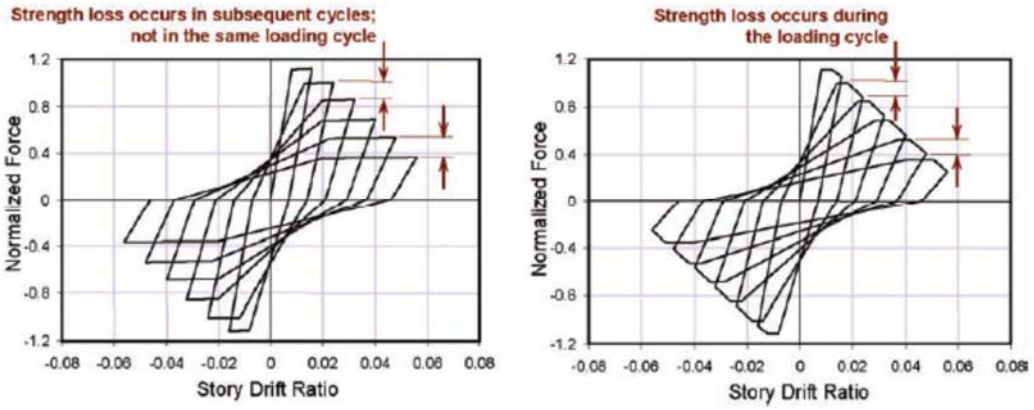

a) **b)**

Figure 2.3 Dynamic behaviour of systems with different types of degradation: a) Cyclic degradation; b) In-cycle degradation (FEMA 2009)

Nonetheless, in instability prone systems, cyclic deterioration may accelerate sidesway collapse of the structural system (Lignos and Krawinkler 2010). The degree of acceleration depends on the hysteretic behaviour of the elements and on the stiffness of the structure. The hysteretic behaviour is a function of the material properties and the detailing of structural components. In regard to the influence of stiffness in the level of cyclic deterioration, it is generally accepted that flexible structures are less susceptible to cyclic deterioration than rigid ones as the latter exhibit more cycles of response under dynamic loading (Ibarra and Krawinkler 2005).

This investigation is focused on design of ductile structures for which appropriate detailing and proportioning of structural components should be provided, hence, the effects of cycle deterioration and in-cycle degradation are not considered. The study is focused on P-Delta induced dynamic instability since, as shall be shown in the following, ductile structures may exhibit an instability condition immediately after significant yielding in structural element.

2.2 P-Delta effects in structures

2.2.1 Effect of gravity loads in the lateral stiffness and strength of structural systems

Second order effects, also referred to as P-Delta effects, is the name given to the amplification of demands of a structure subjected to lateral displacements due to the action of vertical loads over its deformed shape. P-Delta effects can be classified in two types:

1) Major second order effects, P-Δ, which refers to the effect of gravity loads in the response of the structure due to the displacements of its storey joints.
2) Minor second order effects, P-δ, defined as to the local demand amplification within structural components due to their deformation between its end joints.

The latter type is seldom significant in the global seismic response of structures (PEER/ATC 2010), hence, major P-Delta effects are the type addressed in this study.

2.2.2 P-Delta effects in SDOF systems

The basic mechanics that rule major P-Delta effects in structures can be understood from examination of a SDOF system of height H comprised of a rigid column attached at its base to a flexural spring with bilinear backbone of elastic stiffness K^E and post-yield stiffness, $K^D=\alpha K^E$; a mass, m, and a viscous damper that provides a damping quantity c. Such system is subjected to a lateral load V and a vertical load P (Fig. 2.4).

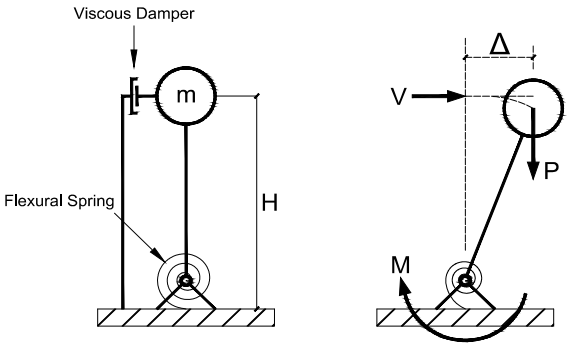

Figure 2.4 SDOF system subjected to lateral dynamic loading and vertical force

As can be observed in the preceding figure, the vertical load generates an additional moment due to the displacement of the system, Δ, thus, the total moment at its base, M, is:

$$M = VH + P\Delta \tag{2.1}$$

The increase in flexural demand with respect to the first order response can be interpreted as a decrease of the system´s lateral strength and stiffness which can be characterized by a geometric transformation. Under such interpretation, the stiffness decrease due to gravity load can be represented via the geometric stiffness

(Eq. 2.2) and, consequently, the effective tangent stiffness of the SDOF system in either its elastic or inelastic stage of behaviour, K^{t}', i.e., second order tangent stiffness, can be defined by Eq. 2.3, in which K^{t} denotes the first order tangent stiffness.

$$K_g = \frac{P}{H} \tag{2.2}$$

$$K^{t\prime} = K^t - K_g \tag{2.3}$$

The parameter commonly used to quantify the influence of P-Delta effects in the lateral stiffness of a structure is the so-called stability coefficient θ, defined as the ratio of stiffness decrease to first order elastic stiffness, K^{E}. For the SDOF system shown in Fig. 2.4, such parameter, which is the same in any state of the structure, is given by the following equation:

$$\theta = \frac{K^t - K^{t\prime}}{K^E} \tag{2.4}$$

Such decrease in strength and stiffness of the structure due to gravity loads may be interpreted as shearing of its load-deformation capacity relationship in function of the stability coefficient. Accordingly, the effective elastic stiffness of the system can be written in terms of θ as,

$$K^{E\prime} = K^E(1-\theta) \tag{2.5}$$

and the effective yield strength, F_y' of the system can be expressed via the following expression,

$$F_y{}' = F_y(1-\theta) \tag{2.6}$$

Consequently, the effective period of vibration, *i.e.*, second order period, of the SDOF system, T′, considering the influence of gravity loads is,

$$T' = \frac{T}{\sqrt{1-\theta}} \tag{2.7}$$

where T is the first order period,

$$T = \frac{2\pi}{\omega} \tag{2.8}$$

Furthermore, the effective post-yield stiffness in terms of the first order post-yield stiffness ratio, α, can be expressed as

$$K_d{}' = (\alpha - \theta)K_e \tag{2.9}$$

and the effective ultimate strength can be defined by the following equation:

$$F_u{}' = F_y{}'[1 + \alpha'(\mu - 1)] \tag{2.10}$$

where α' is the effective post-yield stiffness which can be related to the first

$$\alpha' = \frac{\alpha - \theta}{1 - \theta} \tag{2.11}$$

Evidently, this "shearing" effect of the load displacement relationship has an influence in the response of SDOF systems under dynamic loading. The consequences of stiffness modification due to gravity loads in the elastic stage of behaviour arise from the period lengthening that influences dynamic response. However, it is in the inelastic stage where P-Delta effects influence significantly the system's response as the first order tangent stiffness in such instance (K^D) is considerably less than that of the elastic stage, hence, the effect of gravity loads in the lateral stiffness of the system is more severe. In fact, the stiffness reduction may be of such magnitude that an instability condition arises, i.e, the postyield stiffness being negative ($\alpha' < 0$), which, in turn, may lead to collapse of the system due to dynamic instability.

A particular feature of systems with negative post-yield stiffness is that, even though the displacement and, accordingly, the ductility associated to dynamic instability are infinite by definition, its displacement response under dynamic loading is bounded by the static (monotonic) collapse ductility μ_{cst} given by Eq. 2.12. (Jäger and Adam 2013), defined as the ductility value for which the system reaches zero ultimate strength under monotonic loading; such expression is obtained by equating F_u to zero (Eq. 2.10). Therefore, collapse ductility can be conveniently defined as μ_{cst}.

$$\mu_{cst} = \frac{1 - \alpha}{\theta - \alpha} \tag{2.12}$$

The slope of the post-yield stiffness (stability coefficient) provides insight of the instability potential of the system; in a SDOF system with a given yield strength, the larger the stability coefficient, the more likely dynamic instability will occur. This trend may be recognized by inspection of Equation 2.12; as the stability coefficient is larger the collapse ductility boundary is reduced. Furthermore, the yield strength of the system also plays a significant role in the occurrence of dynamic stability since the decrease of strength in the post-yielding stage, i.e, $\alpha'(\mu\text{-}1)F_y'$, necessary to attain null ultimate strength is larger as the yield strength is increased. Hence, systems with larger stability coefficients require larger lateral strength to avoid dynamic instability.

Moreover, dynamic instability depends on the hysteretic model that rules the response of the system. Several studies show that systems with bilinear behaviour are more susceptible to dynamic instability than peak-oriented models (Rahnama and Krawinkler 1993, Pettinga and Priestley 2007, Adam and Jäger 2012a). According to such studies, this is due to the fact that the response of bilinear systems remains in larger and more lapses of time in a negative segment, thus, the displacement increase in a single direction is more severe than that of systems with peak-oriented behaviour.

2.2.3 P-Delta effects in MDOF systems

Second order effects in MDOF structures may be described using a similar approach as the aforementioned for SDOF systems via the geometric stiffness matrix, $[K_g]$, which represents the stiffness decrement due to gravity loading of the vertical load carrying components of the structure in terms of their axial load to storey height ratios. Accordingly, the effective tangent stiffness matrix of the system, $[K^{t'}]$, *i.e.*, second order stiffness matrix, of an MDOF structure in any stage of behaviour can be expressed as.

$$[K^{t\prime}] = [K^t] - [K_g] \tag{2.13}$$

where $[K^t]$ is the first order tangent stiffness matrix.

An estimation of the effect of gravity loads in the global stiffness of a MDOF structure in a particular damage state may be attained from the comparison of the results of first and second order modal analyses, expressed by the following equations,

$$([K^t] - \lambda[M])\{\phi\} = 0 \tag{2.14}$$

$$([K^{t\prime}] - \lambda'[M])\{\phi'\} = 0 \tag{2.15}$$

where, [M] is the mass matrix, λ and λ' are the first and second order eigen-values respectively; ϕ and ϕ' are their corresponding eigen-vectors, *i.e.,* modal shapes.

It is evident from inspection of the preceding equations that the stiffness decrease due to gravity loads leads to a modification of all eigen-values and eigen-vectors. For lower modes such reduction is higher since the eigen-values are smaller. For this reason, the influence of P-Delta in the tangent global stiffness of a MDOF structure in a certain damage state may be measured by the stability coefficient θ^t associated with the properties of the first mode of the structure, which may be defined as:

$$\theta^t = \frac{\Gamma_1^t \lambda_1^t - \Gamma_1^{t\prime} \lambda_1^{t\prime}}{\Gamma_1^t \lambda_1^t} \tag{2.16}$$

where Γ_1^t is the first order eigen-value of the fundamental mode and λ_1^t the corresponding modal participation factor and $\Gamma_1^{t'}$ and $\lambda_1^{t'}$ are the corresponding second order properties.

In this equation the stability coefficient is denoted with subindex t to denote the tangent stiffness associated to a particular damage state as in MDOF structures this parameter varies from one damage state to another, unlike SDOF systems in which the stability coefficient is the same regardless of the damage state of the structure. Such difference between stability coefficients in MDOF structures is a consequence of the difference between modal properties from one damage state to another. Moreover, as the first and second order dynamic properties of a particular damage state are different, the stability coefficient given by Eq. 2.16 is normalized to the first order modal participation factor to provide a reference with respect to the first order modal stiffness.

In actual structures, the stiffness modification due to gravity loads is usually negligible in the elastic stage, however, as in SDOF systems, it may be significant in the inelastic stage since the elements of the first order tangent stiffness matrix are small due to the damage of structural components and, consequently, the effect of gravity loads in the lateral system is more severe. Moreover, its effect may be of such magnitude that an instability condition arises, *i.e.,* the effective stiffness matrix not being positive definite (Bernal 1998).

If at least one negative eigen-value occurs, the structure presents a static instability condition for the associated modal shape. In a similar manner as in SDOF systems, the fundamental eigen-value provides insight of the instability potential of the structure; the larger the negative eigen-value, the more susceptible the structure is to fail in a sidesway mode. The magnitude of the eigen-value increases as the damage state of the structure is more severe since the elements of the geometric stiffness matrix are small. In fact, the

difference between the effective (tangent) stiffness matrix in the inelastic phase of response and that of the elastic stage may lead to a significantly different modal composition and, consequently, to a displacement response drastically different. For this reason, the stability coefficient of the structure may be quite different in a damaged state to that in the elastic state (Medina and Krawinkler 2003). For instance, a frame structure whose stability coefficient corresponding to a soft storey-mechanism with yielding in several beams is larger than the stability coefficient corresponding to strong column-weak beam damaged state with yielding of the same beams, and the latter is closer in value to the elastic stability coefficient.

Furthermore, if the second-order modal properties were significantly different in the inelastic stage, both, the magnitude and distribution of forces would be significantly different from the magnitude and distribution in the elastic stage and could not be estimated properly from first order analysis. Evidently, this is an important issue for design of new structures as the existing design approaches for P-Delta effects are based in the extrapolation of the results of first or second order elastic analysis; such issue shall be discussed later on.

In accordance with the aforementioned concepts, the level of vulnerability of structures to the P-Delta effect is a function of its geometry, the distribution of stiffness of its structural components and the distribution of strength, since the global stability depends significantly on the damage state developed in the structure (Bernal 1998). Due to their characteristics, multi-storey frame structures are particularly vulnerable to P-Delta effects. Moreover, P-Delta effects governs sidesway collapse of flexible frames with gravity load induced negative stiffness where the influence of cyclic deterioration is relatively not important (Ibarra and Krawinkler 2005).

Several studies such as Adam and Jäger (2012b) show that collapse of P-Delta vulnerable regular frames is governed by the first mode of vibration. Partial or local mechanisms may be generated by the destabilizing effect of the gravity loads depending on the aforementioned factors; however, it is possible that a local mechanism does not affect the global stability of the system. Nonetheless, if the storey drift remains approximately uniform along the height of the building, the prediction of P-Delta induced sidesway collapse may be carried out with a sufficient degree of approximation by means of a SDOF system characterizing the fundamental mode of vibration whose properties are defined from pushover analysis (Adam and Jäger 2012a). Such is the approach followed in simplified collapse assessment procedures proposed by some authors as an alternative to rigorous assessment via non-linear dynamic analyses; both approaches are discussed in the following section.

2.3 Assessment of sidesway collapse of structures subjected to seismic loading

2.3.1 Incremental dynamic analysis

Incremental dynamic analysis (IDA) (Vamvatsikos and Cornell 2001) is a state of the art assessment tool that has been used extensively in recent years to estimate the performance of structures under increasing seismic intensities, particularly for assessment of sidesway collapse. IDA consists in a series of non-linear dynamic analysis of a record or set of records scaled to various intensity levels from which the dynamic capacity of the structure is estimated.

The characterization of seismic intensity is carried out via an intensity measure (IM), which is usually a scalar quantity such as peak ground acceleration (PGA), peak ground velocity (PGV), or spectral pseudo-acceleration ($Sa=Sa\ (T_1,\xi)$) of a linear elastic system whose properties correspond to the first mode of the

structure for a given level of damping. As seismic hazard curves are usually defined for Sa, this parameter is frequently used as an IM. Structural response is characterized through a measure of seismic demand referred to as engineering demand parameter (EDP); typically, maximum interstorey drift amongst all floors is used for such purpose.

The results of the series of non-linear analysis for a given record are usually depicted in the so-called IDA curve, the plot of EDP vs. IM, which depicts the pattern of structural response under a particular record scaled to different intensities. Such curves are different from one record to another, in fact, the trends of behaviour may be notoriously distinct, due to the natural variability of structural response to different acceleration time histories, *i.e.,* record to record variability. Fig. 2.5 (Vamvatsikos and Cornell 2002) depicts the IDA curves of a 5-storey braced frame corresponding to 4 different records, where the aforementioned issue can be observed.

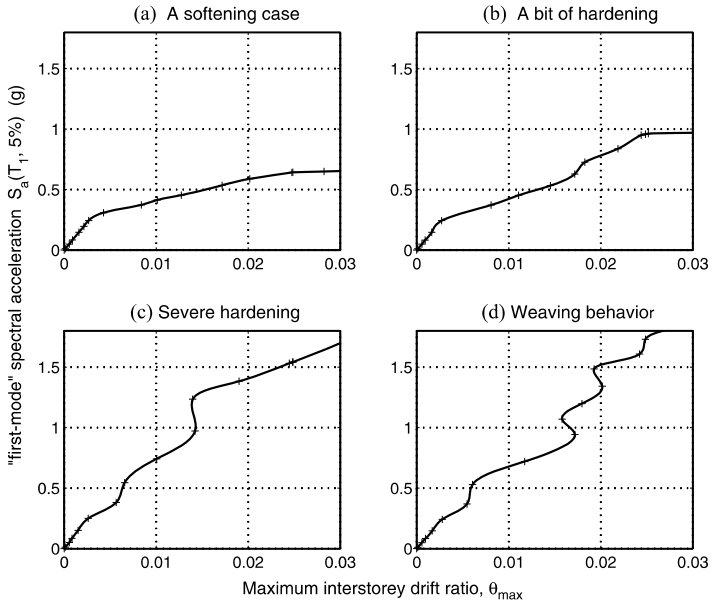

Figure 2.5 IDA-curves of a 8-storey steel braced frame of period T_1 = 1.8 s

Moreover, the degree of record to record variability is related to the IM employed since this measure is a parameter that characterizes the ground motion intensity and, although related to structural response, it does not capture all of the record's characteristics that may influence its response (Iervolino and Manfredi 2008). An intensity measure is said to be "efficient" when the dispersion of structural response is the least possible. For instance, Sa is more efficient than PGA as the former considers in a better way the relation between response and frequency content than the latter.

Extreme softening or flattening of an IDA curve (Fig. 2.5.a) indicates the collapse capacity of the structure as for that level of intensity a disproportionate displacement, *i.e,* numerical instability, occurs. A particular feature of IDA curves is that, opposite to common intuition, they are not necessarily monotonic, *i.e.,* structural response may be lower for higher intensities, since, as the structure is scaled to higher intensities, yielding of the structure occurs at weaker cycles and the properties of the structure are altered for the subsequent cycles due to damage (Iervolino and Manfredi 2008). Such characteristic may be observed in Figs. 2.5c and 2.5d. An extreme consequence of such feature is that it is possible that an IDA curve may

exhibit more than one collapse point. This type of behaviour is given the name of "structural resurrection". In such cases, for simplicity sake, the first collapse point obtained from the series of analysis is considered as the collapse capacity of the structure (Vamvatsikos and Cornell 2002).

According to Vamvatsikos and Cornell (2002) a probabilistic characterization of structural response for a given site can be extracted from a multi-record IDA using a representative set of records. Moreover, if the record set is robust, *i.e.,* the median response calculated with the unscaled records is similar to the median response calculated with scaled records, and an "efficient" intensity measure that allows to consider, ideally, conditional independence of structural response with respect to the earthquakes's magnitude and source distance, performance in terms of mean annual frequency can be calculated from the results of multi-record IDA (Iervolino and Manfredi 2008).

Under the aforementioned assumptions, seismic performance at different intensity levels can be estimated using IDA via two approaches: the EDP-based approach and the IM-based approach. In the former, the probabilistic representation is based on the probability of the EDP considered exceeds a given threshold ($EDP_{c)}$) assumed as collapse, *i.e.,* $P[EDP_d > EDP_c/IM=IM_i]$. Alternatively, in the IM-based approach the probability of collapse is given directly as a function of the collapse intensity, IM_c, *i.e.,* $P[IM_c < IM_i]$. The latter approach is more appropriate for collapse assessment as the variability of the displacement response at the onset of collapse poses a problem for the characterization of probability of collapse via the EDP approach. (Ibarra and Krawinkler 2005).

Even though IDA is a powerful tool for collapse assessment of structures under seismic loading it has the disadvantage of being considerably time consuming and computationally expensive as a large number of non-linear dynamic analysis are needed. Thus, its use in current practical engineering application is still not generalized. For such reason, investigations focused on the development of alternative simplified design and assessment procedures based on the ESDOF system approach that provide sufficiently approximate results have been carried out in recent years.

2.3.2 Simplified assessment procedures for collapse capacity estimation

Bernal (1998) developed a simplified method to assess collapse for instability prone systems that is based on the use of mean collapse spectra. The stability coefficients are calculated either by pushover analysis or from simplified expressions that depend on an expected controlling mechanism of the structure, from which the corresponding collapse spectra is selected. Subsequently, the yield spectral acceleration is obtained from such spectra and its associated base shear is compared with that of the base structure. The method was validated by comparing expected response vs. the average response of a suite of 24 records on hard sites.

Shafei (2011) proposes a simplified method based on non-linear static analysis applicable to regular structures. From the parameters of the backbone curve of the structure, obtained from a pushover analysis using a constant load pattern, median and dispersion are calculated using closed-form equations obtained from multivariate regression analysis of a set of generic frames and a record set of 40 hard soil type records.

Adam and Jäger (2012a) proposed the so-called collapse capacity spectra method which is similar to the approach of Bernal but more refined. To estimate the elastic and inelastic stability coefficients a pushover analysis of the structure is performed. From such analysis the ESDOF is defined and its yield strength is compared with the corresponding ordinates of 16%, 50% and 84% collapse capacity spectra in terms of relative intensity, from which the fragility curve can also be constructed. The method has been extensively

validated via IDA using the far field record set recommended for collapse assessment by the FEMA-P695 provisions (FEMA 2009).

2.4 P-Delta effects in seismic design

2.4.1 Force based design approach

The most common approach followed in force-based design procedures contained in building codes to include P-Delta effects in structural design relies on elastic analysis. Foremost, a first order analysis of an elastic model is performed from which the storey stability coefficients are estimated. If all stability coefficients are smaller than a prescribed threshold, second order effects may be ignored. If the opposite holds true, they should be taken into account in the design of structural elements via two options. The first option is to account for second order effects by modifying the flexural demands obtained from first order elastic analysis with amplification factors. The second option is to calculate P-Delta effects directly with second order analysis of the elastic structural model.

However, this approach is not appropriate for the reasons given in section 2.2, as the displacement response in the inelastic stage may be significantly different than that obtained from elastic analysis even if second order analysis is carried out, since the modification in stiffness due to gravity loads is more severe in the inelastic stage than in the elastic stage. For the same reason, the distribution of forces in the inelastic stage may also be affected significantly by second order effects, thus, control of a desirable failure mechanism of a ductile structure may not be achieved, leading to ill performance control. Even though, building code procedures intend to provide control of gravity induced instability by limiting the deformations of the structures, such approach is not theoretically consistent (Bernal 1998).

2.4.2 Displacement based design approaches

Investigations focused on the development of displacement based procedures have been carried out as they provide a more rational basis to performance oriented design than force-based procedures. The most widely known of the latter methods is the direct-displacement based (DDBD) method proposed by Priestley *et al.* (2007), hence, the general approach of such method and proposals to account for P-Delta effects in DDBD are presented herein.

The DDBD method is based on the use of the so-called substitute structure artifice, in which a non-linear MDOF system is characterized through an equivalent linear SDOF system with secant stiffness to maximum displacement response and an equivalent viscous damping ratio that accounts for the hysteretic energy as a function of the ductility demand and the considered hysteresis rule. For a given design interstorey drift, the design displacement of the substitute structure is defined via empirical equations that are a function of the number of storeys and their height. The yield displacement is estimated using an empirical formula that is a function of the material and geometric properties of structural components. From the resulting design ductility, the corresponding hysteretic viscous damping ratio is defined; the equivalent viscous damping ratio of the substitute structure is the sum of the elastic and hysteretic viscous damping ratios. Subsequently, the required period of the equivalent SDOF system is attained from a design elastic spectrum (in terms of displacements) associated with the equivalent viscous damping ratio. The structural model is then analysed under a force vector associated with the displacement demand and the structural components are designed considering capacity design principles to ensure strong column-weak beam behaviour.

Pettinga and Priestley (2007) proposed a simplified criterion to account for P-Delta effects for the design of moment frames in which the strength of the system is increased in function of the stability coefficient and the hysteresis rule considered, in such a way that the secant stiffness of the substitute structure considering second order effects is the same as that without P-Delta effects. The basis of this criterion is the assumption that the stiffness increase will ensure stable response of the system. The case studies considered in their research is limited to single 4-storey frame subjected to several levels of axial load and the validation was carried out via non-linear dynamic analysis using seven real earthquake records adjusted to closely match a site-specific elastic displacement spectrum, from which the average responses vs. the design target displacements were compared. The authors conclude that their proposal allows to mitigate severe second order effects in the designed frames.

Asimakopoulos *et al.* (2007) developed an equation to calculate a yield displacement amplification factor as a function of the design ductility and the stability coefficient to consider second order effects for design of steel moment frames for the life safety limit state using the DDBD method, although sidesway collapse check is also possible. Such amplification factor modifies the secant stiffness and strength of the design linear ESDOF system. The stability coefficient is estimated from an equation that is a function of the number of storeys and the column to beam stiffness ratios, which was defined from linear regression of the results of non-linear analyses of 8- to 15-storey frame structures. The seismic demands employed in such analyses were three sets of five synthetic spectrum-compatible records generated from the EC8 design spectra (CEN 2001); each set accounts for a different soil condition. The validation of their approach was carried out by comparison of the base shear amplification due to second order effects estimated with their approach and the shear amplification calculated using the EC8 criterion (CEN 2001) and a simplified equation proposed by Miranda and Akkar (2003) for SDOF systems. Hence, the criterion proposed in this article was validated at the ESDOF level only, as non-linear dynamic analysis of the multi-storey frames was not carried out.

It should be noted that, as highlighted by MacRae (1994) and Pettinga and Priestley (2007), there is a conceptual problem regarding the consideration of P-Delta effects via the substitute structure as this artifice is based on the assumption that the equivalent system is self-centred, *i.e.,* the response is reversible, assumption that is inconsistent with the behaviour of structures with severe P-Delta effects in which ratcheting of response occurs. Furthermore, P-Delta effects appear to be considered only at the ESDOF level without taking into account its influence in the distribution of storey design forces. Besides these conceptual problems, these proposals have been validated with a relatively limited size of synthetical or semi-synthetical records.

The approach followed in the method proposed, based on a reference SDOF system representation of a MDOF system, is to ensure a design damage state, *i.e.,* predetermined mechanism, consistent with a design displacement shape for a given demand level, from which consistent design forces are estimated. Thus, this approach is more appropriate to design P-Delta induced instability prone systems and shall be presented in the following chapter. Moreover, in this investigation a full scale validation was carried out for a larger ensemble of real records obtained at soft and stiff soil sites.

CHAPTER 3

FUNDAMENTALS OF THE METHOD PROPOSED

3.1 Reference SDOF system

The main assumption of the method proposed is that it is possible to describe, in a primary manner, the seismic behaviour of an inelastic MDOF structure by means of the behaviour of an inelastic SDOF system whose properties are consistent with those of the fundamental (first) mode of the structure in both its elastic and inelastic stages of behaviour. In the framework of this method, this SDOF system is termed as reference SDOF system, RSDOF, (Ayala 2001) and, accordingly, the main characteristic used to estimate the maximum response of a given structure is the backbone curve of spectral displacement, Sd, *vs.* spectral pseudo-acceleration (strength per unit mass), Sa, *i.e.,* the so-called behaviour curve of the reference SDOF oscillator.

This artifice is analogous to that of the conventional ESDOF system, however, the SDOF system employed is considered to serve as a reference of the behaviour of the corresponding MDOF structure and not as being actually "equivalent" to it, as the contribution of higher modes is taken into account in the definition of the RSDOF system as shall be explained later in this section.

The design approach followed in the method proposed is the definition of a design behaviour curve that provides the stiffness and strength required by the structure to satisfy a given performance objective (PO). For the case of a PO comprised of a serviceability limit state (SLS) and a collapse prevention limit state (CPLS), a design bilinear behaviour curve is built (Fig. 3.1). The characteristic points that define this curve are: origin (0, 0), yield (Sd_y, Sa_y) and ultimate (Sd_u, Sa_u).

The first branch of this curve characterizes the elastic stage of behaviour of the structure. Its slope, λ^E, is limited in such a way that the interstorey drift thresholds for both the SLS or ULS are not exceeded for the demand levels given by the corresponding design spectra. The demand associated to the SLS is given by the point (Sd_s, Sa_s). The second branch of the curve portrays the structural post-yielding behaviour, whose slope, $\alpha\lambda^E$, is a function of the design damage state, *e.g.,* strong column-weak beam, at maximum inelastic response under the design demand considered for the ULS.

The yield displacement, Sd_y depends on the material and geometric properties of the structural elements; the ultimate displacement, Sd_u, is set so that the interstorey drift threshold of the ULS is not exceeded for

the corresponding demand level. The yield spectral pseudo-acceleration, Sa_y, is directly related to the design forces of the structural elements that are expected to yield in accordance with the considered design damage state, whereas the ultimate spectral pseudo-acceleration, Sa_u, is associated with the force levels of the structural components that should remain elastic or develop, at most, limited inelastic behaviour. The remainder of Sa_y and Sa_u is referred as post-yield spectral pseudo-acceleration, Sa_{py}, which is related to the redistribution of forces up to the point of maximum inelastic response of the structure.

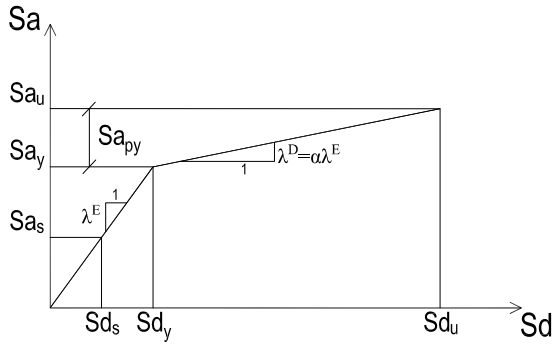

Figure 3.1 Behaviour curve of the reference SDOF system for a two-limit state performance objective

In order to define the design behaviour curve, a structural model is built considering a preliminary proposal of structural element sizes, as it is carried out in any conventional design procedure. The design yield and ultimate displacements and the post-yield stiffness ratio of the RSDOF system can be estimated from the properties of the preliminary structure via two different options. The first option, which requires the model to be non-linear, consists of performing static pushover analysis of the preliminary structure from which the parameters of the RSDOF are estimated with appropriate relations concerning the ESDOF system approach. The second alternative consists on calculating such parameters from the results of modal analyses of elastic structural models representative of the elastic and inelastic stages of behaviour, hence, any structural analysis program that performs elastic analysis can be employed. The latter option is the one considered herein and shall be described in the following section.

3.2 Elastic and "damaged" model

In the same manner as in a conventional design procedure that relies on elastic analysis, a model is built with the elastic properties of the proposed structural elements, such as nominal moments of inertia of available steel shapes or cracked moments of inertia of reinforced concrete elements. Furthermore, a replica of the elastic model is created, in which the plastic hinges assumed in the design damage state are characterized by rotational springs whose stiffnesses matches the post-yield stiffnesses of the structural components. Such replica is referred to as damaged model (Fig. 3.2) and is used to calculate the dynamic properties of the structure associated with its maximum response.

From the modal analysis of the aforementioned structural models, the eigen-values and eigen-vectors, *i.e.,* modal stiffnesses and shapes, are obtained. As the models characterize the stiffness of the structure in its elastic and inelastic stage of behaviour, from structural dynamics concepts regarding the modal superposition approach the slopes of the Sd vs. Sa relations of each mode j in the spectral space can be taken as the associated eigen-values λ^E_j and λ^D_j, respectively (Ayala 2001). This scheme implicitly considers that the modal masses of the structure in its elastic stage are equal than those of the damage state. However, the modal masses of a MDOF structure associated with severe damage may be different to those corresponding

to elastic behaviour, especially for the fundamental mode. Bearing in mind that the behaviour of a MDOF structure is to be characterized through SDOF systems, in which the mass is invariant regardless of its damage state, a more appropriate estimation of the modal post-yield stiffness ratios is given by Eq. 3.1

$$\alpha_j = \frac{\Gamma_j^D \lambda_j^D}{\Gamma_j^E \lambda_j^E} \tag{3.1}$$

where Γ_j^D and Γ_j^D are the modal participation factors of mode j of the elastic and damaged models respectively.

The post-yield stiffness ratio of the RSDOF system, α, is equal to α_1 of the corresponding MDOF structure (see Fig. 3.1). In the following, the variables corresponding to the parameters and demands of the RSDOF system are denoted without a subindex to differentiate them from those of the higher modes of the actual MDOF structure where the mode numbers are indicated.

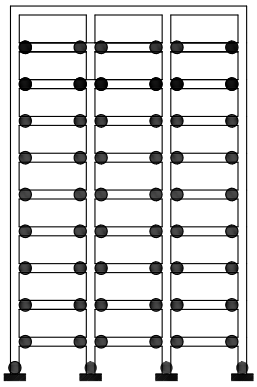

Figure 3.2 Damaged model representing a strong column-weak beam damage state

3.3 Definition of design displacement shapes

It is a well-recognized fact that the displacement response of framed structures during seismic events is usually governed by the response of their fundamental mode of vibration. Thus, a reasonable approximation of the design drift and displacement shape associated with a given limit state, at least a preliminary one, may be estimated with the fundamental mode shape obtained from the eigen-value analyses of the elastic and damaged models.

This estimation is carried out by equating the interstorey drift threshold of the corresponding limit state to the largest difference of modal coordinates of successive levels, which, consequently, defines the critical storey of the frame (Fig. 3.3). From this equality, the target displacements of the PO can be obtained. Hence, for the serviceability limit state considered in this study, where elastic behaviour of the structure is a requirement, Sd_s, is calculated with the following expression:

$$Sd_s = \frac{IDR_s H_k}{\Gamma_1^E (\phi_{k\,1}^E - \phi_{k-1\,1}^E)} \tag{3.2}$$

where IDR_s denotes the interstorey drift threshold for the SLS, k is the critical storey in the elastic stage, H_k is the height of the critical storey, $\Phi^E_{k\,1}$ and $\Phi^E_{k\text{-}1}$ are the fundamental modal coordinates of the critical storey and preceding storey obtained from modal analysis of the elastic model, respectively; Γ^E_1 is the fundamental modal participation factor.

The design yield displacement, Sd_y, is defined in a similar manner as:

$$Sd_y = \frac{IDR_y H_k}{\Gamma_1^E(\phi^E_{k\,1} - \phi^E_{k-1\,1})} \tag{3.3}$$

where IDR_y is the yield interstorey drift which can be estimated with Eq. 3.4 (Priestley, 2007),

$$IDR_y = \frac{\beta_m L}{h_b H} \tag{3.4}$$

in which β_m is a constant that depends on the material and structural type, L is the beam span and h_b is the beam depth.

In order to calculate the ultimate design displacement, Sd_u, associated with inelastic behaviour, it is assumed that the displacement shape of a bilinear MDOF system subjected to severe earthquake excitation is a linear combination of the eigen-vectors corresponding to the elastic and inelastic stages. Therefore, the design spectral displacements of the reference SDOF system may be estimated by means of the following equations:

$$\mu = \frac{Sd_u}{Sd_y} \tag{3.5}$$

$$Sd_u = \frac{IDR_u H_k}{\Gamma_1^{D*}(\phi^{D*}_{k\,1} - \phi^{D*}_{k-1\,1})} \tag{3.6}$$

$$\phi^{D*}_{i\,1} = \frac{1}{\mu}\left[\frac{\Gamma_1^E}{\Gamma_1^D}\phi^E_{i\,1} + (\mu - 1)\phi^D_{i\,1}\right] \tag{3.7}$$

where IDR_u denotes the interstorey drift ratio threshold of the ULS; k, is the critical storey in the inelastic stage; H_k is the height of the critical storey; Γ^E_1 and Γ^D_1 identifies the modal participation factor of the first mode attained from the eigen-analyses of the elastic and inelastic model, respectively; $\Phi^E_{i\,1}$ and $\Phi^D_{i\,1}$ are the elastic and inelastic modal shapes of the fundamental mode, respectively; $\Phi^{D*}_{i\,1}$ identifies the design modal shape for the ULS; $\Phi^{D*}_{k\,1}$ and $\Phi^{D*}_{k\text{-}1\ 1}$ denote the coordinates of the modal shape corresponding to the critical storey and the preceding storey, respectively. It should be noted that the critical storey k in the inelastic stage of the structure is not necessarily the same critical storey in the elastic stage. In frames that develop a strong column-weak beam damage state with yielding at the bases of the first floor columns, the maximum inelastic interstorey drift usually occurs at the base storey or at its vicinity. Therefore, k in Eqs. 3.3 and 3.6 will likely be different.

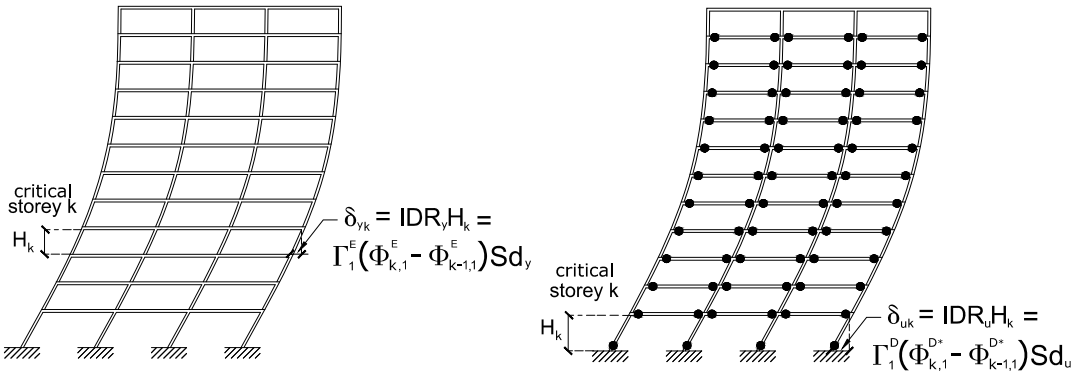

Figure 3.3 Design displacement shapes

Accordingly, design displacement profiles (first mode only), D_s, D_y and D_u, corresponding to the SLS, yield and ULS of the structure, respectively, can be defined via the following equations.

$$\Delta_{s\,i} = \Gamma_1^E \phi_{i\,1}^E Sd_s \tag{3.8}$$

$$\Delta_{y\,i} = \Gamma_1^E \phi_{i\,1}^E Sd_y \tag{3.9}$$

$$\Delta_{u\,i} = \Gamma_1^D \phi_{i\,1}^{D*} Sd_u \tag{3.10}$$

3.4 Definition of design demands of reference SDOF system

Given the design displacements of the RSDOF system, the required periods for each limit state that comprise the PO are obtained from design spectra associated with the respective design intensities. In accordance with the definition of the SLS considered herein, which stipulates that the structure should remain in the elastic range, the design period, T_s is read from the considered SLS design elastic-displacement spectrum (Fig. 3.4a). For ULS design, where inelastic behaviour is expected, the required period for such limit state, T_u, is obtained from the ULS design inelastic-displacement spectrum associated with the design ductility and post-yield stiffness ratio of the design RSDOF system (Fig. 3.4b). The design period of the RSDOF system, T_{des}, is taken as the least value of the aforementioned periods, thus, defining the stiffness requirement of the structure to satisfy the considered PO.

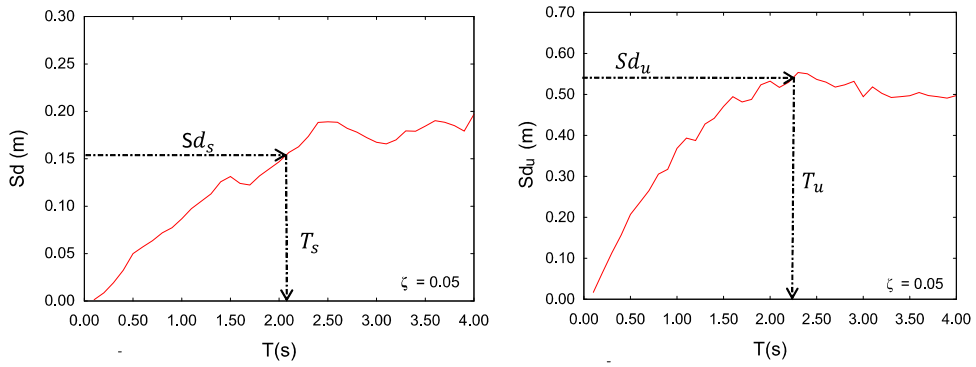

a) **b)**

Figure 3.4 Definition of required periods for SLS and ULS design

Accordingly, the structure is then modified so that its period matches or at least approximates the required one; both elastic and damaged models are adjusted. If such modification is carried out without altering significantly the distribution of element´s stiffness considered in the preliminary structure, the displacement shape of the final design structure shall be consistent with the former. In practical design applications, design groups of structural elements, *i.e.,* sets of elements with the same structural section, are considered in the proposal of a preliminary structure and the final design of the structure is usually carried out considering similar element grouping, thus, the final distribution of structural elements should not be radically different from that originally proposed.

3.5 Definition of design demands of higher modes

According to Sullivan (2008) the contribution of higher modes to force demands may be significant in frame structures in comparison with the displacement response, thus, it is necessary to take them into account in its design. The criterion employed to account for higher mode contribution in the method proposed is based on the fact that both the yield and ultimate demands of an MDOF structure, are the combination of the individual modal responses up to the elastic limit and maximum demand, respectively. The demand of higher modes is consequently defined as a function of the properties of the structure in the elastic and inelastic stages of behaviour such as it is carried out for the RSDOF system. Hence, under such criterion, knowledge of the post-yield properties and ductility demands of higher modes is needed.

Several studies regarding the use of the modal superposition procedure for analysis of inelastic structures have shown that modes do not necessarily share the same strength reduction factors, R, nor develop equal ductilities (Chopra and Goel 2002, Sasaki *et al.* 1998; Sullivan *et al.* 2008). This may be attributed to the following issues:

1) As damage occurs in an MDOF structure the tangent stiffness matrix changes and, generally, such alteration leads to post-yield stiffness ratios of higher modes that are significantly different to those of the fundamental mode.
2) Modal coupling is present in an inelastic MDOF system as the tangent stiffness matrix associated with a damaged state is not diagonalizable with respect to the elastic stiffness matrix (Clough and Penzien 1994). Thus, inelastic modal responses cannot be strictly independently calculated as it can be carried out for an elastic MDOF system.

Nonetheless, Chopra and Goel (2002) state that it is possible to approximate the inelastic response of frame structures via the modal combination of individual modal responses obtained from pushover analysis using the respective modal load patterns and discarding inelastic modal coupling. Hence, according to such approach, the yield strength and the damage progression is independent from one mode to another, *i.e.,* modal interaction in the design damage state is not considered. From numerical analyses carried out in their study using such approach, the ductilities of higher modes attained are lower than that of the first mode.

Even though the criterion regarding higher mode contribution used in the method proposed in this investigation is significantly different to that of Chopra and Goel (2002), as the modal properties are assumed to be dependent on the yielding and the damage progression of the structure, an upper bound of the ductility of higher modes, μ_j, equal to that of the RSDOF system, $\mu_1 = \mu$, is considered appropriate for design purposes. With the assumed μ_j and the post-yield stiffness ratios of higher modes, α_j, associated with

the design damage state given by Eq. 3.1, the design behaviour curves (the Sd *vs.* Sa relations) of each mode can be defined in a similar fashion as it is carried out for the RSDOF system.

3.5.1 Definition of modal force demands

Under the aforementioned assumptions, the individual modal yield demands could be obtained from the corresponding design yield pseudo-acceleration spectrum associated with $\mu_j=\mu$ and α_j. However, considering that actual modal yield demands cannot be known with certainty unless time history analyses of the structure are carried out to design the structure, it would be unjustified to use such a complex scheme to calculate assumed demands that would lead to a more laborious design procedure. Thus, for the sake of simplicity, each modal yield pseudo-acceleration, $Sa_{y\,j}$, including that of the first mode, is defined directly from the yield pseudo-acceleration spectrum corresponding to the properties of the RSDOF system, assuming that such spectrum is representative of the demand of higher modes up to the yield point of the structure (Fig. 3.5).

The maximum inelastic demands are defined assuming that higher modes develop the same ductility as the first mode and that inelastic coupling is negligible. Hence, the ultimate pseudo-acceleration of the j-th mode, $Sa_{u\,j}$, including that of the RSDOF system, is given by the following equation:

$$Sa_{u\,j} = Sa_{y\,j}\left[1 + \propto_j (\mu - 1)\right] \tag{3.11}$$

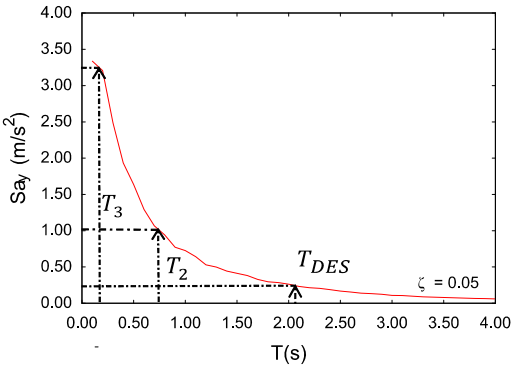

Figure 3.5 Definition of higher mode yield-pseudo-accelerations

3.6 Modal spectral analysis

In accordance with the assumptions regarding the contribution of higher modes, the design demands for the elastic and inelastic stages of behaviour are obtained via modal spectral analysis of the simplified models using conventional modal combination rules, such as SRSS, CQC, as applicable. The considered inelastic strength per unit mass spectrum is employed in the modal spectral analysis of both simplified models. As mentioned in the foregoing section, the modal demands of the elastic model are defined directly from the ordinates of such spectra. For the damaged model, the modal demands are defined by the post-yield strength, $Sa_{py\,j}$, which is given by

$$Sa_{py\,j} = Sa_{y\,j} \propto_j (\mu - 1) \tag{3.12}$$

The ULS design forces are calculated via the modal combination of the maximum inelastic responses, global and local, of all modes. If the SRSS rule is employed, the design forces, $F_{k,}$ of each structural component, *i.e.,* design moments, shears and axial forces; are estimated with the following equation,

$$F_k = \sqrt{\sum_j^n (F^E_{k\,j} + F^D_{k\,j})^2} \tag{3.13}$$

where $F^E_{k\,j}$ denotes the demand of element k corresponding to mode j obtained from the modal spectral analysis of the elastic model; $F^D_{k\,j}$ is the demand of element k associated with mode j attained from the modal spectral analysis of the damaged model and n is the number of modes considered.

Furthermore, for the sake of consistency, the design displacement shape may be calculated by means of modal combination considering the aforementioned assumptions regarding higher mode contribution. This can be carried out by calculating the displacement shapes for each mode via Eqs. 3.14 to 3.18, using the demands obtained from the design spectra associated with the ductility calculated previously considering the fundamental mode only, and then combining them through the selected modal combination rule. Such adjustment of the displacement shape is usually not necessary, but it can be used to attain a rough estimation of higher mode contribution for long period structures for which it may be significant.

$$\Delta_{s\,i} = \sqrt{\textstyle\sum_{j=1}^{n}\left[\beta_j \Gamma_j^E (\phi^E_{k\,j} - \phi^E_{k-1\,j}) Sd_s\right]^2} \tag{3.14}$$

$$\Delta_{y\,i} = \sqrt{\textstyle\sum_{j=1}^{n}\left[\beta_j \Gamma_j^E (\phi^E_{k\,j} - \phi^E_{k-1\,j}) Sd_y\right]^2} \tag{3.15}$$

$$\Delta_{u\,i} = \sqrt{\textstyle\sum_{j=1}^{n}\left[\beta_j \Gamma_j^{D*} (\phi^D_{k\,j} - \phi^{D*}_{k-1\,j}) Sd_u\right]^2} \tag{3.16}$$

$$\phi^{D*}_{i\,j} = \frac{1}{\mu}\left[\frac{\Gamma_j^E}{\Gamma_j^D}\phi^E_{i\,j} + (\mu - 1)\phi^D_{i\,j}\right] \tag{3.17}$$

$$\beta_j = \frac{Sd_j}{Sd_1} \tag{3.18}$$

where βj is the displacement of mode j normalized by the displacement of the RSDOF system.

3.7 DESIGN FOR SIDESWAY COLLAPSE DUE TO P-DELTA EFFECTS

Due to the way in which the framework of the method proposed is built, second order effects can be considered in a straightforward manner through modal analysis of simplified models using the geometric stiffness matrix formulation. If at least a negative eigen-value is obtained, that for regular frame structures will most likely be the one associated with the first mode, the slope of the second branch of its behaviour curve would be negative, thus, indicating that the system is prone to be dynamically unstable for the design demands corresponding to the ULS (Bernal 1998). In such case, under the assumption that it is cost efficient to design a structure for a "negative stiffness", it is necessary that the strength of the reference SDOF system is defined in such a way that, for a given seismic intensity, its displacement response is stable. For such

purpose, an auxiliary SDOF system (Ibarra and Krawinkler 2005) is used, and the design demand is defined from particular collapse capacity spectra or constant ductility spectra for structures that are susceptible to P-Delta induced sidesway collapse.

3.7.1 Auxiliary SDOF system

The auxiliary system, developed by Ibarra and Krawinkler (2005), is an artifice employed to approximate the collapse capacity of a MDOF structure with P-Delta induced negative stiffness via an equivalent SDOF system. It consists on the definition of a SDOF system whose second order backbone matches the corresponding of the equivalent SDOF system (Fig. 3.6). It is necessary to employ this artifice since the stability coefficients in the elastic and inelastic stages of behaviour in MDOF systems are usually different (Medina and Krawinkler 2003), whereas in SDOF systems the stability coefficient is the same regardless of its damage state. In the method proposed, the stability coefficients of the MDOF structures are estimated via Eqs. 3.19 and 3.20,

$$\theta^E = \frac{\Gamma^E \lambda^E - \Gamma^{E\prime} \lambda^{E\prime}}{\Gamma^E \lambda^E} \tag{3.19}$$

$$\theta^I = \frac{\Gamma^D \lambda^D - \Gamma^{D\prime} \lambda^{D\prime}}{\Gamma^D \lambda^D} \tag{3.20}$$

where $\lambda^{E\prime}$ and $\Gamma^{E\prime}$, λ^E, and Γ^E, are the elastic fundamental eigen-values and modal participation factors with and without P-Delta effects, respectively; $\lambda^{D\prime}$ and $\Gamma^{D\prime}$, λ^D, and Γ^D are the inelastic fundamental eigen-values and modal participation factors of the structure with and without P-Delta effects, respectively. The period and stability coefficient of the auxiliary SDOF system are calculated by means of the following equations (Ibarra and Krawinkler 2005):

$$T_{AUX} = T_1 \sqrt{\frac{1-\alpha}{1-\alpha-\theta^E+\theta^I}} \tag{3.21}$$

$$\theta_{AUX} = \frac{\theta^I - \alpha\theta^E}{1-\alpha-\theta^E+\theta^I} \tag{3.22}$$

where T_1 and α are the fundamental period and the corresponding post-yield stiffness ratio of the MDOF system without considering P-Delta effects, *i.e.,* the first order stiffness properties of the RSDOF.

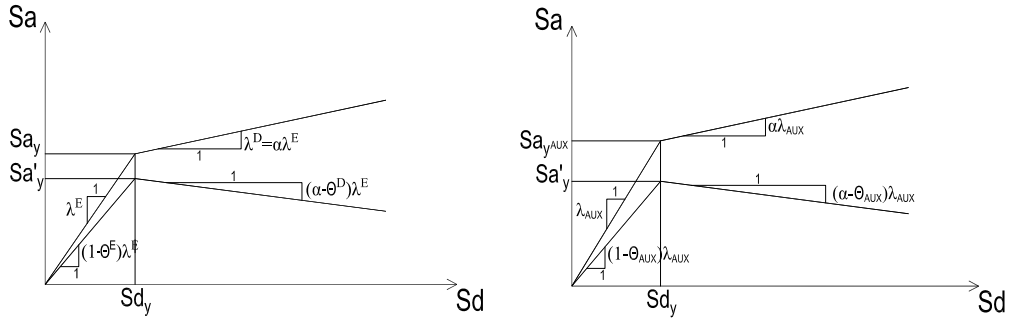

Figure 3.6 First and second order design SDOF systems: a) reference; b) auxiliary

3.7.2 Collapse capacity and constant ductility spectra of SDOF systems with negative post-yield stiffness branch

A collapse capacity spectrum, as defined by Adam and Jäger (2012a), is the plot of the first order initial period T vs. the relative intensity, Sa_e/Sa_y, of SDOF systems that exhibit a P-Delta induced negative post-yield stiffness, for which instability occurs under dynamic loading (Adam and Jäger 2012a); where Sa_e is the spectral pseudo-acceleration of the corresponding elastic SDOF system. The parameters that define such type of spectra are an effective post-yield stiffness ratio, *i.e.,* the difference of stability coefficient and hardening ratio, $\theta - \alpha$; a damping ratio, damping coefficient ζ; and a hysteresis rule. In a similar manner, Jäger and Adam (2013) defined constant ductility spectra for SDOF systems with P-Delta induced negative stiffness in terms of the same parameters and a given target ductility μ, for the purpose of collapse assessment consistent with a near-collapse limit state approach.

Collapse capacity spectra in terms of the median of Sa_e/Sa_y, of a set of records have been employed extensively by Adam and Jäger (2012a) for assessment of P-Delta induced sidesway collapse of MDOF structures under increasing seismic demands as an alternative to IDA, in accordance with the collapse assessment approach proposed by Ibarra and Krawinkler (2005) in which collapse capacity is measured in terms of a relative intensity. According to this approach, the median intensity in terms of Sa_e can be obtained in a straightforward manner by multiplying the ordinate of the collapse capacity spectra corresponding to the auxiliary period T_{AUX} of the structure by its yield strength.

In this study, percentile collapse capacity spectra and constant ductility spectra (16%, 50%, 84% and 90%) were built for two sets of records. The first one is the FEMA-P695 far field set (FEMA 2009), comprised of 44 real records, corresponding to hard rock and stiff soil sites in the US. The second record set considered in this investigation is that used by Ruiz Garcia and Miranda (2002), referred here as VM set, comprised of 100 records, recorded at soft soil sites in the Valley of Mexico. Both sets of spectra were calculated considering aleatory uncertainty, *i.e.,* record to record variability, only.

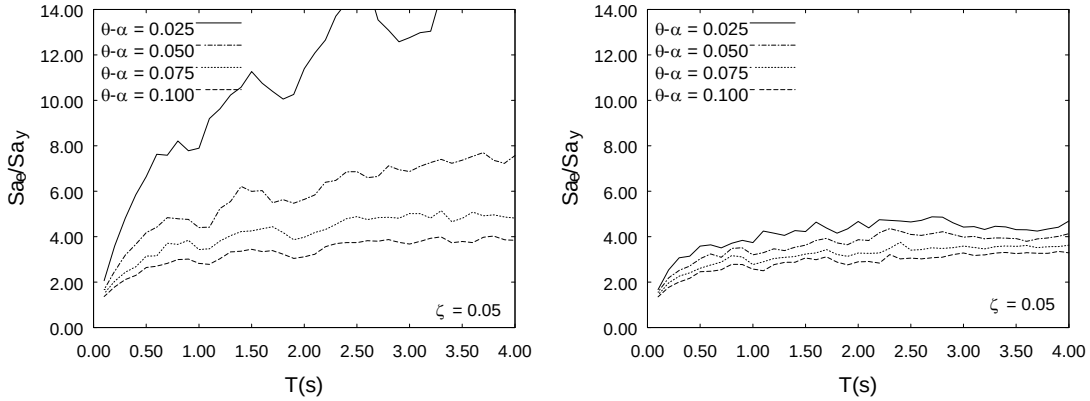

Figure 3.7 Median spectra in terms of relative intensity of SDOF systems with P-Delta induced negative post-yield stiffness of the FEMA-P695 far field record set for various θ -α values: a) collapse capacity ; b) constant ductility μ=5.00

Fig. 3.7 illustrates sets of collapse capacity spectra and constant ductility spectra of one of the FEMA-P695 set of records in terms of median relative intensity of non-deteriorating SDOF systems with bilinear behaviour for various $\theta - \alpha$ values and $\zeta = 0.05$. As it can be observed in such figure, the steeper the effective stiffness, $(\alpha - \theta)\,\lambda^E$, the lesser the collapse capacity, and the smaller the period, the larger the collapse capacity required, characteristics that are consistent with the behaviour trends of bilinear SDOF systems with negative post-yield stiffness.

In the design method proposed, collapse and constant ductility spectra in terms of yield pseudo-acceleration (strength per unit mass), Sa_y, and ultimate spectral displacement, Sd_u, are employed rather than spectra in terms of relative intensity, since the goal is to provide the required strength to the considered structure to control its displacement response for the level of seismic demand considered, whereas the goal of collapse assessment is the opposite.

For near collapse limit state design, the design demands are obtained from constant ductility spectra corresponding to the design ductility, μ_{DES}, calculated as discussed in section 3.3. On the other hand, the demands for actual collapse prevention design may be obtained from collapse spectra. If such is the case a convenient definition of collapse displacement is necessary. Even though the displacement and, accordingly, the ductility associated to dynamic instability are infinite by definition, the displacement response prior to collapse of SDOF systems with negative post-yield stiffness is bounded by the static collapse ductility, μ_{cst}, given by Eq. 3.23 (Jäger and Adam 2013).

$$\mu_{cst} = \frac{1 - \alpha}{\theta - \alpha} \tag{3.23}$$

Therefore, the dynamic collapse ductility, μ_c, may be conveniently defined as μ_{cst}. Under such assumption, collapse spectra can be considered as constant ductility spectra corresponding to μ_{cst}. Fig. 3.8 depicts a set of collapse capacity spectra ($\mu = \mu_{cst}$) and constant ductility spectra ($\mu = 5$) of the aforementioned set of records in terms of median yield pseudo-acceleration and median ultimate displacement for various $\theta - \alpha$ values and $\zeta = 0.05$.

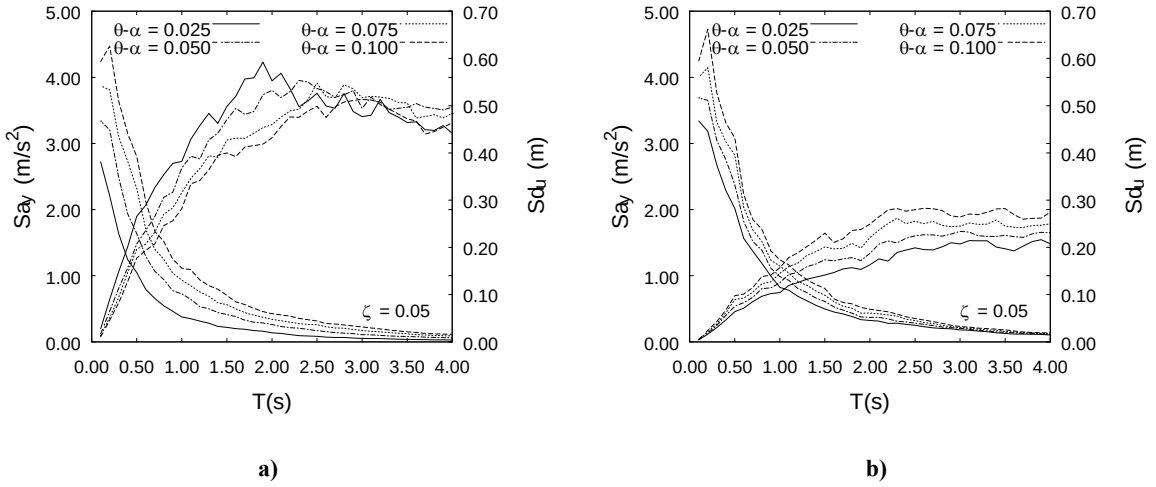

Figure 3.8 Median spectra in terms of yield pseudo-acceleration and ultimate displacement of SDOF systems with P-Delta induced negative post-yield stiffness of the FEMA-P695 far field record set for various θ-α values: a) collapse capacity, $\mu=\mu_{cst}$; b) constant ductility $\mu=5.00$.

However, in the method proposed the design demands are a function of the design ductility (section 3.5), thus, the component of the design demand corresponding to post-yield behaviour would be large if μ_{cst} is considered in an actual collapse design application. This issue would be particularly relevant for frames with small stability coefficients that would be those most likely to be considered for design purposes of actual frame structures (MacRae 1993). Nonetheless, a more convenient definition of collapse post-yield demands is possible using constant ductility spectra associated with a smaller collapse ductility value, based on the fact that displacement response at the onset of dynamic instability of SDOF systems with negative post-yield stiffness is very sensitive to its relative intensity (Ibarra and Krawinkler 2005).

Fig. 3.9 shows the comparison between median collapse capacity spectra and median constant ductility spectra (relative intensity) for two negative post-yield stiffness ratios $\theta - \alpha$ and several μ values. As it can be readily observed, the ordinates of the constant ductility spectra approximate those of the collapse capacity spectra as the ductility is larger, and, as the effective stiffness is larger, the ductilities for which this occurs are smaller, a consequence of the high variability of the displacement response with respect to Sa_e/Sa_y.

Therefore, for actual collapse design it would not be necessary to design for demands given by collapse spectra (in terms of yield strength and ultimate displacement) since the relative intensities related to collapse and to the attainment of lower ductility values are very close, thus, allowing the use of constant ductility spectra instead. For this reason, in this thesis the actual collapse design applications were carried out employing constant ductility spectra associated with a μ value for which the relative intensity at the period of the auxiliary SDOF system of the considered structure was less than 10% of the relative intensity associated with actual collapse.

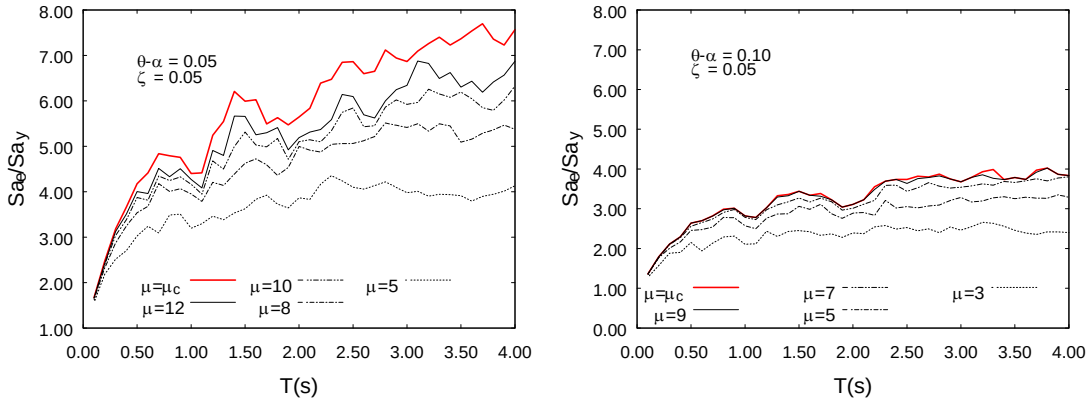

a) **b)**

Figure 3.9 Constant ductility and collapse capacity spectra in relative intensity format of the FEMA-P695 far field record set for several μ values: a) θ – α=0.05; b) θ – α=0.10

3.7.3 Design procedure

The application of the method proposed to design an instability prone frame due to P-Delta effects aimed to satisfy a two-limit state PO, considering actual collapse prevention or deformation control associated with a near collapse condition, can be summarized in the following steps.

1. Pre-dimensioning of the structural elements based on designer's experience or a rough force-based design. Consequently, an elastic model is built in a structural analysis program.
2. Modal analysis of the elastic model without considering P-Delta effects. From the first order elastic properties, the required SLS displacement, d_s, is calculated using Eq. 3.2
3. The required first order period T_s corresponding to d_s is obtained from the design displacement spectra associated with the SLS. Subsequently, the elastic model is modified so that its fundamental period matches T_s.
4. Gravity load and modal analyses of the elastic model considering P-Delta effects. From the results the stability coefficient, θ^E, is calculated with Eq. 3.19.
5. Definition of the design damage distribution corresponding to strong-column weak-beam behaviour with inelastic action in first storey column bases for the ULS and construction of the "damaged model" in accordance with section 3.2.
6. Modal analyses of the "damaged model" considering P-Delta effects. If a negative eigen-value is attained, modal analysis without P-Delta effects is carried out. Subsequently, the period of the auxiliary SDOF system associated with the required stiffness for the SLS, T_{AUXS}, and the corresponding stability coefficient, θ_{AUX}, are calculated via Eqs. 3.20 to 3.22.
7. For a deformation control-based design, the yield and ultimate displacements are calculated with Eqs. 3.5 to 3.7, hence, the design ductility μ_{DES} is defined. If the application is oriented towards sidesway collapse control, μ_{DES} may be taken as μ_{cst} or a smaller ductility value in accordance with section 4.2.
8. From the ULS design ultimate displacement spectrum corresponding to μ_{DES} and $\theta_{AUX} - \alpha$, the required auxiliary period for such limit state, T_{AUXU}, is obtained.
9. Definition of the final design auxiliary period, T_{DES}, as the smaller value of T_{AUXS} and T_{AUXU}. If the latter is the smallest value and is significantly different than T_{AUXS}, recalculate the effective negative post-yield stiffness, $\theta_{AUX} - \alpha$, using the first mode eigen-value calculated in step 5 and repeat steps 6 to 8 until a sufficient approximation of T_{DES} is attained.
10. Modal spectral analysis of the simplified models in accordance with section 3.6 and calculation of design forces of structural elements with Eq. 3.13. It is recommended that in this step the design displacement is calculated using Eqs. 3.14-3.18, since an estimate of higher mode demands is possible at this instance.
11. Design and detailing of structural elements with appropriate criteria regarding the behaviour of materials and structural types according to building codes or other accepted design provisions.

CHAPTER 4

VALIDATION OF THE METHOD PROPOSED

4.1 Overview of the case studies considered and validation approach

Foremost, in order to validate the design displacement based approach in which the method proposed is based, design applications of the method proposed aimed at theoretical P-Delta induced collapse were carried out for 8-,12- and 16 storey non-deteriorating generic frames, regular in elevation. Two sets of generic frames were employed in this investigation. The first set, whose results are also shown in López et al (2015), is comprised of "rigid" frames subjected to the FEMA-P695 (FEMA 2009) far field set of records. The second set corresponds to "flexible" frames subjected to the Valley of Mexico set of records, denoted as VM set, given by Miranda and Ruiz-Garcia (2002).

Each frame was designed for different magnitudes of axial load corresponding to $\theta_{AUX} - \alpha$ values equal to 0.025 to 0.10 in increments of 0.025. To allow flexibility in the validation of the applications of the method proposed for various levels of axial load and ductility values, strength and stiffness independency in structural components is considered in these case studies. Accordingly, the example frames possess a fixed fundamental period calculated with empirical expressions given by Chopra and Goel (2000) that provides mean period values from measurements of actual structures in function of their height and material.

The design was carried out assuming that such fundamental period is that required by the SLS and that the stiffness requirement of the structure is governed by such limit state in accordance with step 3 of section 3.7.3. Subsequently, the strength of structural components was provided according to the design targets of the ULS in conformance with section 3.7.2. To illustrate the application of the method proposed in these case studies, a detailed example of a 16 storey frame is shown in this chapter.

The validation of the design applications was carried out using IDA. For each record the individual intensities associated with collapse were obtained. Moreover, for the purpose of demonstrating that the displacement based approach provides a good approximation of structural response for various levels of ductility, the intensities associated with exceedance of an interstorey drift threshold associated with ductility values ranging from 3 to 8. Subsequently, for the purpose of providing a probabilistic characterization of the data obtained from IDA, the 16^{th}, 50^{th} and 84^{th} collapse intensities were calculated via counted statistics

and were compared with their respective spectral percentile intensities, *i.e.*, the product of the relative intensity attained from the corresponding spectra by the design yield strength of the auxiliary SDOF system as stated in section 3.7.2.

4.2 Characteristics of example frames

All case studies considered, 8-, 12- and 16- storey frames, share the following characteristics: first storey height of 5.00 m, and 3.50 m elsewhere; three spans of 10.00 m; uniform column to beam stiffness ratio of 1.5 at joints. The stiffness of beams and columns decreases 25% every four stories and the masses are distributed uniformly along the height of the frame. The fundamental periods of the set of rigid frames, whose stiffness is representative of reinforced concrete frames, was calculated with Eq. 4.1. On the other hand, the fundamental period considered for the flexible set of frames, representative of steel structures, was obtained from Eq.4.2.

$$T_1 = 0.0524H^{0.90} \tag{4.1}$$

$$T_1 = 0.0905H^{0.80} \tag{4.2}$$

The values of stiffness of structural components and mass of the system are such that the fundamental period (first order) of the frame is approximately the same as that given by the preceding equations. Gravity nodal loads are applied in leaning columns; they are uniformly distributed along the height of the structure and its magnitude is consistent with the considered predefined effective post-yield stiffness values, $\theta_{AUX} - \alpha$: 0.025, 0.05, 0.075 and 0.10; each frame is designed for these levels of axial load. Structural components exhibit bilinear non-deteriorating behaviour; the post-yield stiffness of all beams and columns is zero, *i.e.,* elasto-plastic behaviour, in the first set of frames, and 0.02 in the second set of frames. Furthermore, axial-flexure interaction in columns is neglected and interdependency between strength and stiffness is not considered, as mentioned in the beginning of this chapter.

4.3 Design demands and performance targets

The goal of the design applications is that the interstorey drift threshold in any floor is exceeded or dynamic instability occurs, as applicable, for 50% of the record set at the design target intensity since median yield pseudo-acceleration spectra and median ultimate-displacement spectra are employed to design these case studies. Accordingly, the same approach was used for the assessment of sidesway-collapse and near collapse for other percentile and ductility values.

The first set of frames was designed using the median spectra of the FEMA-P695 set of records; such spectra was scaled in each application in such a way that the design target intensity, in terms of the spectral pseudo-acceleration of the corresponding elastic system of period T_{AUX} (period of the auxiliary SDOF), is Sa_{tar} = 9.81 m/s^2. The second set of frames were designed with the demands attained from the Mexico Valley set of records. In these applications the median spectra was scaled so that the design target intensities of each frame matches the spectral pseudo-acceleration value at period T_{AUX} of the East-West component of the Michoacán Earthquake of 1985, recorded in the SCT station in Mexico City.

Hence, the scaling factors of the median spectra where defined from the median relative intensity, the median yield pseudo-acceleration spectra and the design target intensities considered by means of the following expression,

$$\varsigma = \frac{Sa_{tar}}{50\%Sa_e/Sa_y\,[T_{AUX},\xi,\mu_c,\theta-\alpha]\;50\%Sa_y[T_{AUX},\xi,\mu_c,\theta-\alpha]} \tag{4.3}$$

where $50\%Sa_e/Sa_y\,[T_{AUX},\xi,\mu_c,\theta_{AUX}\text{-}\alpha]$ and $50\%Sa_y[T_{AUX},\xi,\mu_c,\theta_{AUX}\text{-}\alpha]$ are the ordinates at period T_{AUX} of the corresponding median relative intensity spectra and median yield pseudo-acceleration spectra , respectively. The attainment of the relative intensity is depicted in Fig. 4.1. Moreover, assessment of the frame structures for other percentiles and near-collapse ductilities was carried out scaling the spectra using Eq. 4.3 also, but substituting the corresponding percentile and ductility.

For the collapse design applications, the ductilities considered for the definition of design demands were, 30, 12, 8, 7 for effective post-yield stiffness values of 0.025, 0.05, 0.075, 0.100, respectively, in accordance with section 3.7.2. Such ductility values correspond to 70, 75, 60 and 60 percent of the static collapse ductility (Eq. 3.23), respectively. Nonetheless, the attainment of numerical instability in the analyses of the designed frames is interpreted as dynamic instability, *i.e.,* flattening of the IDA curves and, thus, as sidesway collapse.

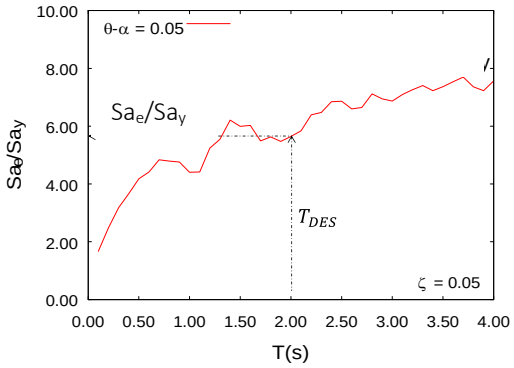

Figure 4.1 Attainment of relative intensity from the corresponding spectrum

The design damage states considered for all frames are consistent with the strong column-weak beam criterion. Since in the method proposed the design displacement shapes are a function of the design damage state, slightly different damage configurations were tested. The 8-storey frame is designed expecting that all beams yield barring those of the roof-level and the 12- and 16-storey frames are designed in such a way that only the beams of the last two floors remain elastic. Yielding at column bases is considered in the design damage states of all case studies.

4.4 Detailed description of design application of 16-storey frame

In this section the detailed design application of the 16-storey frame with $\theta_{AUX} - \alpha = 0.05$ of the first set is shown. As mentioned in the beginning of this chapter, the case studies considered are generic frames with a fixed fundamental period assuming that the stiffness of the frame is that required by the SLS. Hence, the procedure shall be described from step 3 onwards.

From step 3, the required serviceability period $T_s = 2.00$ s and the corresponding eigen-value λ^E are obtained. Subsequently, step 4 of the procedure, second order modal analysis of the modified structure is performed, from which the $\lambda^{E,}$ is attained, allowing the calculation of $\theta^E = 0.045$ with Eq. 3.19. In step 5, a damage distribution is defined: strong column-weak beam considering yielding in column bases and all beams

except those of the last two floors. Subsequently, a "damaged model" is built as described in section 3.2. In step 6 second order modal analysis is performed, thus, providing $\lambda^{D'} = -0.404$. Since the eigen-value is negative, first order modal analysis is carried out, from which λ^{D} is obtained and the first order post-yield stiffness ratio, $\alpha = 0.007$, is calculated with Eq. 3.1. The inelastic stability coefficient is then calculated with Eq. 3.20, $\theta^{I} = 0.054$, hence, allowing the calculation of the auxiliary SDOF system's properties, T_{AUXS}=1.98 s and $\theta_{AUX} = 0.054$, via Eqs. 3.21 and 3.22 and the design shape with Eq. 3.6. Up to this point, the required elastic properties of the frame to satisfy the SLS and, thus, an auxiliary SDOF system corresponding to such properties and the design damage state, have been defined.

In step 7, the yield displacement, Sd_y, and target ultimate displacement, Sd_u, of the auxiliary SDOF system are obtained from Eqs. 3.3 and 3.7, respectively, for the deformation control based design considering IDRy = 0.012 and IDRu = 0.060. These are the resulting interstorey drifts corresponding to the predetermined value of μ=5.00 employed in this example application. In step 8, the required period for the ULS, T_{AUXU}, is attained from the corresponding design spectrum. For the deformation control based design application, such period is obtained from the constant ductility spectrum (in terms of displacement) associated with μ = 5 and $\theta - \alpha = 0.05$ since $\theta_{AUX} - \alpha = 0.047$. In accordance with section 3.7.2, the actual collapse design application may be carried out using a constant ductility spectrum associated with a lower ductility value than μ_{cst}. Accordingly, from visual inspection of the set of spectra shown in Fig. 3.9.a, the ultimate displacement spectra associated with $\mu = 12$ and $\theta - \alpha = 0.05$ is chosen from which the corresponding T_{AUXU} is attained. The ductility value considered is 0.60 of $\mu_{cst} = 20$, hence the global post-yield demand associated with such ductility is 40% smaller than that associated with μ_{cst}.

In step 9, the final design period, T_{DES}, is defined as the smaller value of T_{AUXS} and T_{AUXU}, however, as mentioned before, the correlation between yield and stiffness is not taken into account in this example case and T_{AUXS} is equal to T_{DES} in this example application. Accordingly, the yield and target displacements of the final design auxiliary SDOF system are those previously obtained. From such yield displacement and the design period, the design yield pseudo-acceleration, Sa_{yAUX} is defined (see Fig. 3.5). Furthermore, the design post-yield pseudo-acceleration of the auxiliary SDOF system, Sa_{pyAUX}, is estimated via Eq. 3.12. Hence, the design auxiliary SDOF system has been defined in this step; its design properties are given in Table 1.

Table 1. Properties of the design auxiliary SDOF systems of the 16-storey frame for actual collapse and near collapse design applications

T_{DES} [s]	$\theta_{AUX} - \alpha$	μ_{DES}	Sa_{yAUX} [m/s^2]	Sa_{pyAUX} [m/s^2]	Sd_{uAUX} [m]
1.98	0.047	12.00	1.91	0.028	2.27
		5.00	2.57	0.077	1.27

In step 10, modal spectral analyses of both simplified models are carried out to obtain the design forces of structural components. For the elastic model such analysis is straightforward; the force demands of each mode are obtained directly from the design yield pseudo-acceleration spectrum for the first order periods. However, an artifice is used to obtain post-yield demands from modal analysis of the damaged model, since

the abscissas of the design spectra correspond to the first order initial period and, moreover, a negative eigen-value is attained. This artifice consists on performing modal spectral analysis employing the geometric stiffness matrix formulation where the demands are given by a "post-yield strength spectrum", a plot of second order lengthened periods $T^D{}_j$', *vs.* the corresponding value of modal post-yield demand, $Sa_{py}'_j$, which is built with the modes considered whose eigen-value is positive. $Sa_{py}'_j$ is estimated with Eq. 3.12 using second order post-yield stiffness ratios, α_j', calculated with the second order eigen-values of the higher modes, i.e., $\alpha_j' = \Gamma^{D'}\lambda^{D'}/\Gamma^{E'}\lambda^{E'}$.

Furthermore, to estimate the post-yield force demand associated with the fundamental mode with negative eigen-value, the damaged model is analyzed for a static load pattern consistent with such mode, whose magnitude is defined by the factor $(1-\theta_{AUX})*Sa_{pyAUX}$. Three modes are sufficient to design satisfactorily the structures. Table 2 provides the information necessary to perform modal spectral analysis of the damaged model. Subsequently, the design forces are calculated via SRSS (Eq. 3.13), allowing the design of structural elements (step 11). The design forces of columns are checked to comply with a strong column-weak beam over-strength ratio $F_{SCWB} = 1.50$; the strength of columns is modified accordingly at joints were such ratio is smaller. The F_{SCWB} value considered is larger than the values stipulated in several design codes for the design of ductile structures to increase the possibility that the damage state developed by the structure is consistent with the design damage state considered, in accordance with the recommendations given by Haselton *et al.* (2011).

Table 2. Post-yield spectral design demands of higher modes of 16-storey frame for actual collapse and near collapse design applications

$T^{D'}{}_2$ [s]	$T^{D'}{}_3$ [s]	α_2'	α_3'	μ_{DES}	$Sa_{y\,2}$ [m/s^2]	$Sa_{py}'_2$ [m/s^2]	$Sa_{y\,2}$ [m/s^2]	$Sa_{py}'_3$ [m/s^2]
4.89	1.19	0.004	0.074	12.00	7.09	0.300	12.87	10.47
				5.00	10.29	0.165	18.43	5.45

4.5 Incremental dynamic analysis of designed frames

IDAs of all designed frames were performed with the OpenSees computer program (McKenna *et al.* 2004). Plastic hinges were modelled as zero length rotational spring elements with bilinear behaviour without considering stiffness deterioration. Second order analyses were performed via the geometric matrix formulation. The non-linear step-by-step dynamic analyses of the designed structure were carried out using the Rayleigh damping approximation with damping ratios ζ=0.05, for the first and third modes. The integration of the non-linear equations of motion was carried out using Newmark's Beta method with parameters $\gamma = 0.5$ and $\beta = 0.25$ together with the Newton-Raphson method. IDA was performed using an initial intensity, Sa_e, of 0.20 m/s^2 with increments of 0.20 m/s^2 up to either collapse or exceedance of 1.5 times the design interstorey drift, for the frames designed for actual collapse and deformation control, respectively.

4.6 Evaluation of results

From the IDA of the designed frames the last intensity step of non-exceedance of drift in any floor or non-collapse, in accordance with the definition of collapse considered in their design, was identified for each record, from which the 16th, 50th and 84th intensities, Sa_{eANA}, was calculated via counted statistics. In order to quantify the uncertainty (aleatory) of such parameter, confidence intervals associated with a 0.05 significance level were estimated via the bootstrap technique (DiCiccio and Efron 1996), generating 3000 bootstrap samples. For this number of samples, stability in the values of the confidence limits was attained in all of the case studies.

The results obtained from the analyses of the case studies for ductility valued of 3,4,5 and collapse are depicted graphically in the figures shown in the end of this chapter. Figs. 4.2 to 4.73 illustrate the comparison of the set subjected to the VM set of records and Figs. 4.74 to 4.151 show the results of the set subjected to the FEMA-P695 set of records. From left to right, the first subplot of such figures shows the actual (red) and target (blue) percentile intensities with its corresponding confidence intervals along with the IDA curves. As can be observed in such figures a good approximation was attained. The relative error of the median design intensity was in the range of $\pm$20% and the average relative error among all cases was 9%. Moreover, in most of the cases the target media intensity was localized within confidence intervals associated with a 0.05 significance level. The relative error of 16% and 84% intensities was in the range of $\pm$30% and the average was 15% and, although not as good as that of the median intensities it can be considered sufficient.

The best approximations were obtained from the case studies subjected to the VM set of records. It is the author's belief that this is a consequence of the inherent errors of using a simplified criterion to consider higher mode contributions. The case studies subjected to the VM set are located in the short period region and hence higher mode demands are considerable smaller with respect to those of the fundamental mode. On the other hand, the frames subjected to the FEMA-P695 set are located in a region where spectral demands of the second and third mode are considerably higher than those of the fundamental mode. This feature may lead to think that the total force demand could be almost fully dominated by the higher modes, however, as the higher mode participation factors are small, the contributions of fundamental and higher modes to base shear are balanced.

Furthermore, since the method proposed relies on a displacement based approach, a comparison of the design displacement and interstorey drift profiles obtained with Eqs 3.14 and 3.18, with respect to the percentile profiles corresponding to the last non-exceedance intensity step from IDA, was carried out. The profiles corresponding to actual collapse design applications were defined considering $\mu_{DES} = \mu_{cst}$. Figs. 152-163 show the comparison of 50% profiles of the frames subjected to the VM set of records and Figs.164-175 those corresponding to the FEMA-P695 set. In general, the shape of the design displacement profiles match the shape of the median displacement profiles obtained from the analyses. For the purpose of measuring the correspondence between target and actual profiles of IDR, NDR and SVR, the modal assurance criterion (MAC) was employed, given in Equation 4.4 where VEC denotes the response vector (IDR, NDR or SVR), subindexes *dem* and *tar* distinguish the demand and target, respectively.

$$MAC = \frac{(\{VEC_{dem}\} \cdot \{VEC_{tar}\})^2}{(\{VEC_{dem}\} \cdot \{V_{ECdem}\})(\{VEC_{tar}\} \cdot \{VEC_{tar}\})} \tag{4.4}$$

According to this criterion, MAC values larger or equal than 0.90 indicate a good correspondence between shapes. The average MAC value from all cases was 0.95, hence, the correspondence between actual and displacement shapes is good. The difference in magnitudes of the displacements is a consequence of the intensity step used in the IDAs, as the displacement response of structures with negative stiffness is particularly sensible to the demand intensity. Consequently, such differences were larger in the frames subjected to larger levels of axial load, i.e., in the cases where the effective post-yield stiffness was larger, and/or larger ductilities.

Nonetheless, the difference between magnitudes is of secondary importance as the performance of the structures is measured by the approximation of the design target intensity. In fact, the good correspondence between the actual and target intensities is a consequence of the good correspondence of the design displacement profiles attained from the method proposed. Evidently, being this a simplified method, there were individual cases were shape correspondence was not attained, especially in the case studies subjected to the FEMA-P695 set for which higher mode demand is significant. For instance, in the assessment of the 12- and 16-storey frames with low stability coefficient, *i.e.,* 0.025 for a near-collapse ductility of 4, the maximum interstorey drift occurred in the 3rd floor. It appears that in such case the influence of higher modes was underestimated. Nonetheless, the maximum interstorey drift was consistent with the interstorey drift limit estimated by the method proposed, even though it was expected to occur in the first floor.

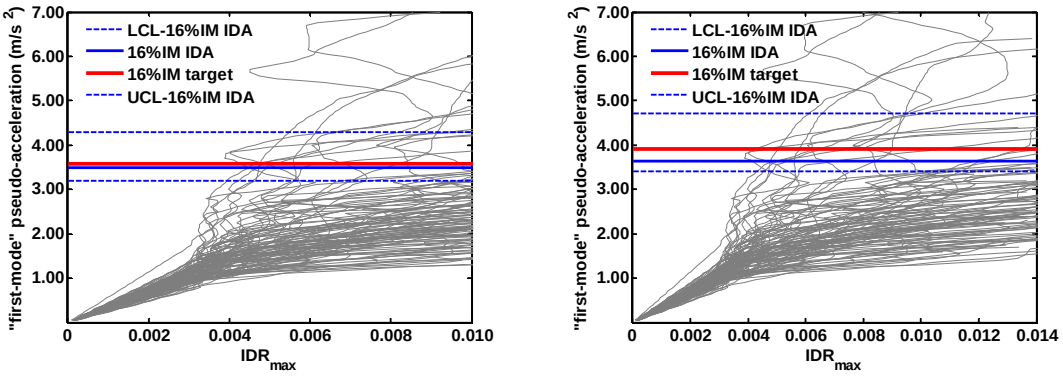

Figure 4.2 IDA curves and 16% collapse intensities of 8-storey frame with T_1=1.40 s and θ_{AUX}-α=0.025 subjected to the VM set of records: a) near collapse μ=4; b) near collapse μ=5

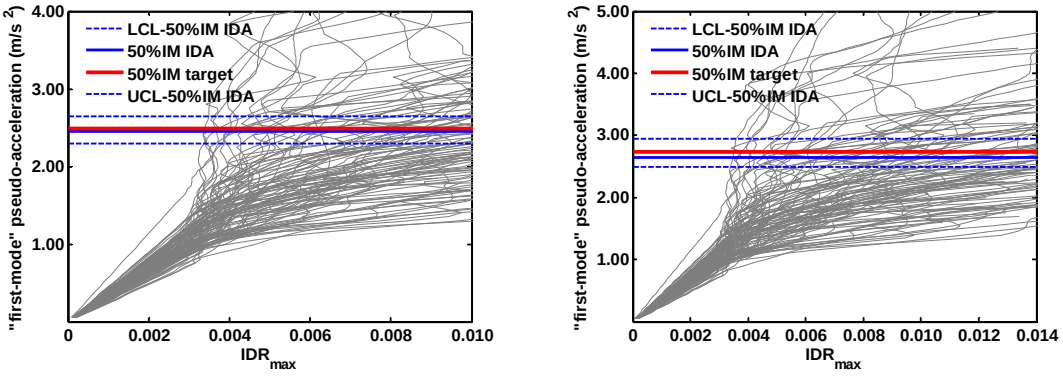

Figure 4.3 IDA curves and 50% collapse intensities of 8-storey frame with T_1=1.40 s and θ_{AUX}-α=0.025 subjected to the VM set of records: a) near collapse μ=4; b) near collapse μ=5

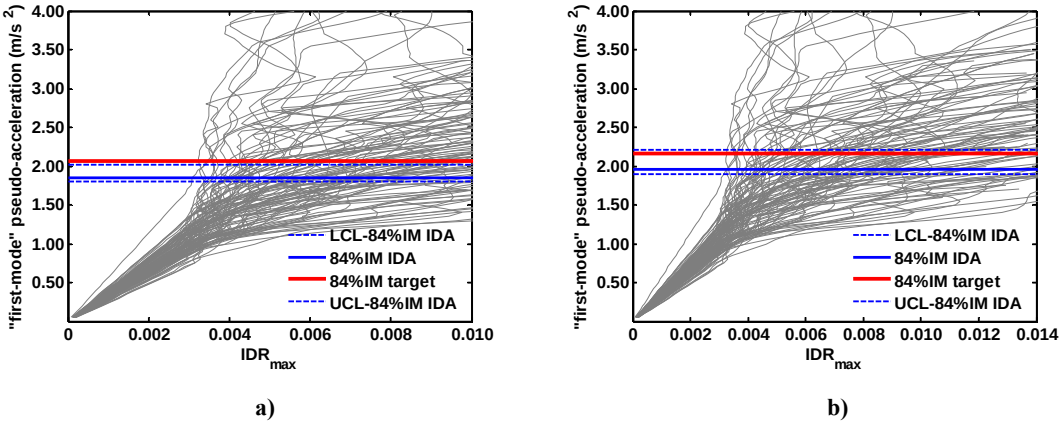

Figure 4.4 IDA curves and 84% collapse intensities of 8-storey frame with T_1=1.40 s and θ_{AUX}-α=0.025 subjected to the VM set of records: a) near collapse μ=4; b) near collapse μ=5

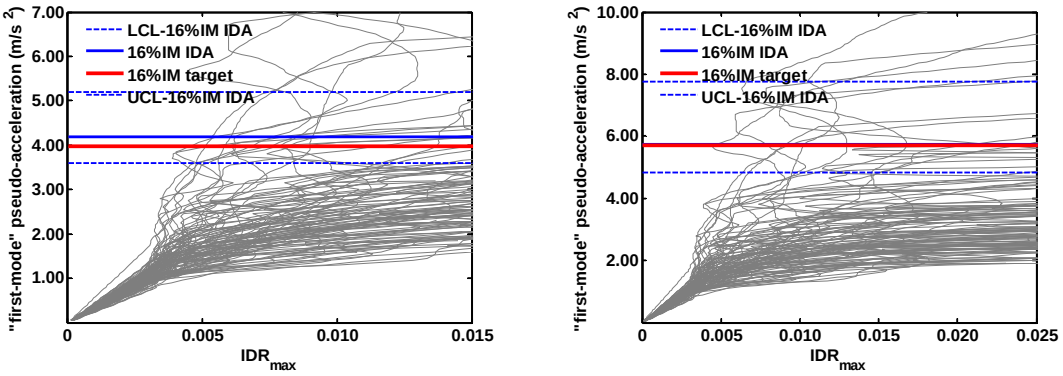

Figure 4.5 IDA curves and 16% collapse intensities of 8-storey frame with T_1=1.40 s and θ_{AUX}-α=0.025 subjected to the VM set of records: a) near collapse μ=6; b) sidesway collapse $\mu=\mu_c$

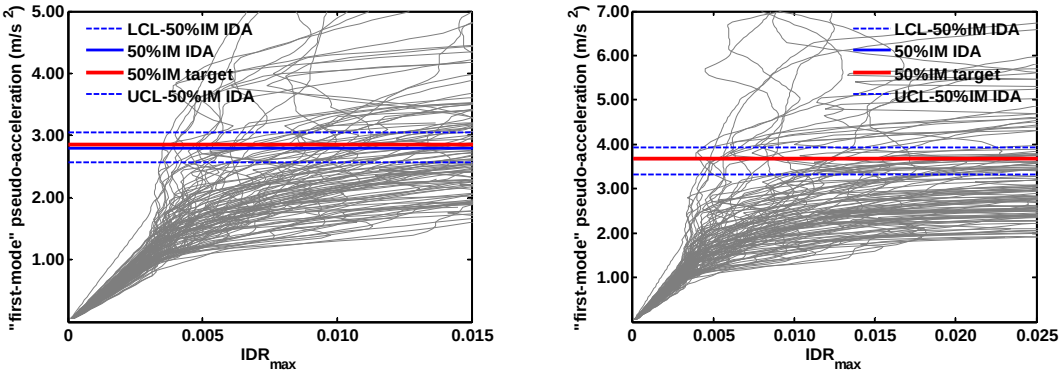

Figure 4.6 IDA curves and 50% collapse intensities of 8-storey frame with T_1=1.40 s and θ_{AUX}-α=0.025 subjected to the VM set of records: a) near collapse μ=6; b) sidesway collapse $\mu=\mu_c$

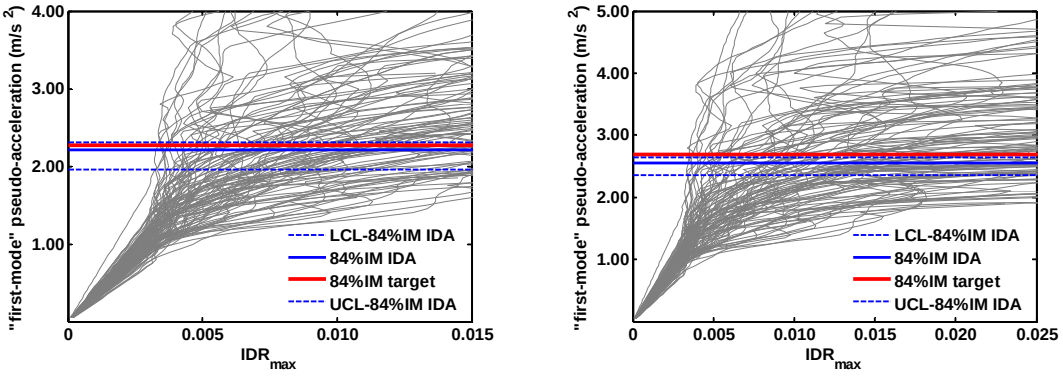

Figure 4.7 IDA curves and 84% collapse intensities of 8-storey frame with T_1=1.40 s and θ_{AUX}-α=0.025 subjected to the VM set of records: a) near collapse μ=6; b) sidesway collapse $\mu=\mu_c$

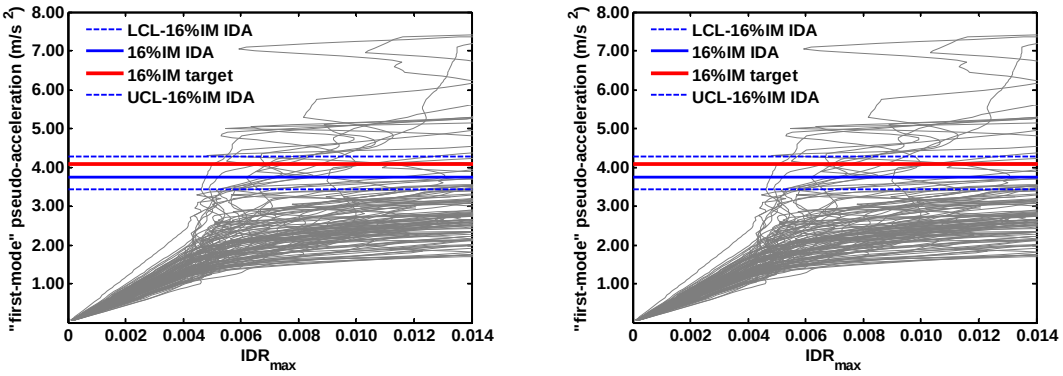

a) b)

Figure 4.8 IDA curves and 16% collapse intensities of 8-storey frame with T_1=1.40 s and θ_{AUX}-α=0.05 subjected to the VM set of records: a) near collapse μ=4; b) near collapse μ=5

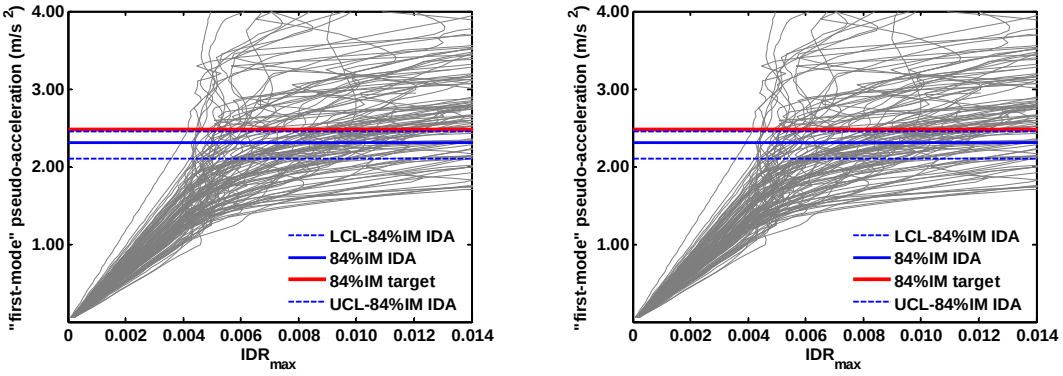

a) b)

Figure 4.9 IDA curves and 50% collapse intensities of 8-storey frame with T_1=1.40 s and θ_{AUX}-α=0.05 subjected to the VM set of records: a) near collapse μ=4; b) near collapse μ=5

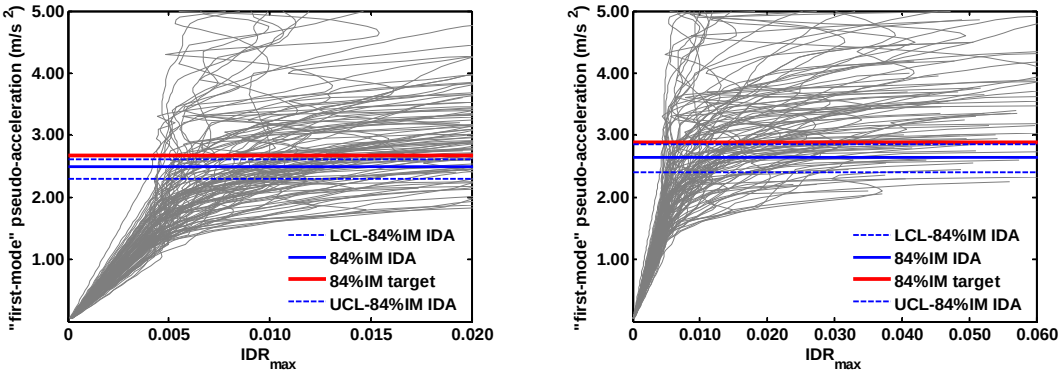

a) b)

Figure 4.10 IDA curves and 84% collapse intensities of 8-storey frame with T_1=1.40 s and θ_{AUX}-α=0.05 subjected to the VM set of records: a) near collapse μ=4; b) near collapse μ=5

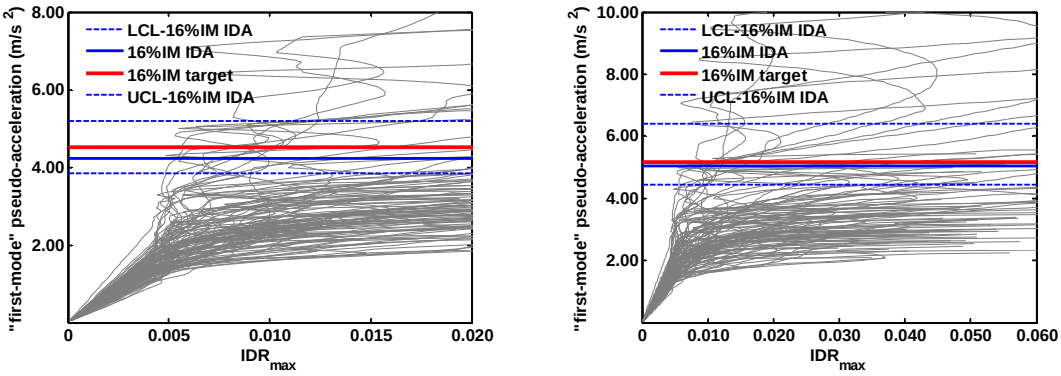

a) b)

Figure 4.11 IDA curves and 16% collapse intensities of 8-storey frame with T_1=1.40 s and θ_{AUX}-α=0.05 subjected to the VM set of records: a) near collapse μ=6; b) sidesway collapse $\mu=\mu_c$

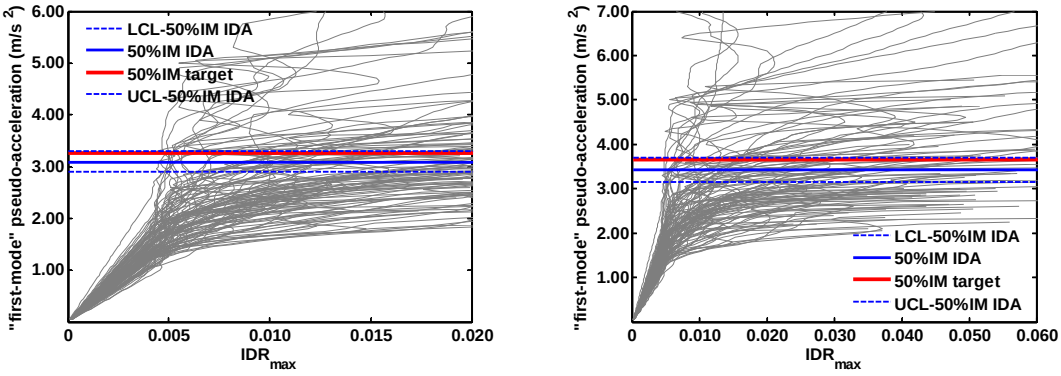

a) b)

Figure 4.12 IDA curves and 50% collapse intensities of 8-storey frame with T_1=1.40 s and θ_{AUX}-α=0.05 subjected to the VM set of records: a) near collapse μ=6; b) sidesway collapse $\mu=\mu_c$

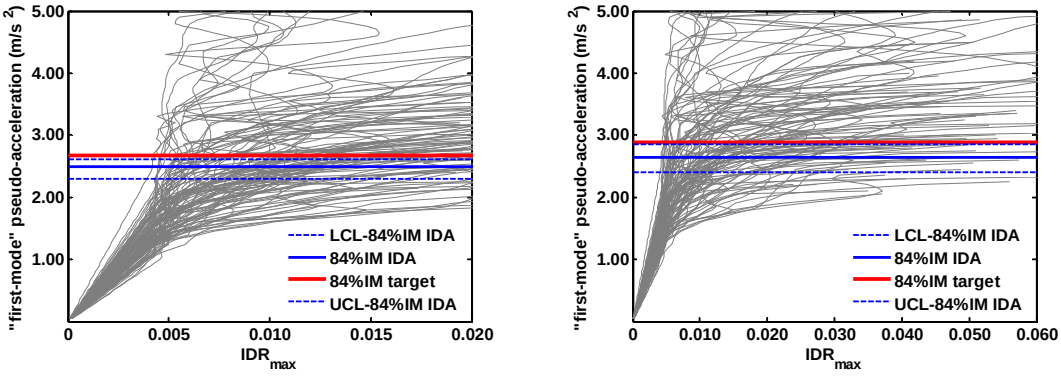

a) b)

Figure 4.13 IDA curves and 84% collapse intensities of 8-storey frame with T_1=1.40 s and θ_{AUX}-α=0.05 subjected to the VM set of records: a) near collapse μ=6; b) sidesway collapse $\mu=\mu_c$

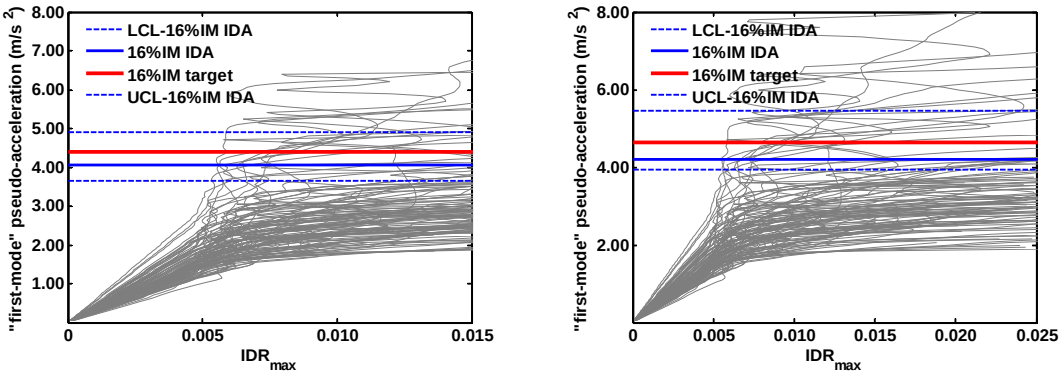

Figure 4.14 IDA curves and 16% collapse intensities of 8-storey frame with T_1=1.40 s and θ_{AUX}-α=0.075 subjected to the VM set of records: a) near collapse μ=4; b) near collapse μ=5

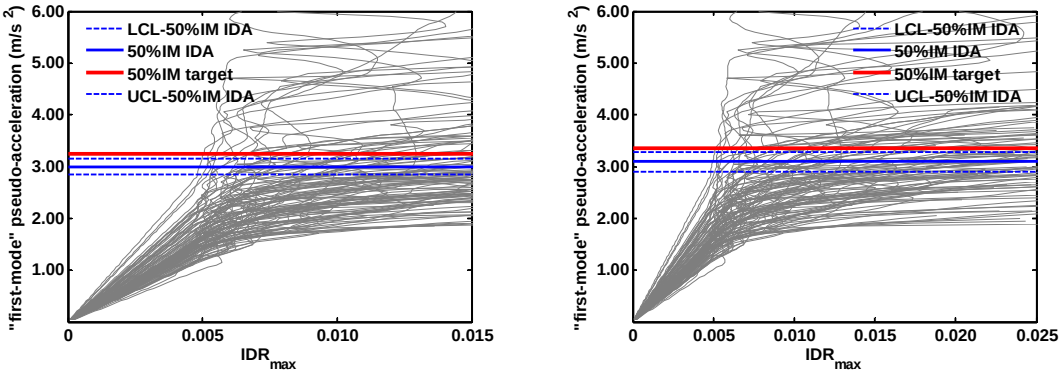

Figure 4.15 IDA curves and 50% collapse intensities of 8-storey frame with T_1=1.40 s and θ_{AUX}-α=0.075 subjected to the VM set of records: a) near collapse μ=4; b) near collapse μ=5

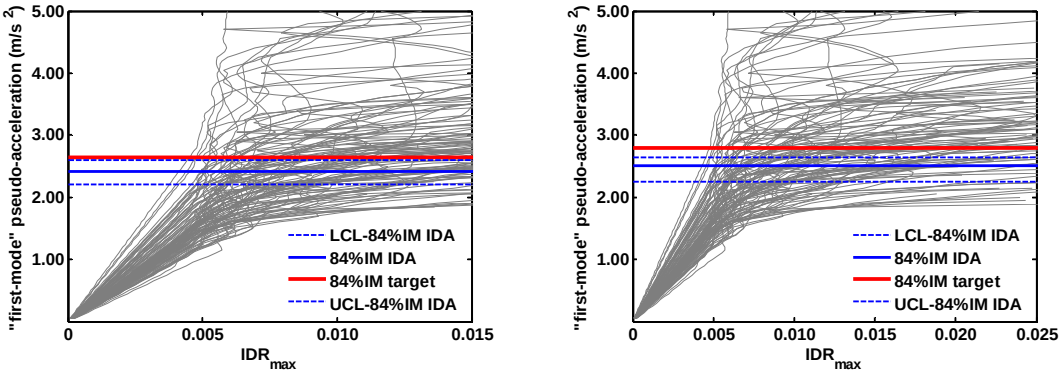

Figure 4.16 IDA curves and 84% collapse intensities of 8-storey frame with T_1=1.40 s and θ_{AUX}-α=0.075 subjected to the VM set of records: a) near collapse μ=4; b) near collapse μ=5

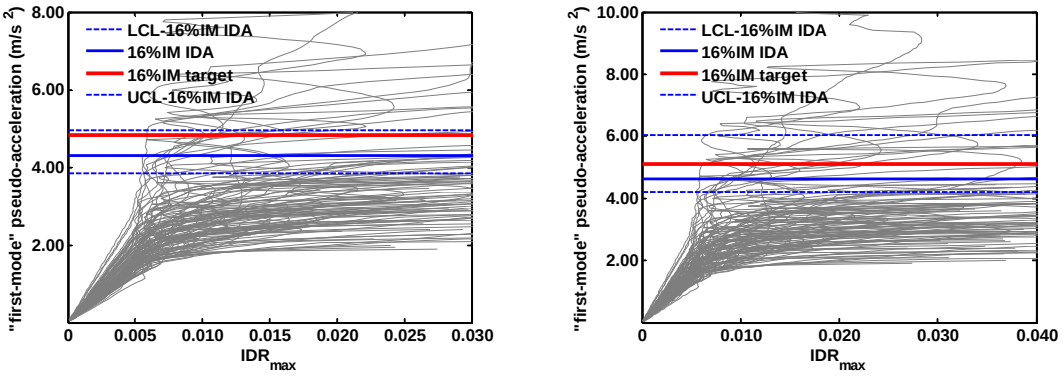

a) b)

Figure 4.17 IDA curves and 16% collapse intensities of 8-storey frame with T_1=1.40 s and θ_{AUX}-α=0.075 subjected to the VM set of records: a) near collapse μ=6; b) sidesway collapse $\mu=\mu_c$

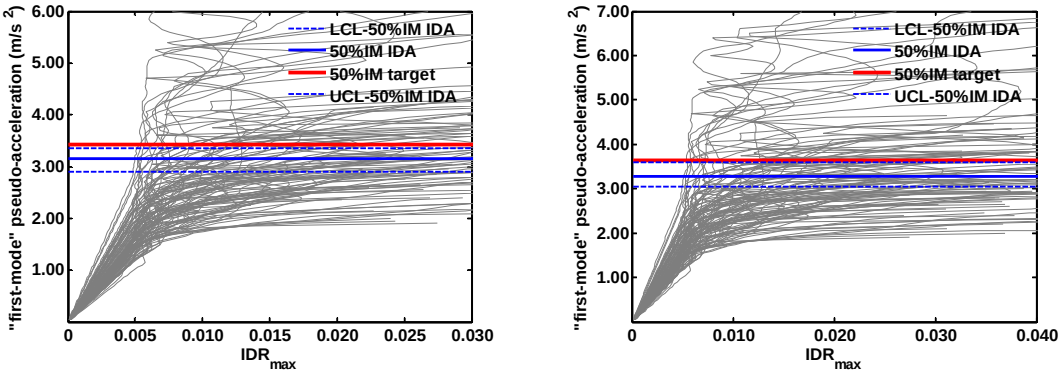

a) b)

Figure 4.18 IDA curves and 50% collapse intensities of 8-storey frame with T_1=1.40 s and θ_{AUX}-α=0.075 subjected to the VM set of records: a) near collapse μ=6; b) sidesway collapse $\mu=\mu_c$

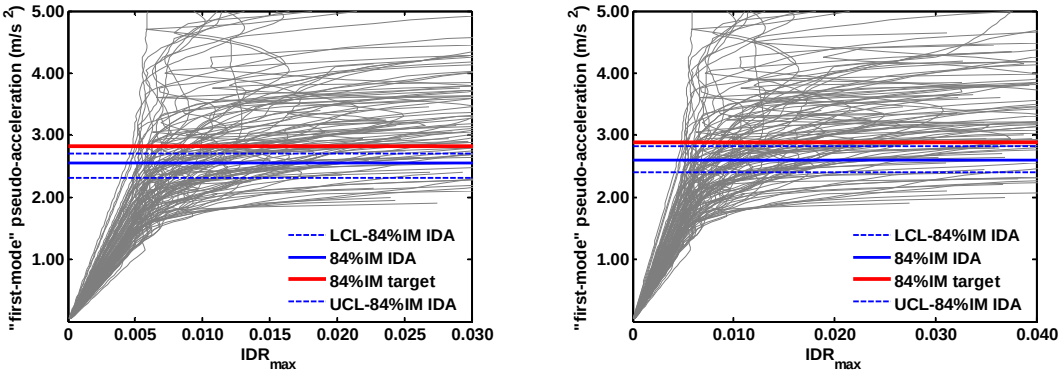

a) b)

Figure 4.19 IDA curves and 84% collapse intensities of 8-storey frame with T_1=1.40 s and θ_{AUX}-α=0.075 subjected to the VM set of records: a) near collapse μ=6; b) sidesway collapse $\mu=\mu_c$

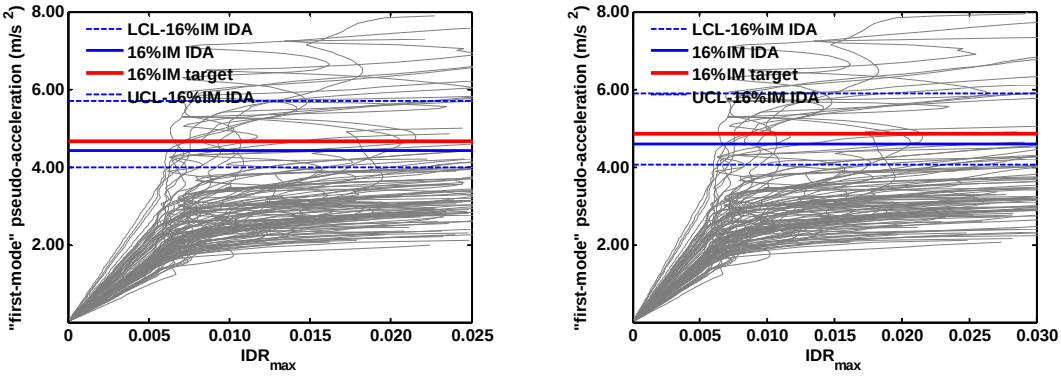

a) b)

Figure 4.20 IDA curves and 16% collapse intensities of 8-storey frame with T_1=1.40 s and θ_{AUX}-α=0.10 subjected to the VM set of records: a) near collapse μ=4; b) near collapse μ=5

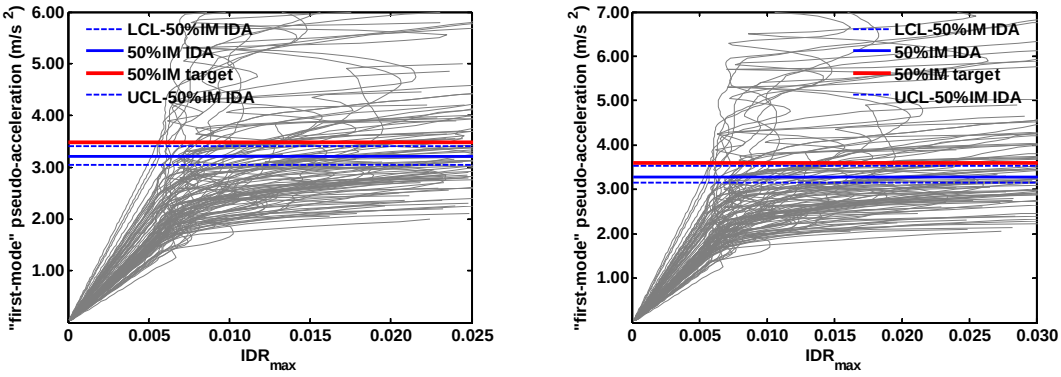

a) b)

Figure 4.21 IDA curves and 50% collapse intensities of 8-storey frame with T_1=1.40 s and θ_{AUX}-α=0.10 subjected to the VM set of records: a) near collapse μ=4; b) near collapse μ=5

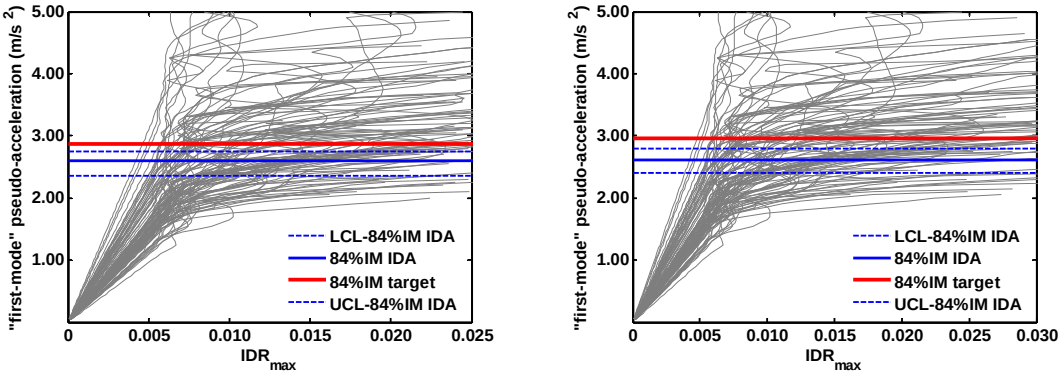

a) b)

Figure 4.22 IDA curves and 84% collapse intensities of 8-storey frame with T_1=1.40 s and θ_{AUX}-α=0.10 subjected to the VM set of records: a) near collapse μ=4; b) near collapse μ=5

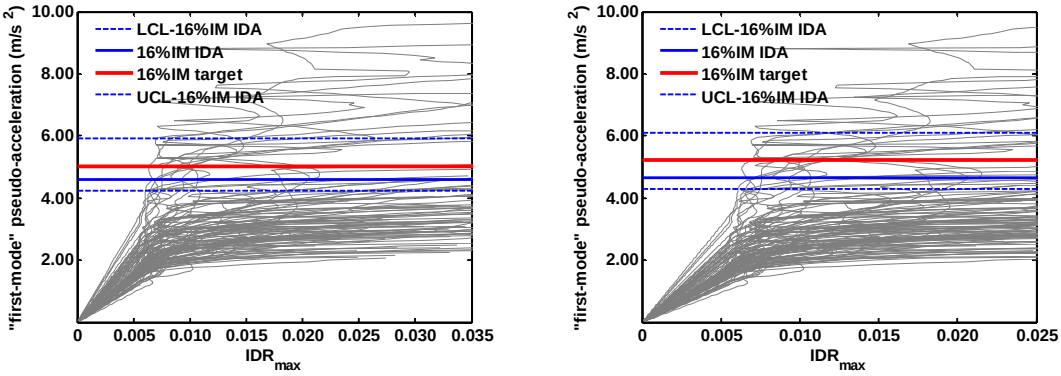

a) b)

Figure 4.23 IDA curves and 16% collapse intensities of 8-storey frame with T_1=1.40 s and θ_{AUX}-α=0.10 subjected to the VM set of records: a) near collapse μ=6; b) sidesway collapse $\mu=\mu_c$

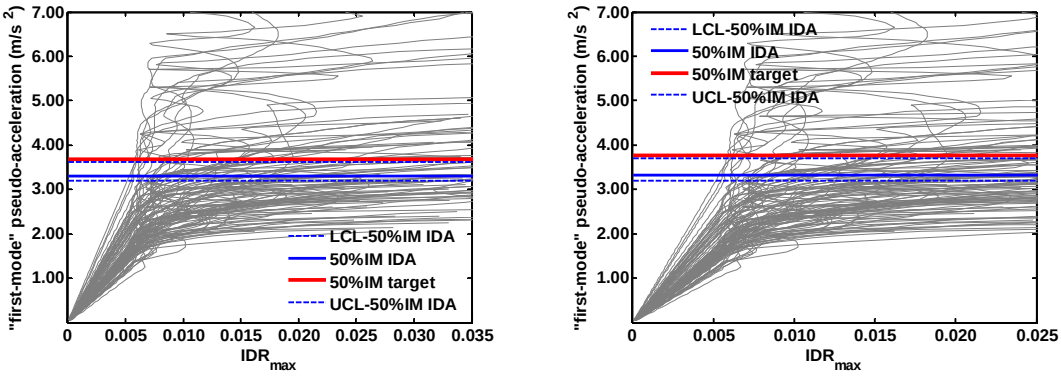

a) b)

Figure 4.24 IDA curves and 50% collapse intensities of 8-storey frame with T_1=1.40 s and θ_{AUX}-α=0.10 subjected to the VM set of records: a) near collapse μ=6; b) sidesway collapse $\mu=\mu_c$

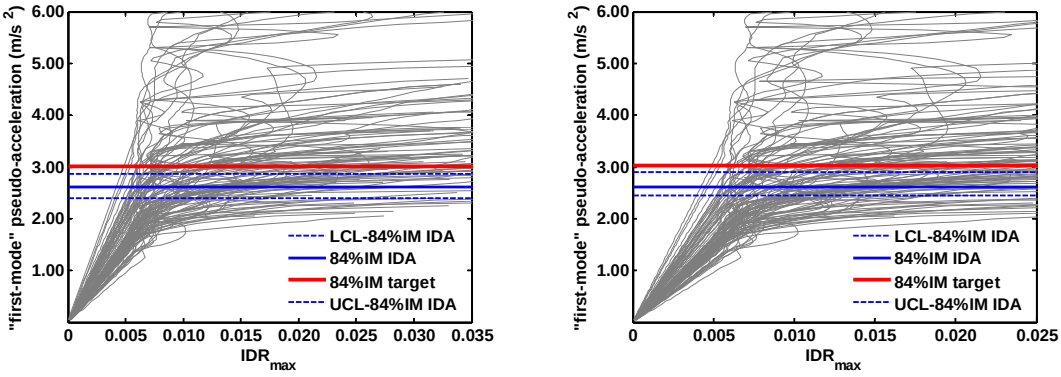

a) b)

Figure 4.25 IDA curves and 84% collapse intensities of 8-storey frame with T_1=1.40 s and θ_{AUX}-α=0.10 subjected to the VM set of records: a) near collapse μ=6; b) sidesway collapse $\mu=\mu_c$

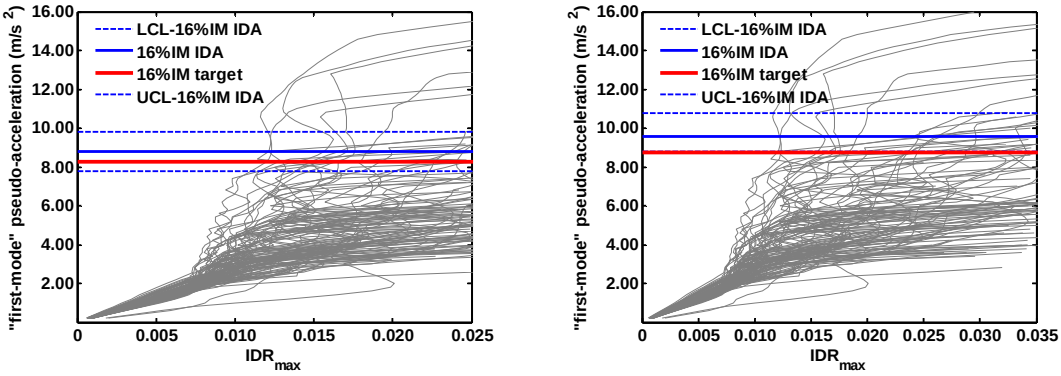

Figure 4.26 IDA curves and 16% collapse intensities of 12-storey frame with T_1=1.90 s and θ_{AUX}-α=0.025 subjected to the VM set of records: a) near collapse μ=4; b) near collapse μ=5

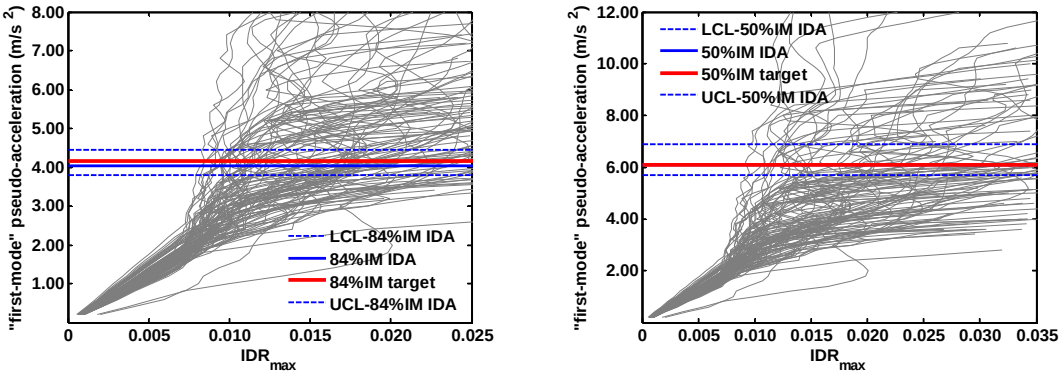

Figure 4.27 IDA curves and 50% collapse intensities of 12-storey frame with T_1=1.90 s and θ_{AUX}-α=0.025 subjected to the VM set of records: a) near collapse μ=4; b) near collapse μ=5

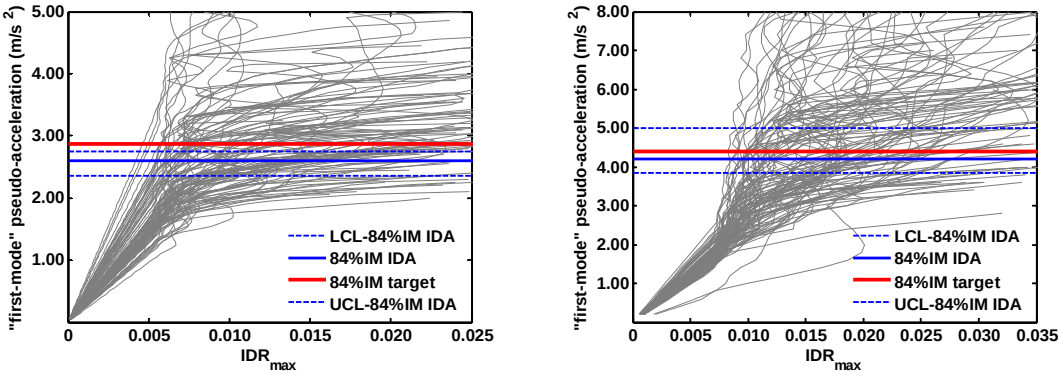

Figure 4.28 IDA curves and 84% collapse intensities of 12-storey frame with T_1=1.90 s and θ_{AUX}-α=0.025 subjected to the VM set of records: a) near collapse μ=4; b) near collapse μ=5

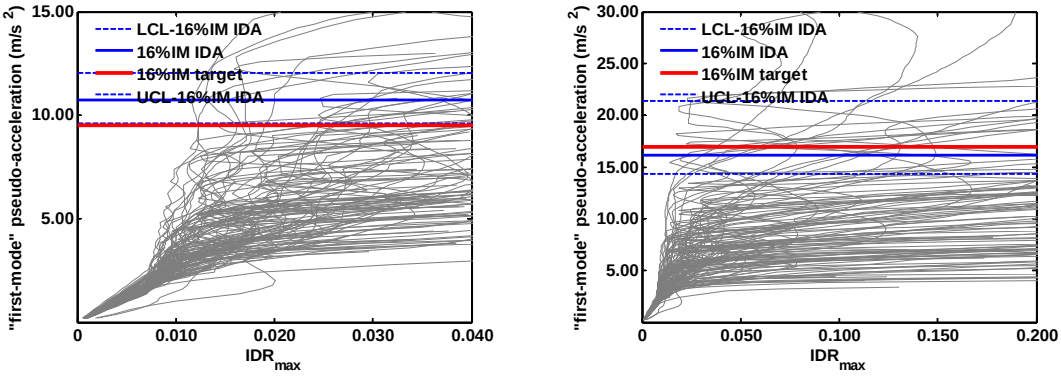

a) b)

Figure 4.29 IDA curves and 16% collapse intensities of 12-storey frame with T_1=1.90 s and θ_{AUX}-α=0.025 subjected to the VM set of records: a) near collapse μ=6; b) sidesway collapse $\mu=\mu_c$

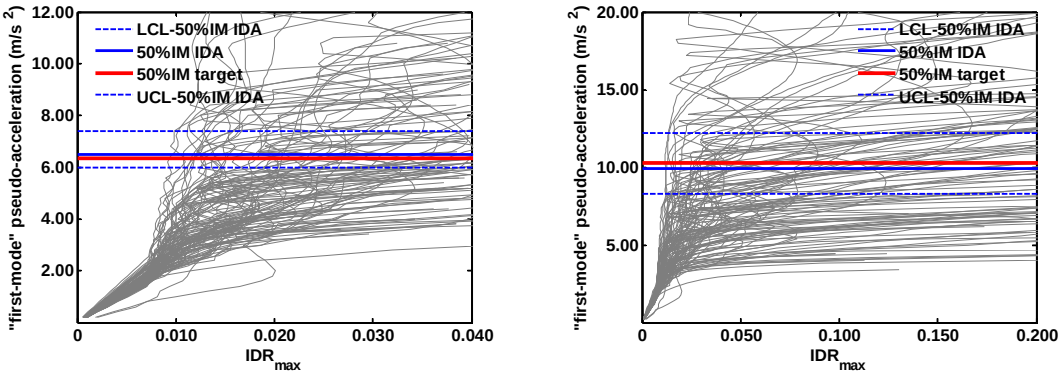

a) b)

Figure 4.30 IDA curves and 50% collapse intensities of 12-storey frame with T_1=1.90 s and θ_{AUX}-α=0.025 subjected to the VM set of records: a) near collapse μ=6; b) sidesway collapse $\mu=\mu_c$

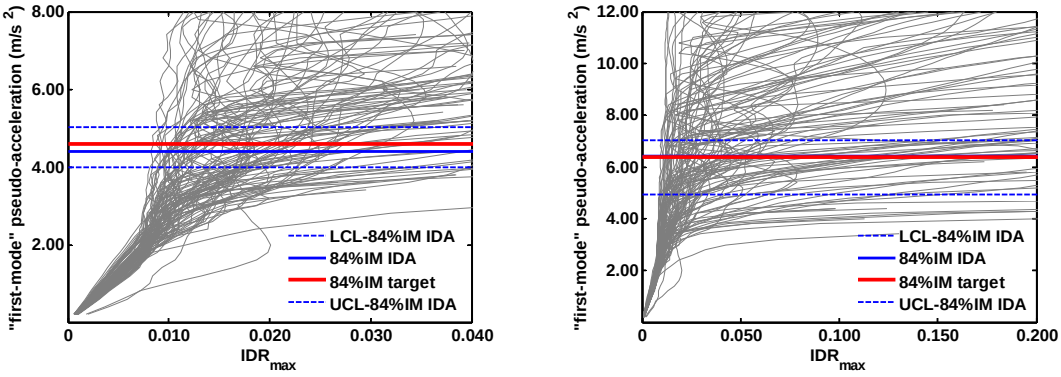

a) b)

Figure 4.31 IDA curves and 84% collapse intensities of 12-storey frame with T_1=1.90 s and θ_{AUX}-α=0.025 subjected to the VM set of records: a) near collapse μ=6; b) sidesway collapse $\mu=\mu_c$

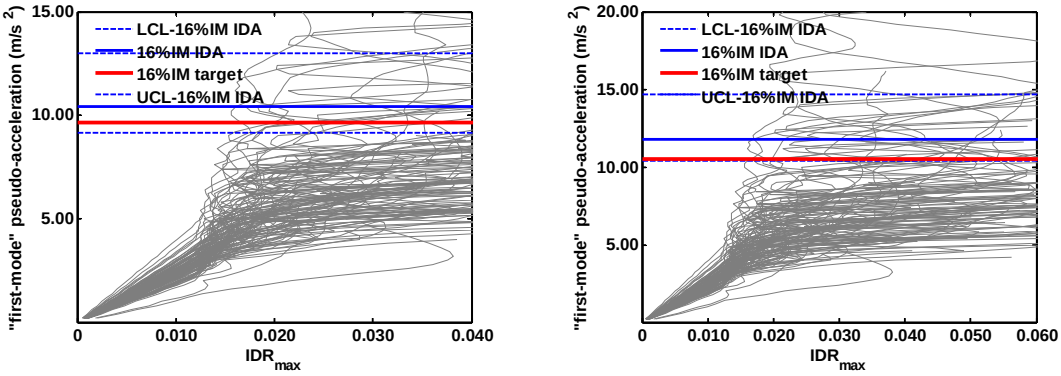

a) b)

Figure 4.32 IDA curves and 16% collapse intensities of 12-storey frame with T_1=1.90 s and θ_{AUX}-α=0.05 subjected to the VM set of records: a) near collapse μ=4; b) near collapse μ=5

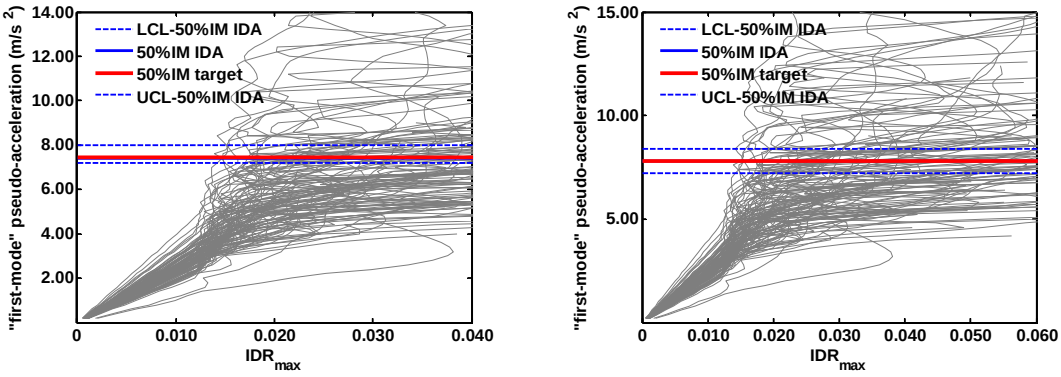

a) b)

Figure 4.33 IDA curves and 50% collapse intensities of 12-storey frame with T_1=1.90 s and θ_{AUX}-α=0.05 subjected to the VM set of records: a) near collapse μ=4; b) near collapse μ=5

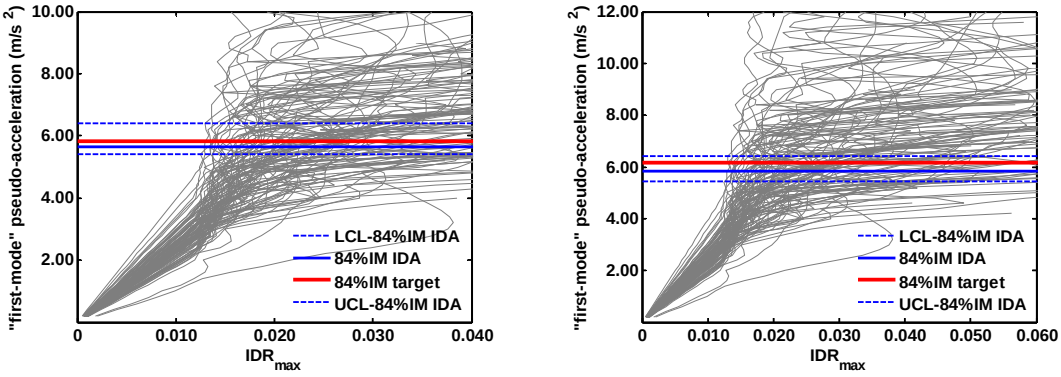

a) b)

Figure 4.34 IDA curves and 84% collapse intensities of 12-storey frame with T_1=1.90 s and θ_{AUX}-α=0.05 subjected to the VM set of records: a) near collapse μ=4; b) near collapse μ=5

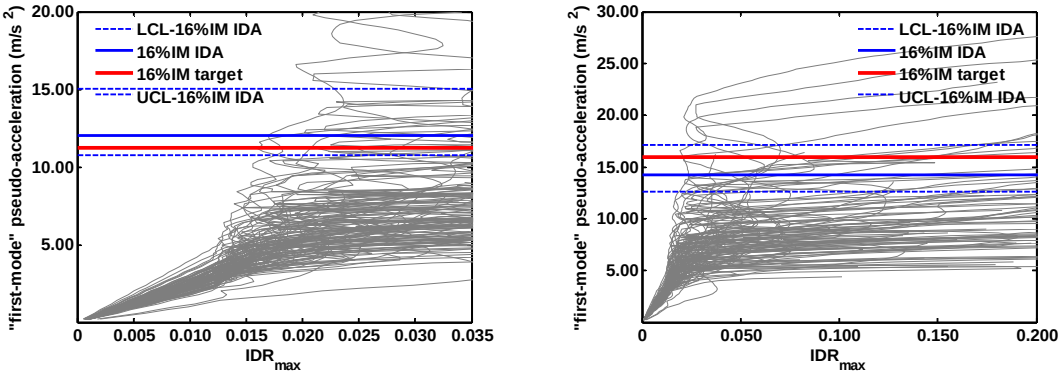

Figure 4.35 IDA curves and 16% collapse intensities of 12-storey frame with T_1=1.90 s and θ_{AUX}-α=0.05 subjected to the VM set of records: a) near collapse μ=6; b) sidesway collapse $\mu=\mu_c$

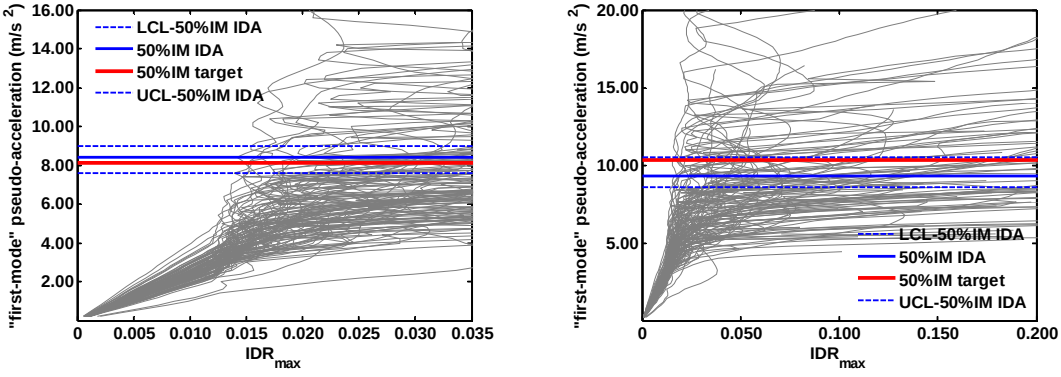

Figure 4.36 IDA curves and 50% collapse intensities of 12-storey frame with T_1=1.90 s and θ_{AUX}-α=0.05 subjected to the VM set of records: a) near collapse μ=6; b) sidesway collapse $\mu=\mu_c$

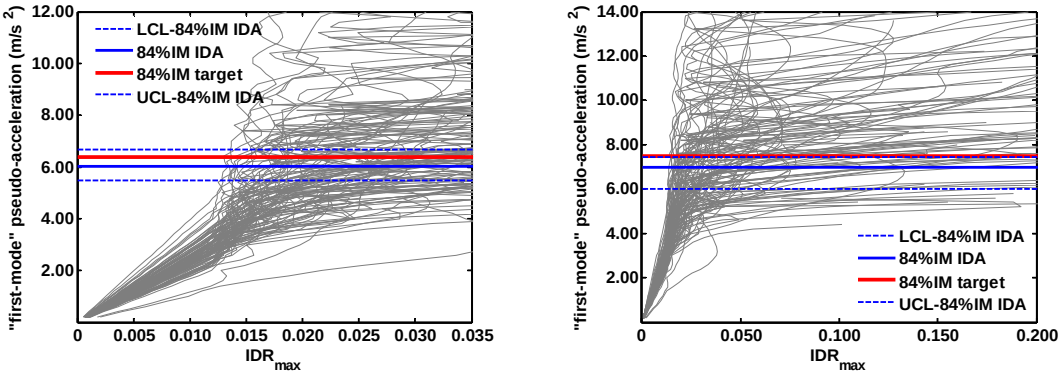

Figure 4.37 IDA curves and 84% collapse intensities of 12-storey frame with T_1=1.90 s and θ_{AUX}-α=0.05 subjected to the VM set of records: a) near collapse μ=6; b) sidesway collapse $\mu=\mu_c$

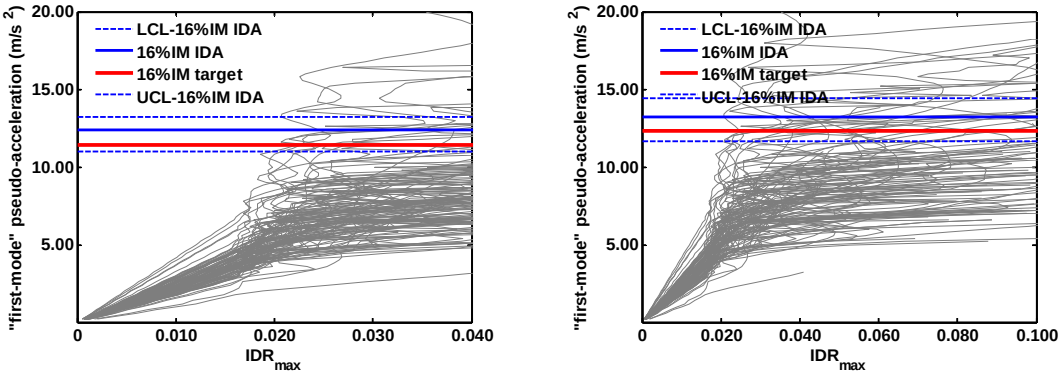

a) b)

Figure 4.38 IDA curves and 16% collapse intensities of 12-storey frame with T_1=1.90 s and θ_{AUX}-α=0.075 subjected to the VM set of records: a) near collapse μ=4; b) near collapse μ=5

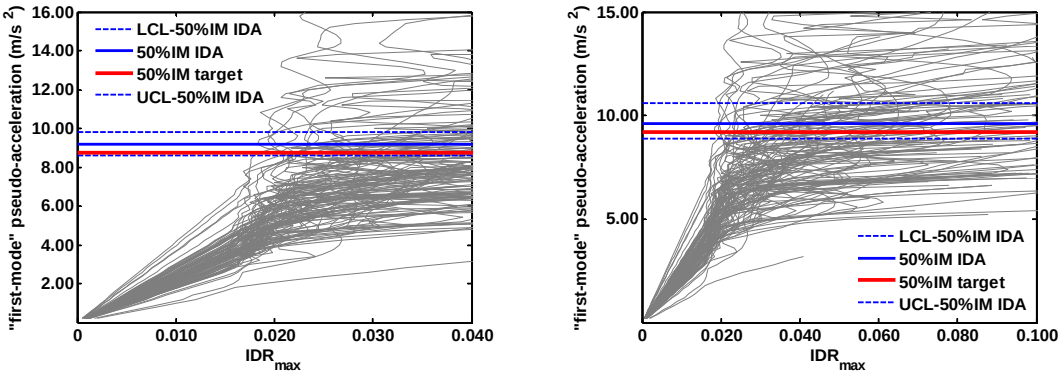

a) b)

Figure 4.39 IDA curves and 50% collapse intensities of 12-storey frame with T_1=1.90 s and θ_{AUX}-α=0.075 subjected to the VM set of records: a) near collapse μ=4; b) near collapse μ=5

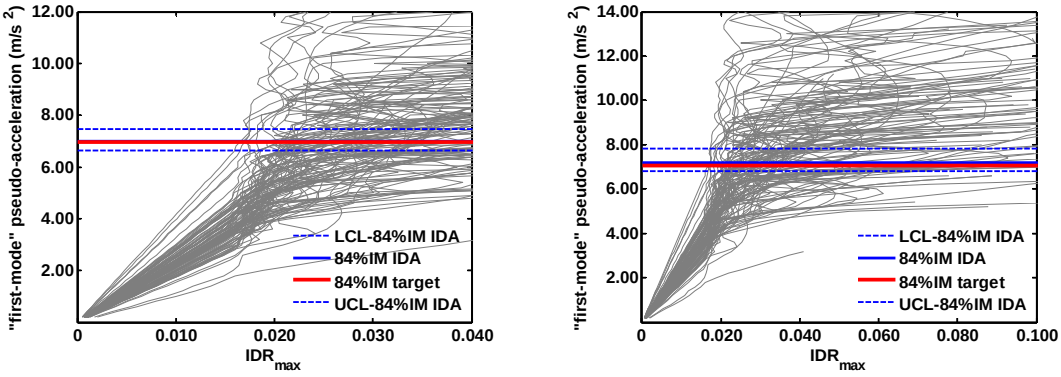

a) b)

Figure 4.40 IDA curves and 84% collapse intensities of 12-storey frame with T_1=1.90 s and θ_{AUX}-α=0.075 subjected to the VM set of records: a) near collapse μ=4; b) near collapse μ=5

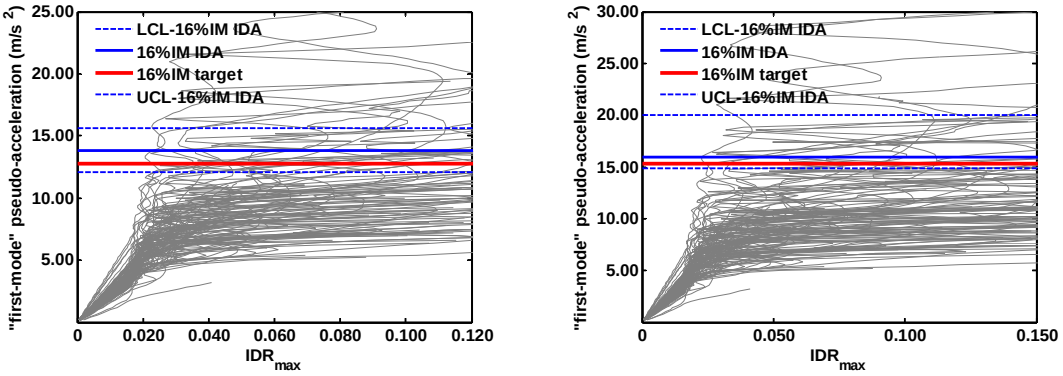

a) b)

Figure 4.41 IDA curves and 16% collapse intensities of 12-storey frame with T_1=1.90 s and θ_{AUX}-α=0.075 subjected to the VM set of records: a) near collapse μ=6; b) sidesway collapse $\mu=\mu_c$

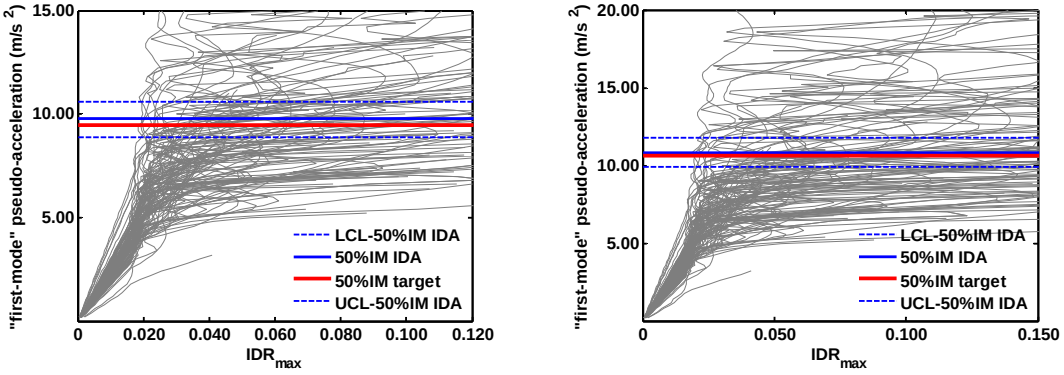

a) b)

Figure 4.42 IDA curves and 50% collapse intensities of 12-storey frame with T_1=1.90 s and θ_{AUX}-α=0.075 subjected to the VM set of records: a) near collapse μ=6; b) sidesway collapse $\mu=\mu_c$

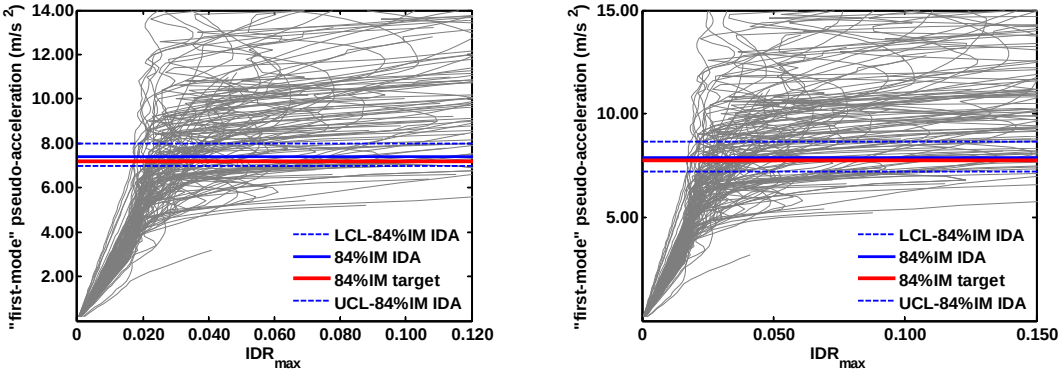

a) b)

Figure 4.43 IDA curves and 84% collapse intensities of 12-storey frame with T_1=1.90 s and θ_{AUX}-α=0.075 subjected to the VM set of records: a) near collapse μ=6; b) sidesway collapse $\mu=\mu_c$

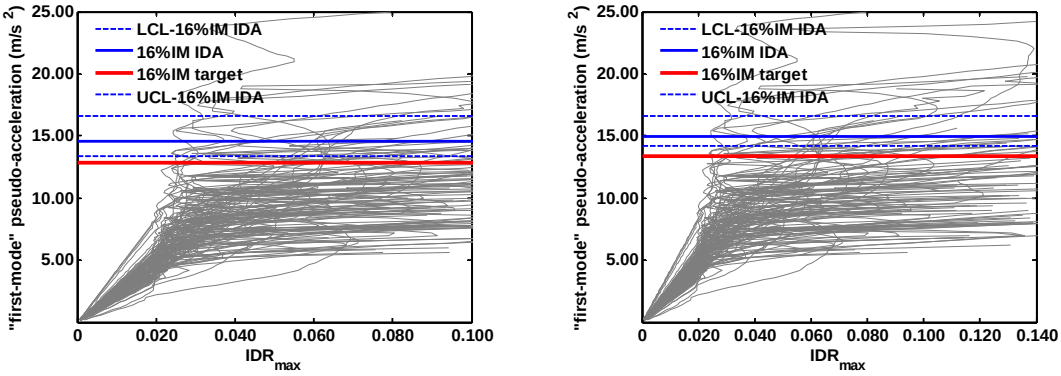

a) **b)**

Figure 4.44 IDA curves and 16% collapse intensities of 12-storey frame with T_1=1.90 s and θ_{AUX}-α=0.10 subjected to the VM set of records: a) near collapse μ=4; b) near collapse μ=5

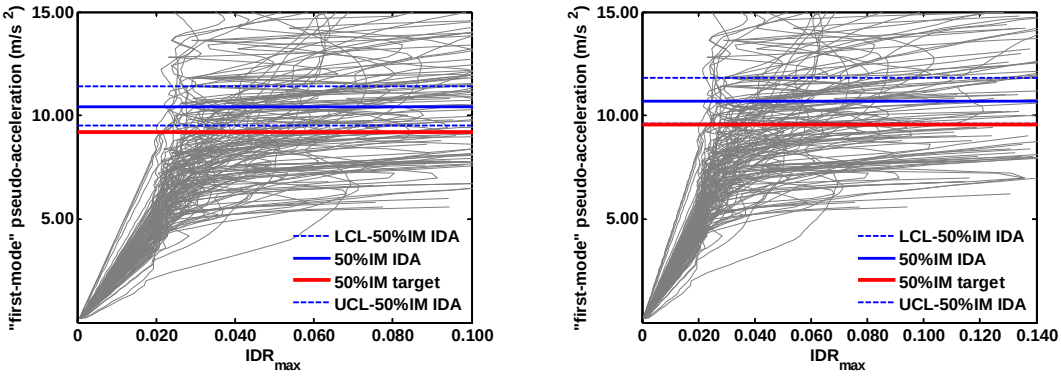

a) **b)**

Figure 4.45 IDA curves and 50% collapse intensities of 12-storey frame with T_1=1.90 s and θ_{AUX}-α=0.10 subjected to the VM set of records: a) near collapse μ=4; b) near collapse μ=5

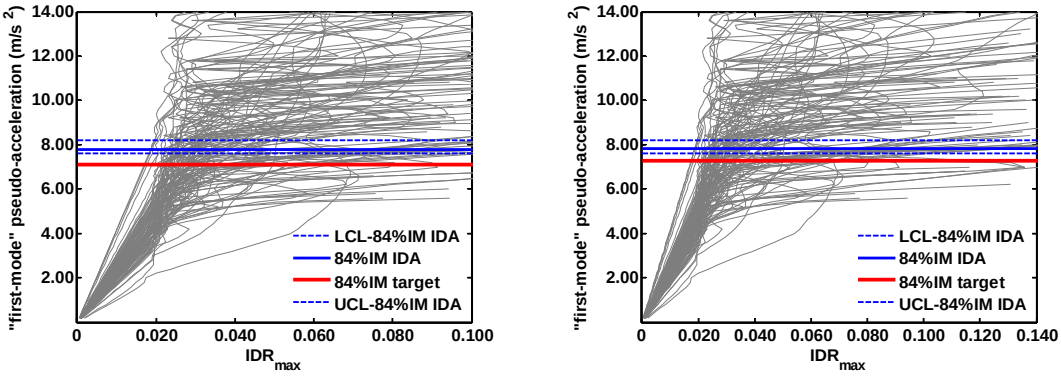

a) **b)**

Figure 4.46 IDA curves and 84% collapse intensities of 12-storey frame with T_1=1.90 s and θ_{AUX}-α=0.10 subjected to the VM set of records: a) near collapse μ=4; b) near collapse μ=5

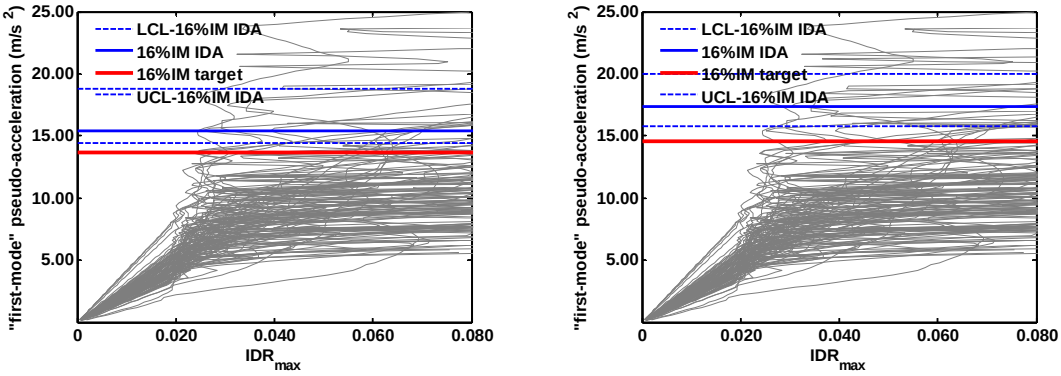

a) b)

Figure 4.47 IDA curves and 16% collapse intensities of 12-storey frame with T_1=1.90 s and θ_{AUX}-α=0.10 subjected to the VM set of records: a) near collapse μ=6; b) sidesway collapse $\mu=\mu_c$

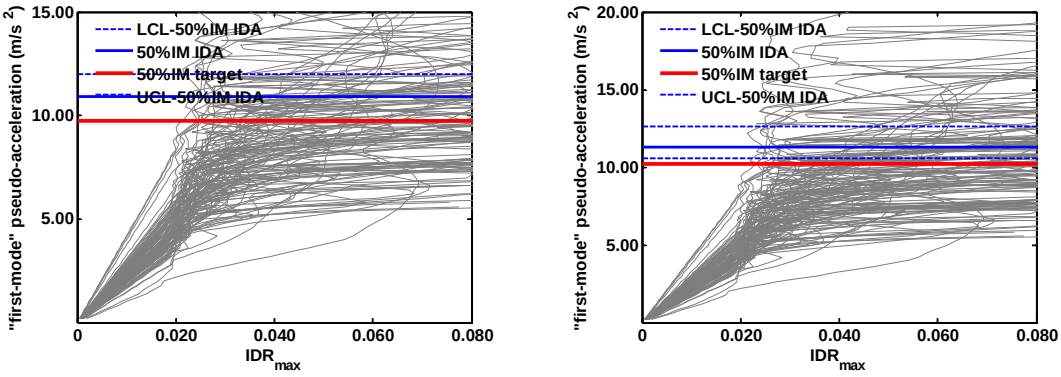

a) b)

Figure 4.48 IDA curves and 50% collapse intensities of 12-storey frame with T_1=1.90 s and θ_{AUX}-α=0.10 subjected to the VM set of records: a) near collapse μ=6; b) sidesway collapse $\mu=\mu_c$

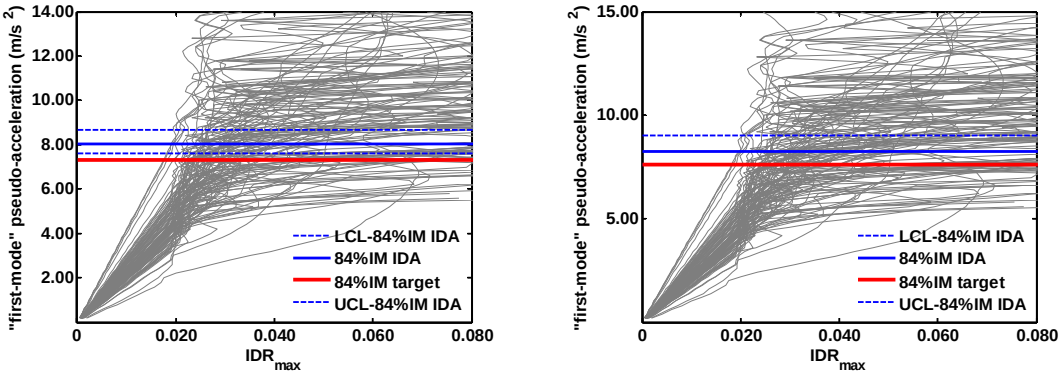

a) b)

Figure 4.49 IDA curves and 84% collapse intensities of 12-storey frame with T_1=1.90 s and θ_{AUX}-α=0.10 subjected to the VM set of records: a) near collapse μ=6; b) sidesway collapse $\mu=\mu_c$

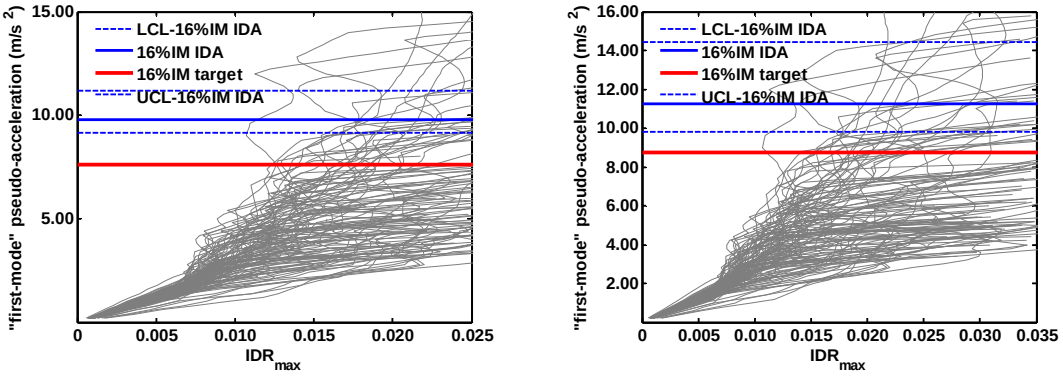

Figure 4.50 IDA curves and 16% collapse intensities of 16-storey frame with T_1=2.30 s and θ_{AUX}-α=0.025 subjected to the VM set of records: a) near collapse μ=4; b) near collapse μ=5

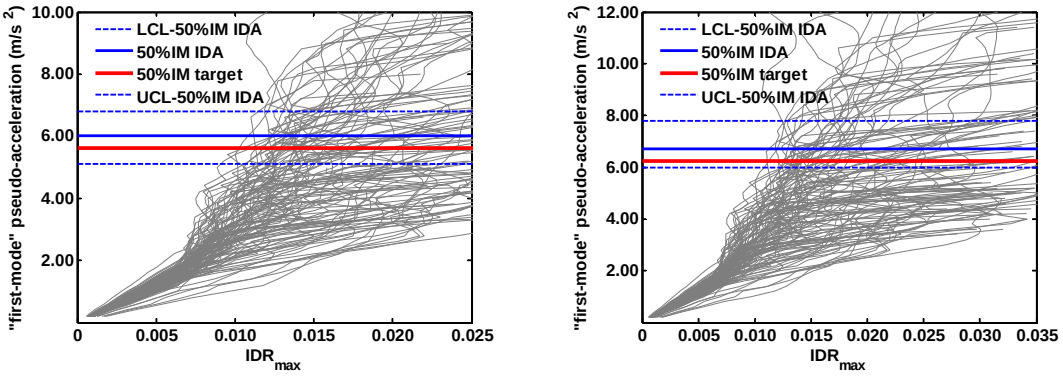

Figure 4.51 IDA curves and 50% collapse intensities of 16-storey frame with T_1=2.30 s and θ_{AUX}-α=0.025 subjected to the VM set of records: a) near collapse μ=4; b) near collapse μ=5

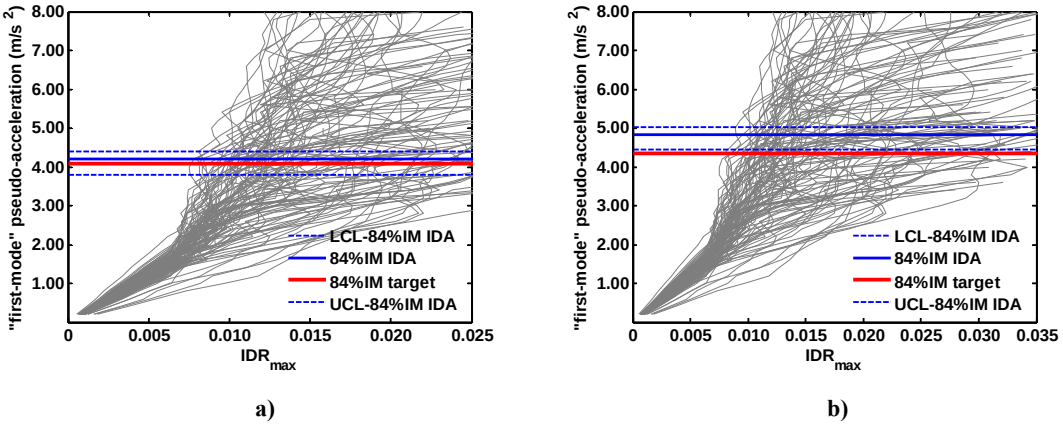

Figure 4.52 IDA curves and 84% collapse intensities of 16-storey frame with T_1=2.30 s and θ_{AUX}-α=0.025 subjected to the VM set of records: a) near collapse μ=4; b) near collapse μ=5

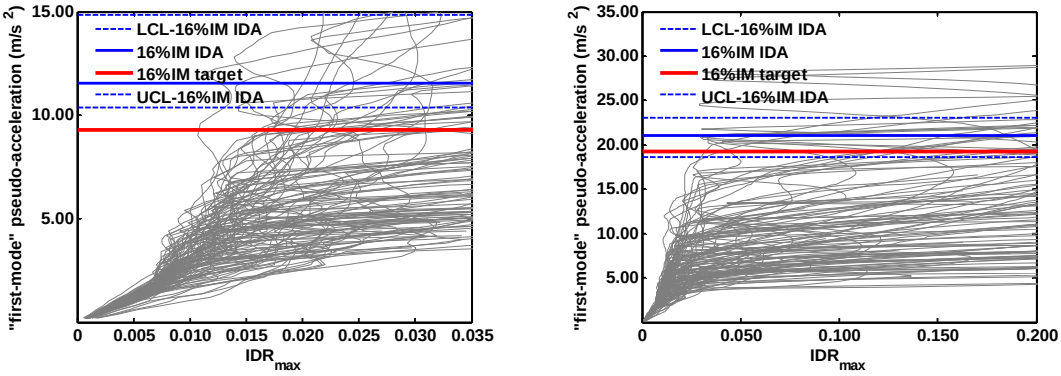

a) b)

Figure 4.53 IDA curves and 16% collapse intensities of 16-storey frame with T_1=2.30 s and θ_{AUX}-α=0.025 subjected to the VM set of records: a) near collapse μ=6; b) sidesway collapse $\mu=\mu_c$

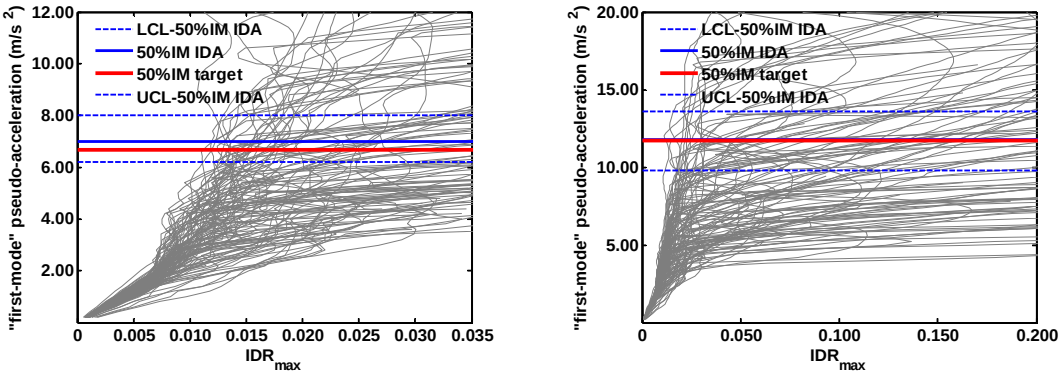

a) b)

Figure 4.54 IDA curves and 50% collapse intensities of 16-storey frame with T_1=2.30 s and θ_{AUX}-α=0.025 subjected to the VM set of records: a) near collapse μ=6; b) sidesway collapse $\mu=\mu_c$

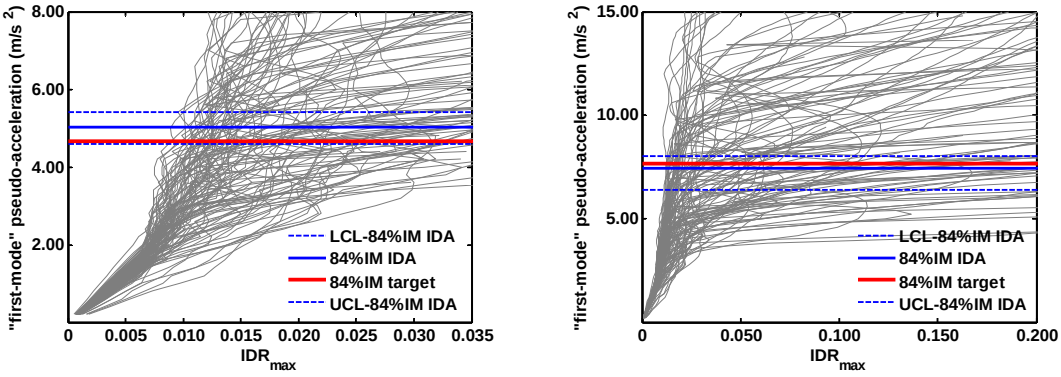

a) b)

Figure 4.55 IDA curves and 84% collapse intensities of 16-storey frame with T_1=2.30 s and θ_{AUX}-α=0.025 subjected to the VM set of records: a) near collapse μ=6; b) sidesway collapse $\mu=\mu_c$

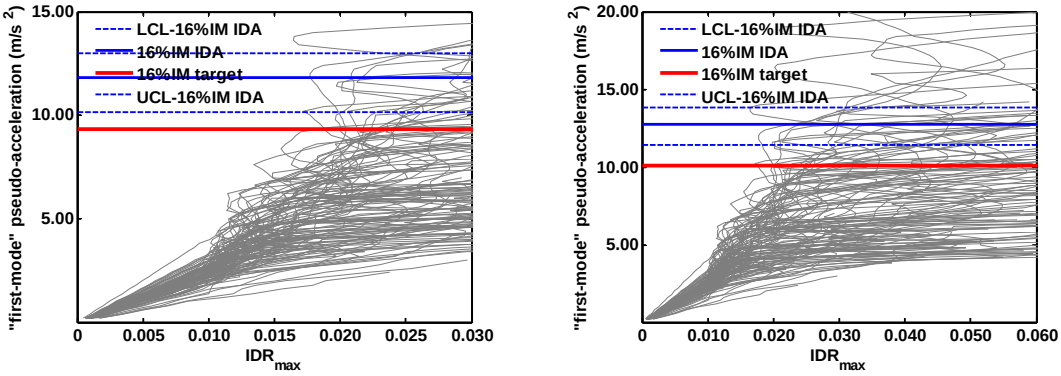

a) b)

Figure 4.56 IDA curves and 16% collapse intensities of 16-storey frame with T_1=2.30 s and θ_{AUX}-α=0.05 subjected to the VM set of records: a) near collapse μ=4; b) near collapse μ=5

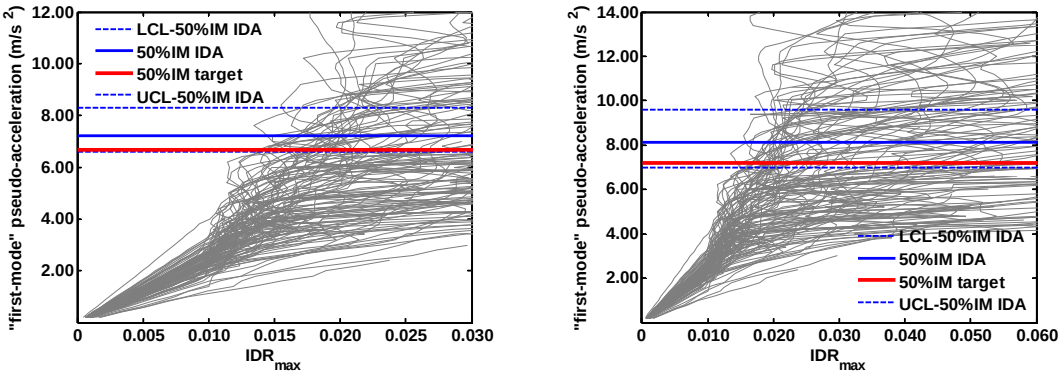

a) b)

Figure 4.57 IDA curves and 50% collapse intensities of 16-storey frame with T_1=2.30 s and θ_{AUX}-α=0.05 subjected to the VM set of records: a) near collapse μ=4; b) near collapse μ=5

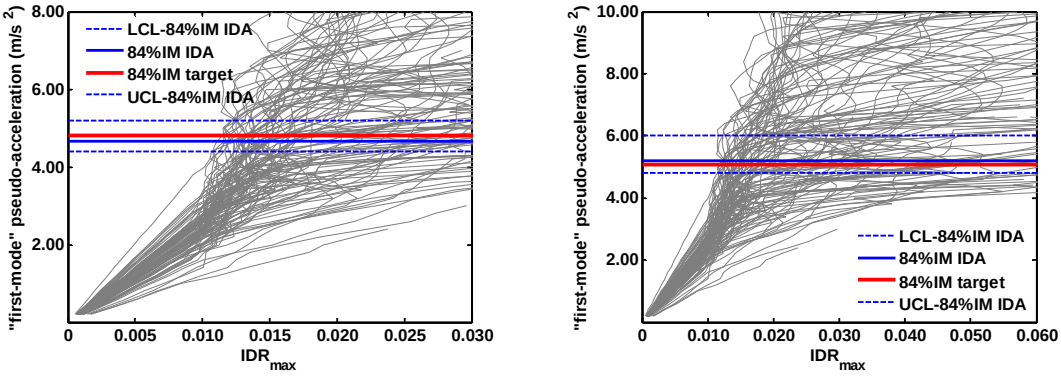

a) b)

Figure 4.58 IDA curves and 84% collapse intensities of 16-storey frame with T_1=2.30 s and θ_{AUX}-α=0.05 subjected to the VM set of records: a) near collapse μ=4; b) near collapse μ=5

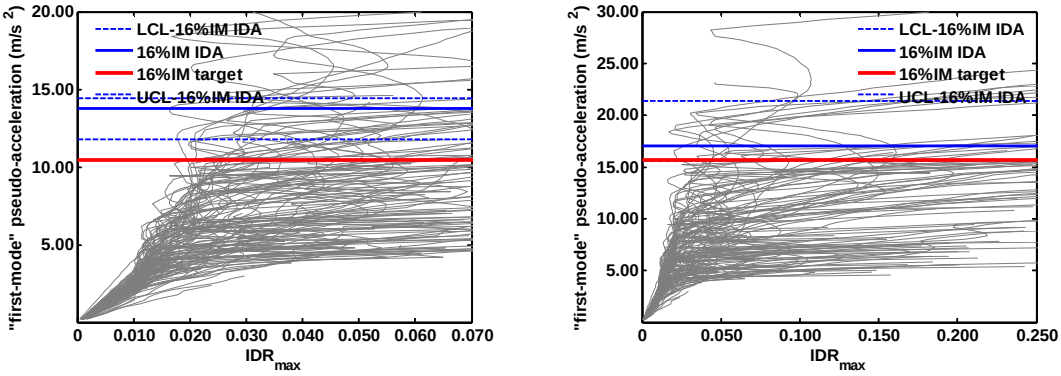

a) b)

Figure 4.59 IDA curves and 16% collapse intensities of 16-storey frame with T_1=2.30 s and θ_{AUX}-α=0.05 subjected to the VM set of records: a) near collapse μ=6; b) sidesway collapse $\mu=\mu_c$

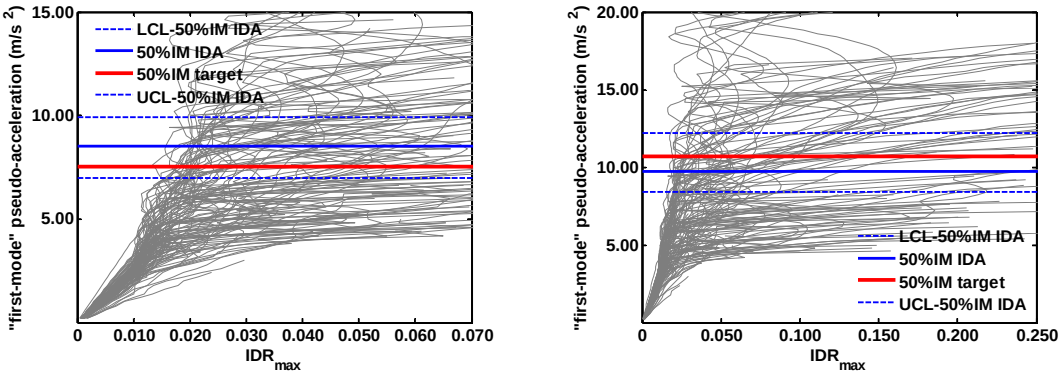

a) b)

Figure 4.60 IDA curves and 50% collapse intensities of 16-storey frame with T_1=2.30 s and θ_{AUX}-α=0.05 subjected to the VM set of records: a) near collapse μ=6; b) sidesway collapse $\mu=\mu_c$

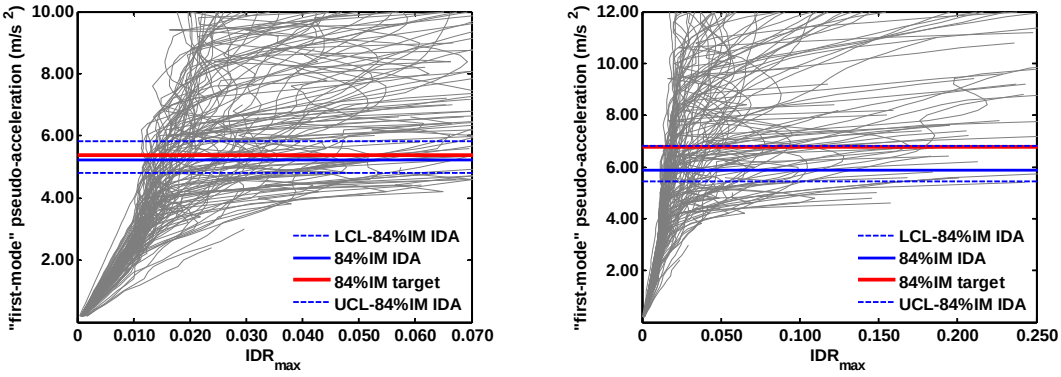

a) b)

Figure 4.61 IDA curves and 84% collapse intensities of 16-storey frame with T_1=2.30 s and θ_{AUX}-α=0.05 subjected to the VM set of records: a) near collapse μ=6; b) sidesway collapse $\mu=\mu_c$

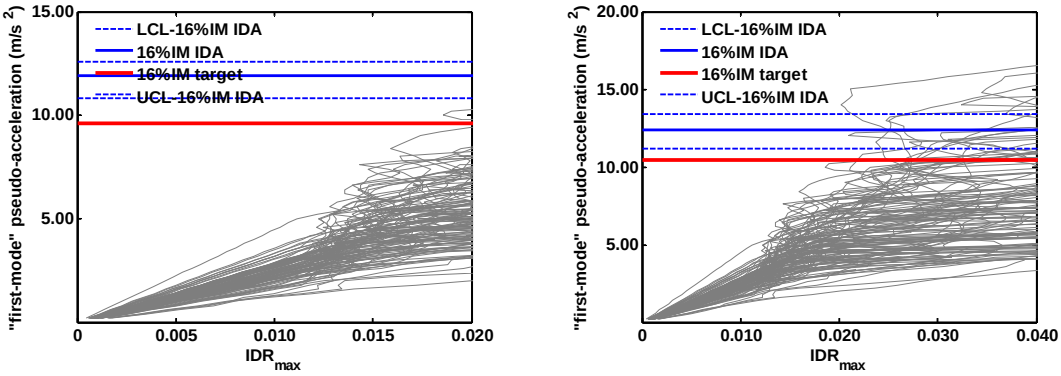

a) b)

Figure 4.62 IDA curves and 16% collapse intensities of 16-storey frame with T_1=2.30 s and θ_{AUX}-α=0.075 subjected to the VM set of records: a) near collapse μ=4; b) near collapse μ=5

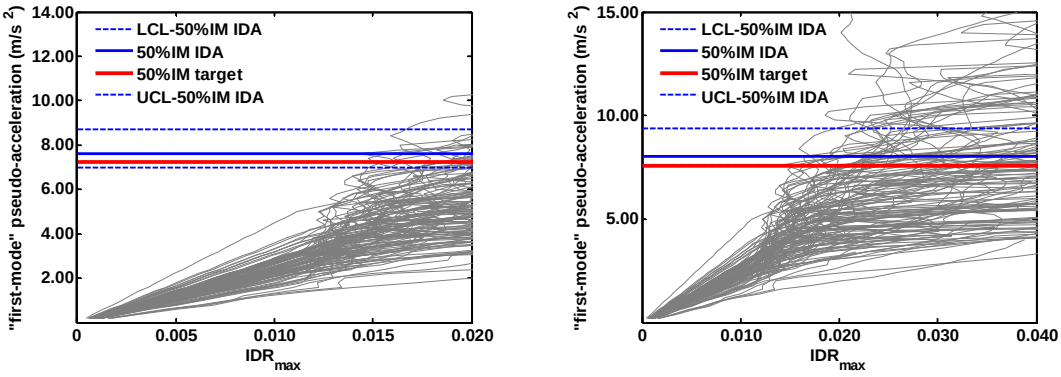

a) b)

Figure 4.63 IDA curves and 50% collapse intensities of 16-storey frame with T_1=2.30 s and θ_{AUX}-α=0.075 subjected to the VM set of records: a) near collapse μ=4; b) near collapse μ=5

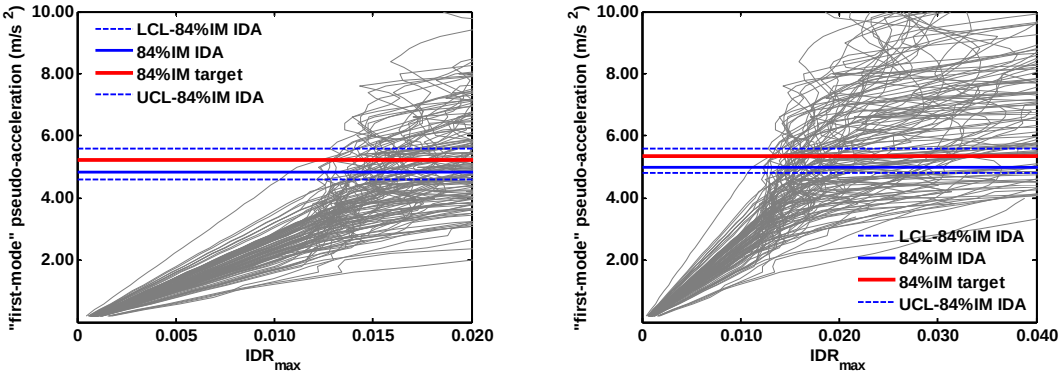

a) b)

Figure 4.64 IDA curves and 84% collapse intensities of 16-storey frame with T_1=2.30 s and θ_{AUX}-α=0.075 subjected to the VM set of records: a) near collapse μ=4; b) near collapse μ=5

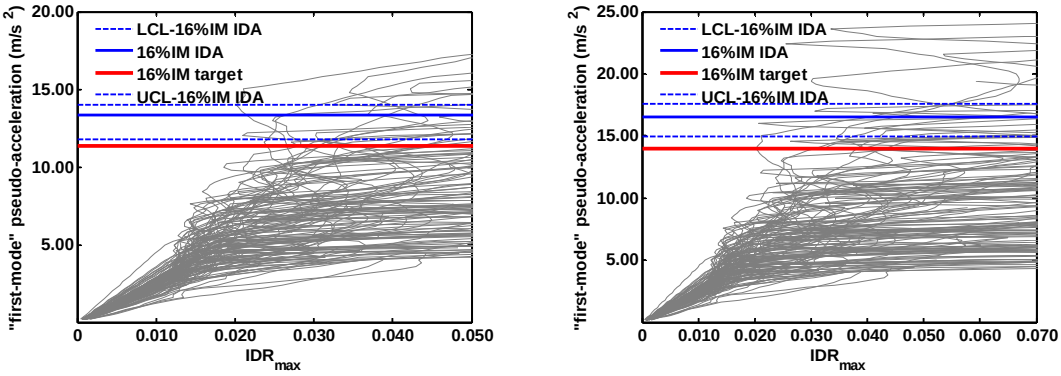

Figure 4.65 IDA curves and 16% collapse intensities of 16-storey frame with T_1=2.30 s and θ_{AUX}-α=0.075 subjected to the VM set of records: a) near collapse μ=6; b) sidesway collapse $\mu=\mu_c$

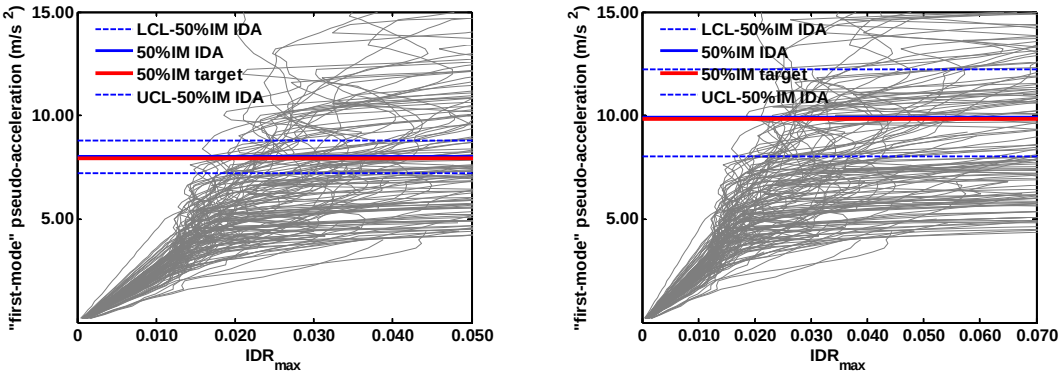

Figure 4.66 IDA curves and 50% collapse intensities of 16-storey frame with T_1=2.30 s and θ_{AUX}-α=0.075 subjected to the VM set of records: a) near collapse μ=6; b) sidesway collapse $\mu=\mu_c$

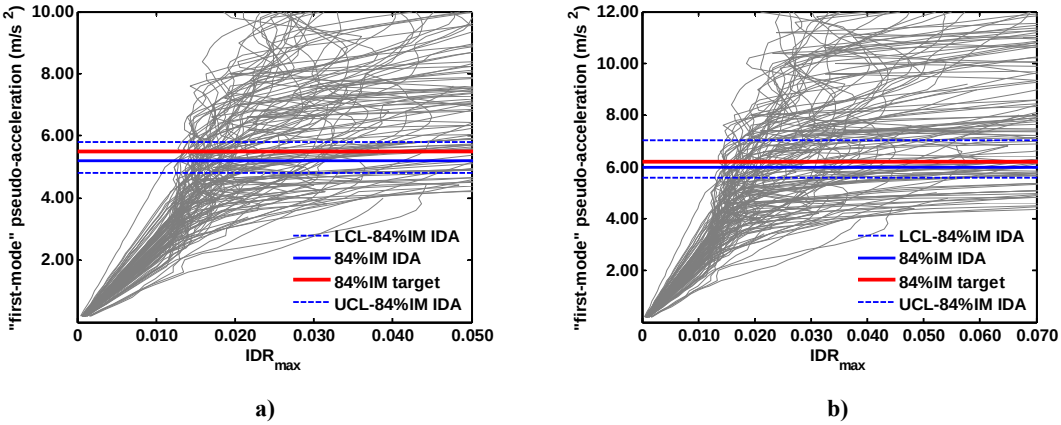

Figure 4.67 IDA curves and 84% collapse intensities of 16-storey frame with T_1=2.30 s and θ_{AUX}-α=0.075 subjected to the VM set of records: a) near collapse μ=6; b) sidesway collapse $\mu=\mu_c$

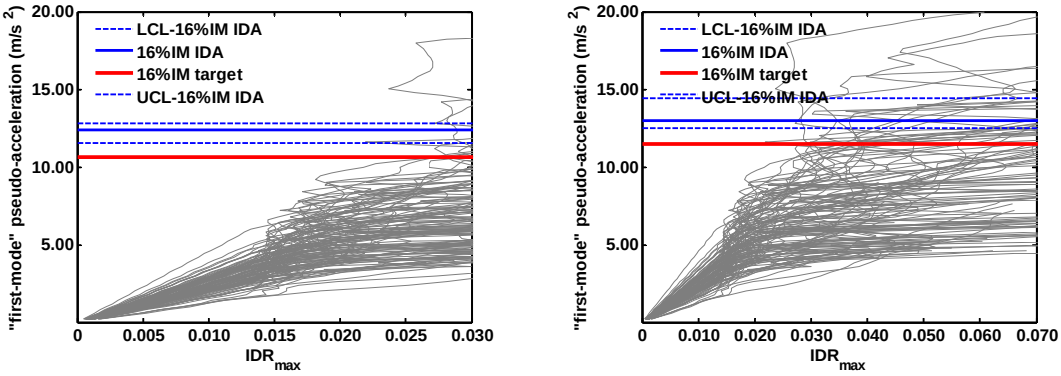

Figure 4.68 IDA curves and 16% collapse intensities of 16-storey frame with T_1=2.30 s and θ_{AUX}-α=0.10 subjected to the VM set of records: a) near collapse μ=4; b) near collapse μ=5

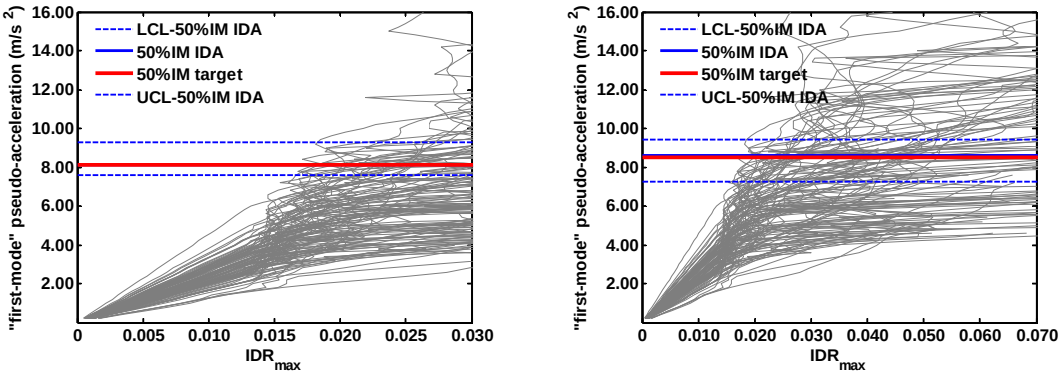

Figure 4.69 IDA curves and 50% collapse intensities of 16-storey frame with T_1=2.30 s and θ_{AUX}-α=0.10 subjected to the VM set of records: a) near collapse μ=4; b) near collapse μ=5

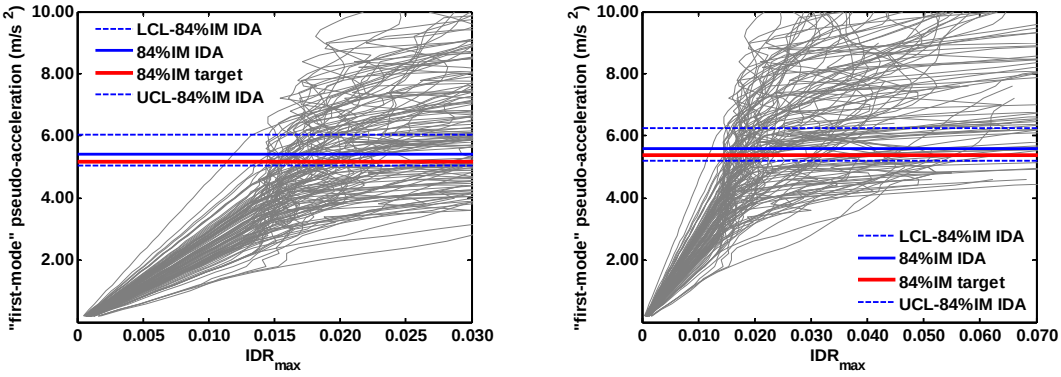

Figure 4.70 IDA curves and 84% collapse intensities of 16-storey frame with T_1=2.30 s and θ_{AUX}-α=0.10 subjected to the VM set of records: a) near collapse μ=4; b) near collapse μ=5

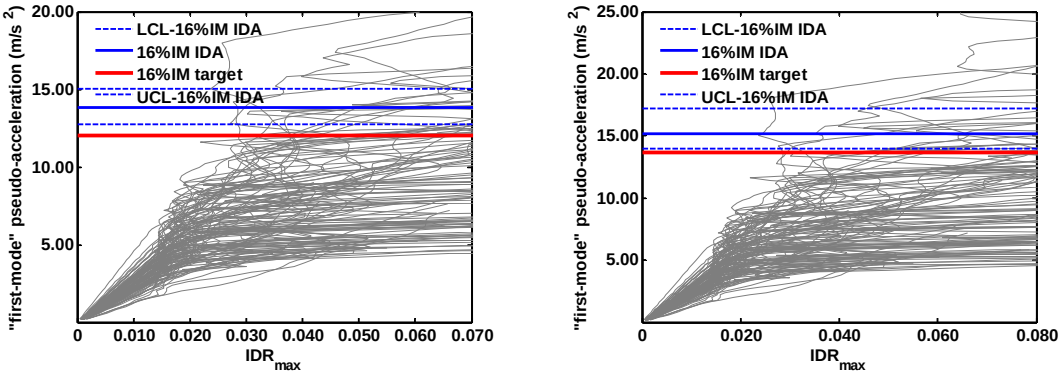

Figure 4.71 IDA curves and 16% collapse intensities of 16-storey frame with T_1=2.30 s and θ_{AUX}-α=0.10 subjected to the VM set of records: a) near collapse μ=6; b) sidesway collapse $\mu=\mu_c$

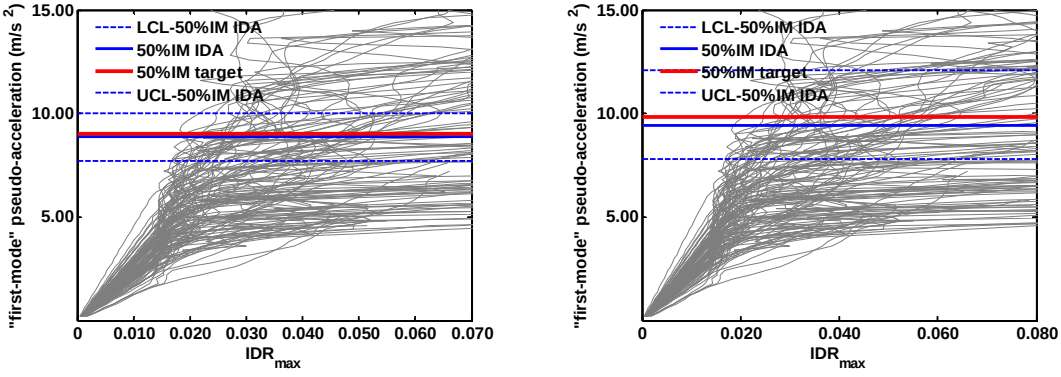

Figure 4.72 IDA curves and 50% collapse intensities of 16-storey frame with T_1=2.30 s and θ_{AUX}-α=0.10 subjected to the VM set of records: a) near collapse μ=6; b) sidesway collapse $\mu=\mu_c$

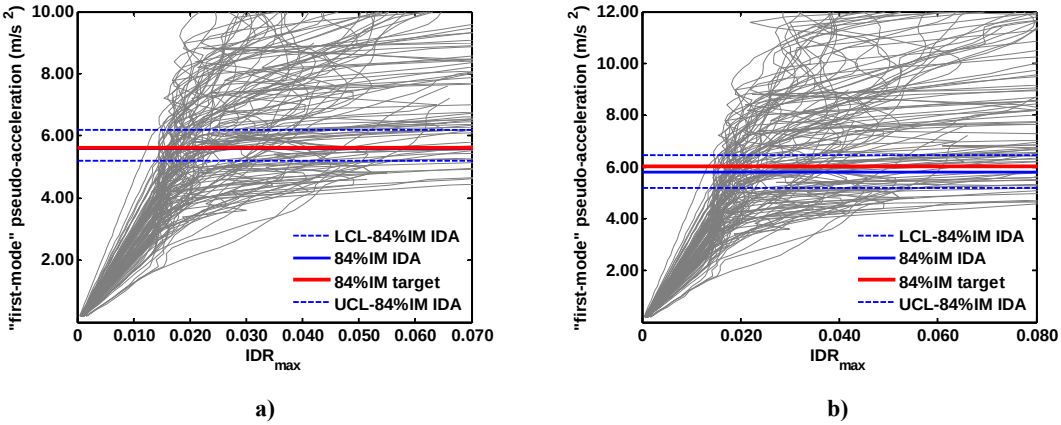

Figure 4.73 IDA curves and 84% collapse intensities of 16-storey frame with T_1=2.30 s and θ_{AUX}-α=0.10 subjected to the VM set of records: a) near collapse μ=6; b) sidesway collapse $\mu=\mu_c$

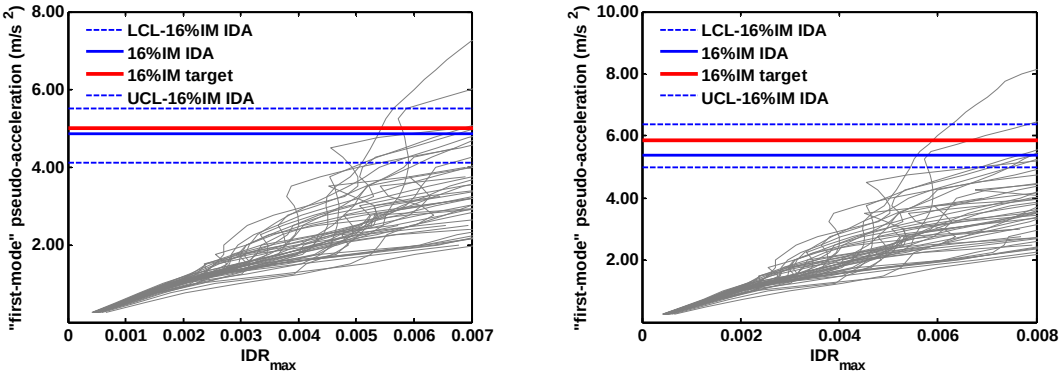

a) b)

Figure 4.74 IDA curves and 16% collapse intensities of 8-storey frame with T_1=1.10 s and θ_{AUX}-α=0.025 subjected to the FEMA-P695 set of records: a) near collapse μ=4; b) near collapse μ=5

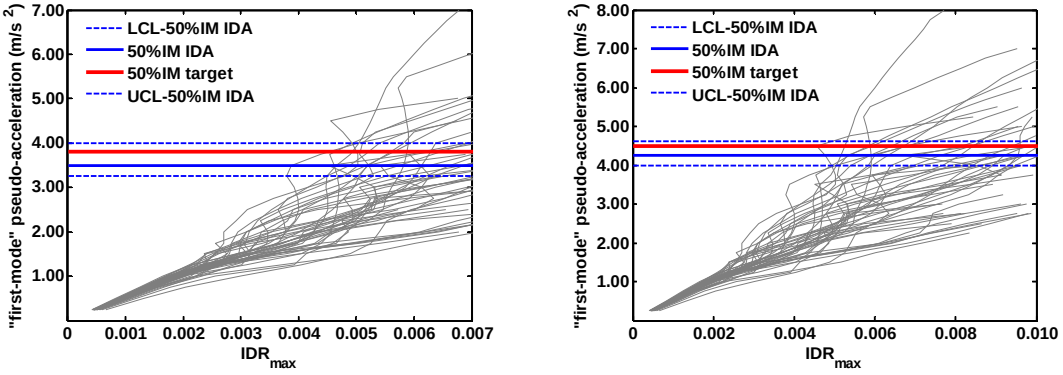

a) b)

Figure 4.75 IDA curves and 50% collapse intensities of 8-storey frame with T_1=1.10 s and θ_{AUX}-α=0.025 subjected to the FEMA-P695 set of records: a) near collapse μ=4; b) near collapse μ=5

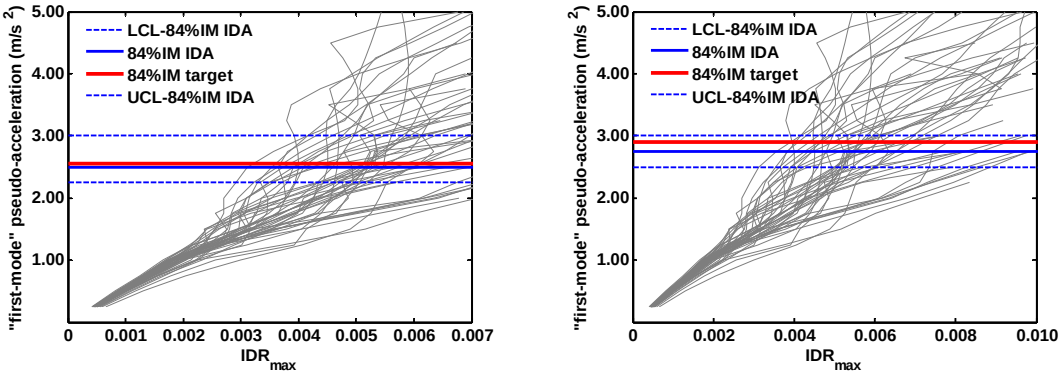

a) b)

Figure 4.76 IDA curves and 84% collapse intensities of 8-storey frame with T_1=1.10 s and θ_{AUX}-α=0.025 subjected to the FEMA-P695 set of records: a) near collapse μ=4; b) near collapse μ=5

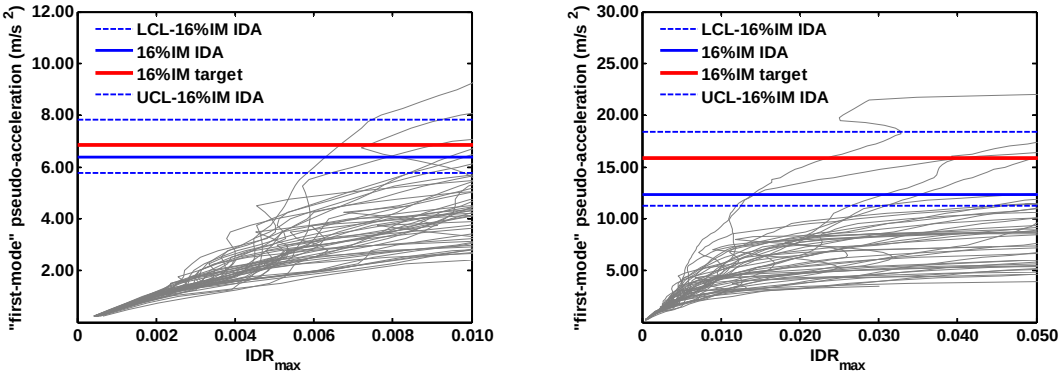

a) b)

Figure 4.77 IDA curves and 16% collapse intensities of 8-storey frame with T_1=1.10 s and θ_{AUX}-α=0.025 subjected to the FEMA-P695 set of records: a) near collapse μ=6; b) sidesway collapse $\mu=\mu_c$

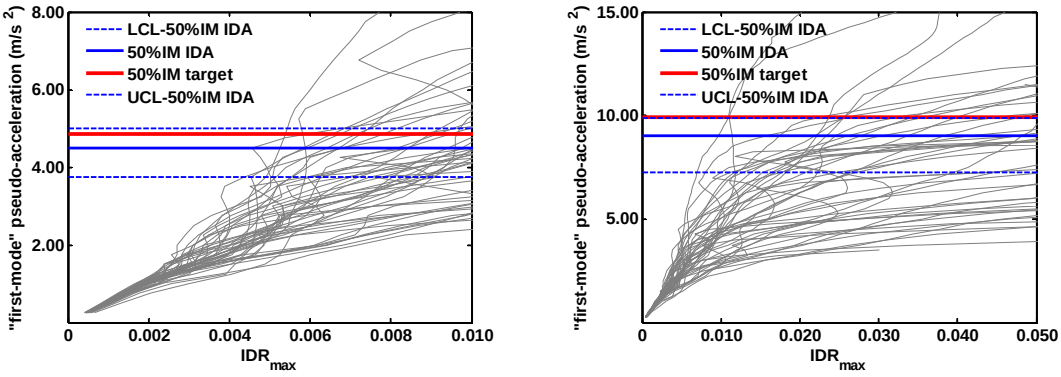

a) b)

Figure 4.78 IDA curves and 50% collapse intensities of 8-storey frame with T_1=1.10 s and θ_{AUX}-α=0.025 subjected to the FEMA-P695 set of records: a) near collapse μ=6; b) sidesway collapse $\mu=\mu_c$

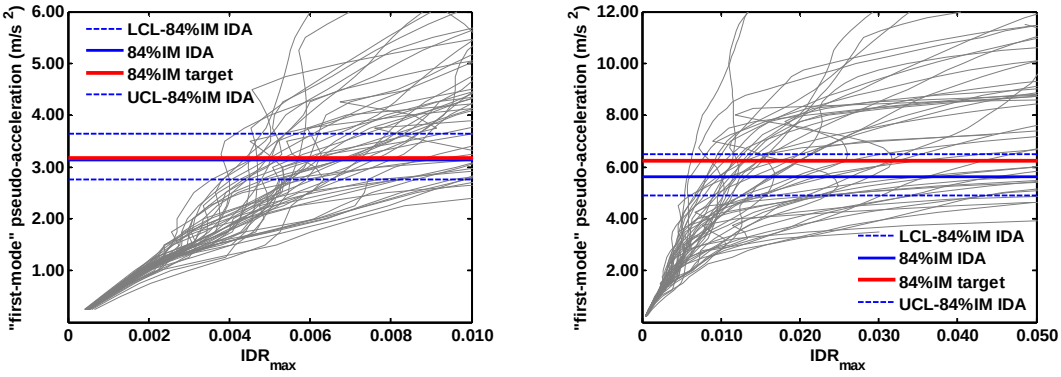

a) b)

Figure 4.79 IDA curves and 84% collapse intensities of 8-storey frame with T_1=1.10 s and θ_{AUX}-α=0.025 subjected to the FEMA-P695 set of records: a) near collapse μ=6; b) sidesway collapse $\mu=\mu_c$

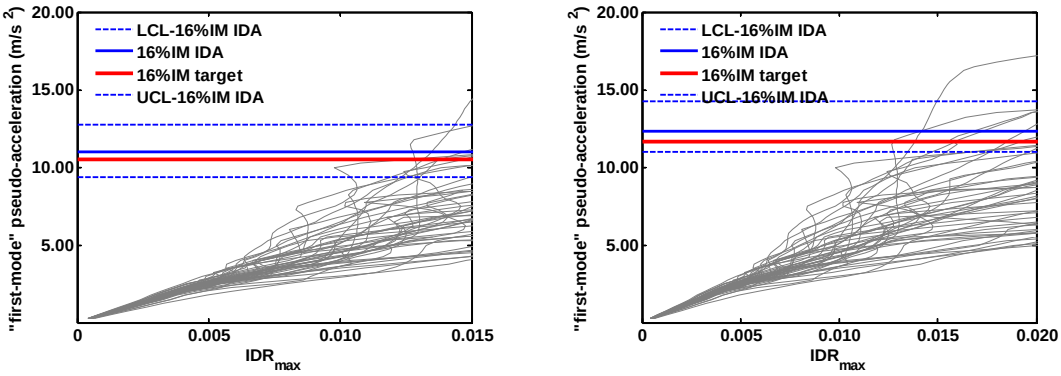

a) b)

Figure 4.80 IDA curves and 16% collapse intensities of 8-storey frame with T_1=1.10 s and θ_{AUX}-α=0.05 subjected to the FEMA-P695 set of records: a) near collapse μ=4; b) near collapse μ=5

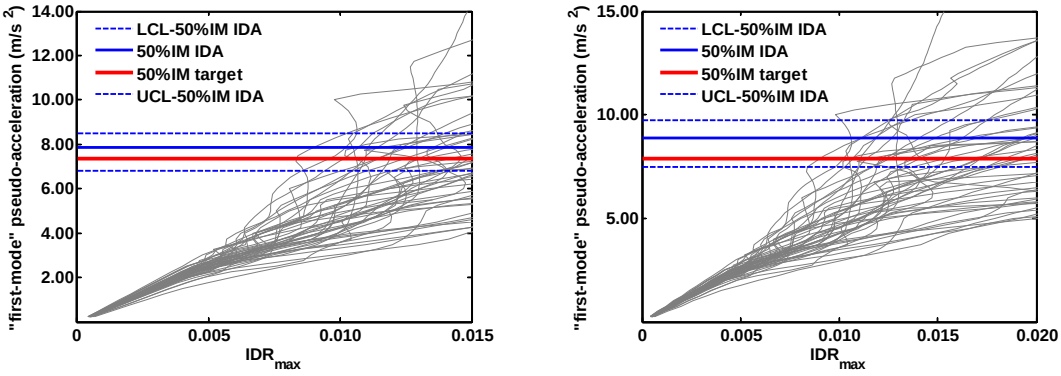

a) b)

Figure 4.81 IDA curves and 50% collapse intensities of 8-storey frame with T_1=1.10 s and θ_{AUX}-α=0.05 subjected to the FEMA-P695 set of records: a) near collapse μ=4; b) near collapse μ=5

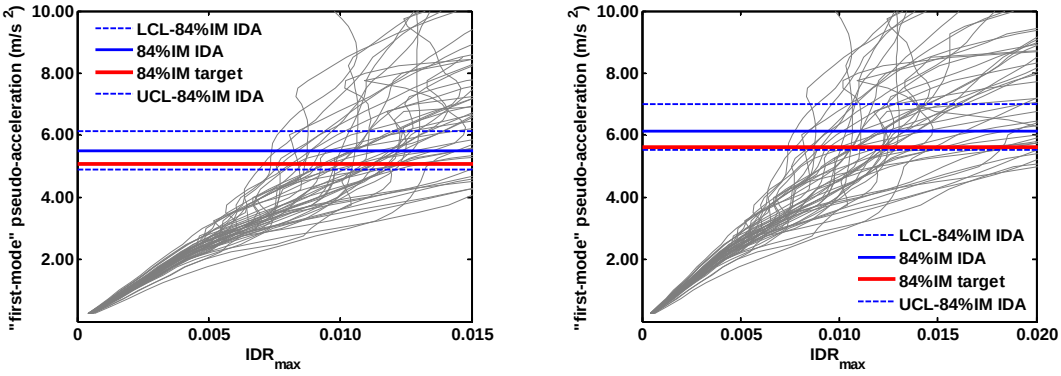

a) b)

Figure 4.82 IDA curves and 84% collapse intensities of 8-storey frame with T_1=1.10 s and θ_{AUX}-α=0.05 subjected to the FEMA-P695 set of records: a) near collapse μ=4; b) near collapse μ=5

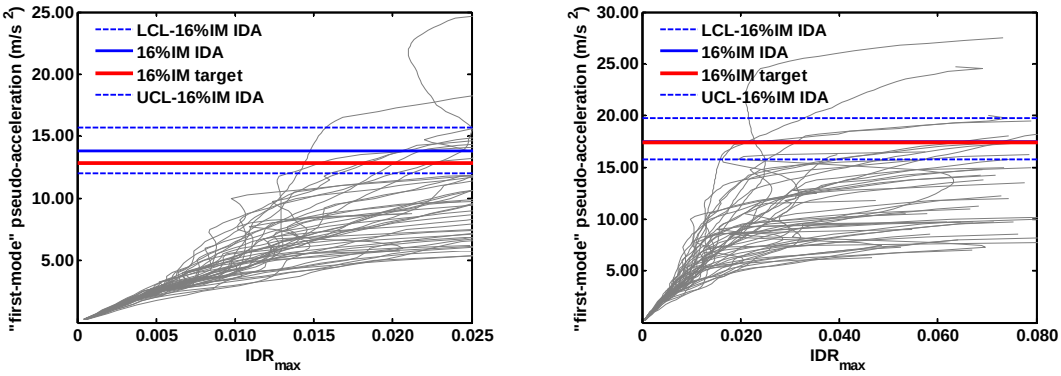

a) b)

Figure 4.83 IDA curves and 16% collapse intensities of 8-storey frame with T_1=1.10 s and θ_{AUX}-α=0.05 subjected to the FEMA-P695 set of records: a) near collapse μ=6; b) sidesway collapse $\mu=\mu_c$

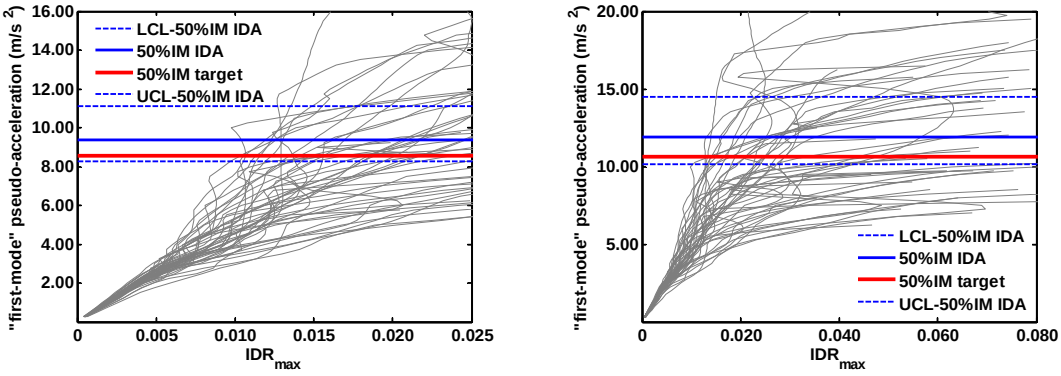

a) b)

Figure 4.84 IDA curves and 50% collapse intensities of 8-storey frame with T_1=1.10 s and θ_{AUX}-α=0.05 subjected to the FEMA-P695 set of records: a) near collapse μ=6; b) sidesway collapse $\mu=\mu_c$

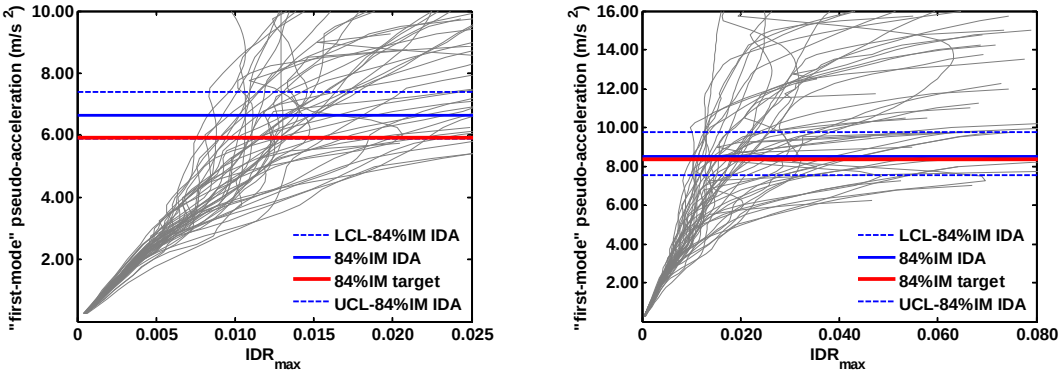

a) b)

Figure 4.85 IDA curves and 84% collapse intensities of 8-storey frame with T_1=1.10 s and θ_{AUX}-α=0.05 subjected to the FEMA-P695 set of records: a) near collapse μ=6; b) sidesway collapse $\mu=\mu_c$

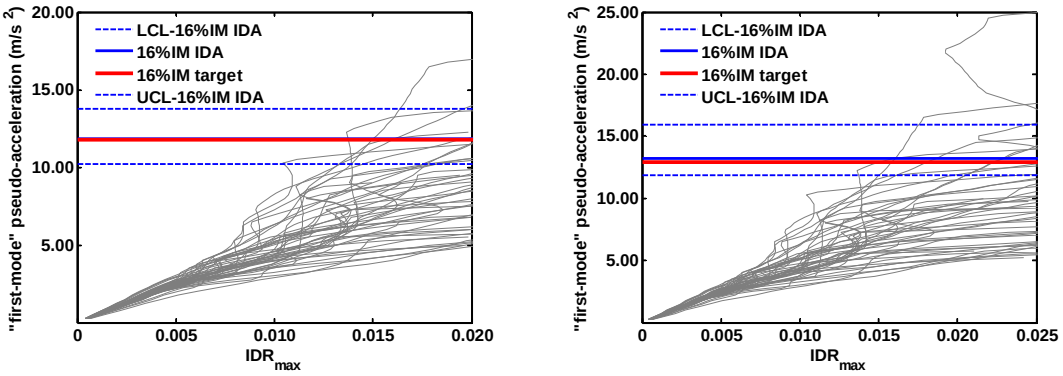

a) **b)**

Figure 4.86 IDA curves and 16% collapse intensities of 8-storey frame with T_1=1.10 s and θ_{AUX}-α=0.075 subjected to the FEMA-P695 set of records: a) near collapse μ=4; b) near collapse μ=5

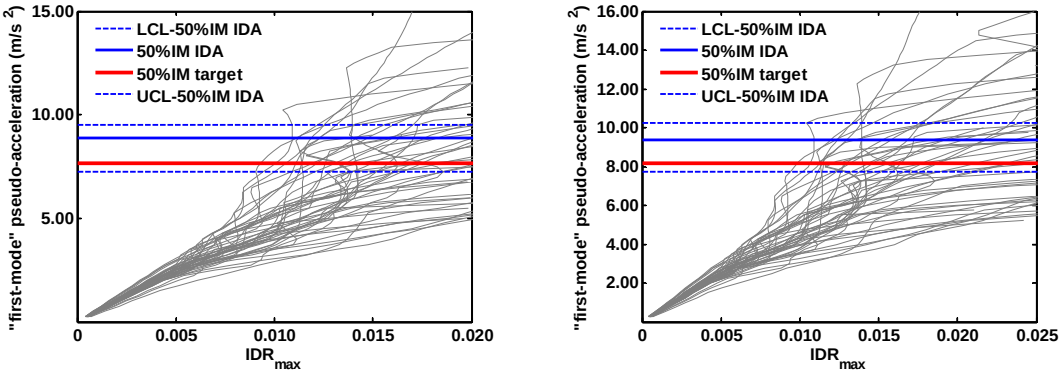

a) **b)**

Figure 4.87 IDA curves and 50% collapse intensities of 8-storey frame with T_1=1.10 s and θ_{AUX}-α=0.075 subjected to the FEMA-P695 set of records: a) near collapse μ=4; b) near collapse μ=5

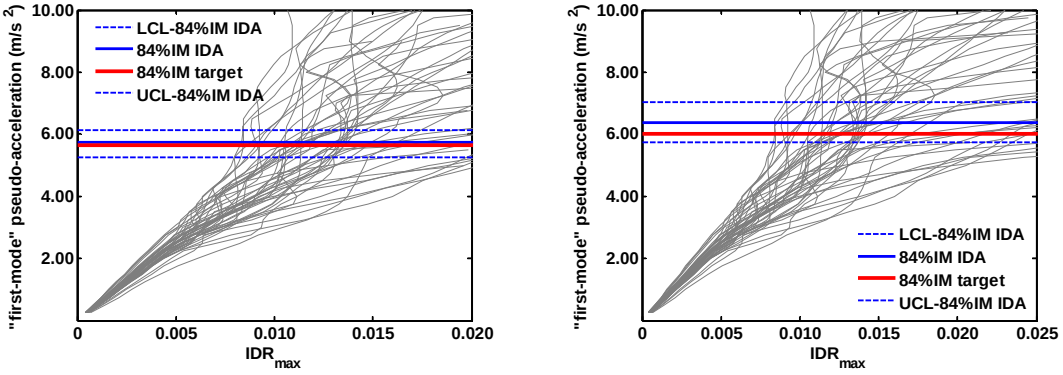

a) **b)**

Figure 4.88 IDA curves and 84% collapse intensities of 8-storey frame with T_1=1.10 s and θ_{AUX}-α=0.075 subjected to the FEMA-P695 set of records: a) near collapse μ=4; b) near collapse μ=5

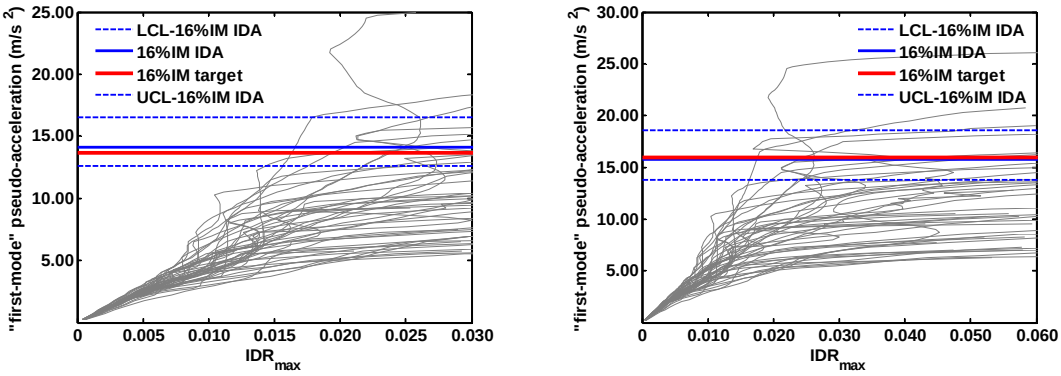

a) b)

Figure 4.89 IDA curves and 16% collapse intensities of 8-storey frame with T_1=1.10 s and θ_{AUX}-α=0.075 subjected to the FEMA-P695 set of records: a) near collapse μ=6; b) sidesway collapse $\mu=\mu_c$

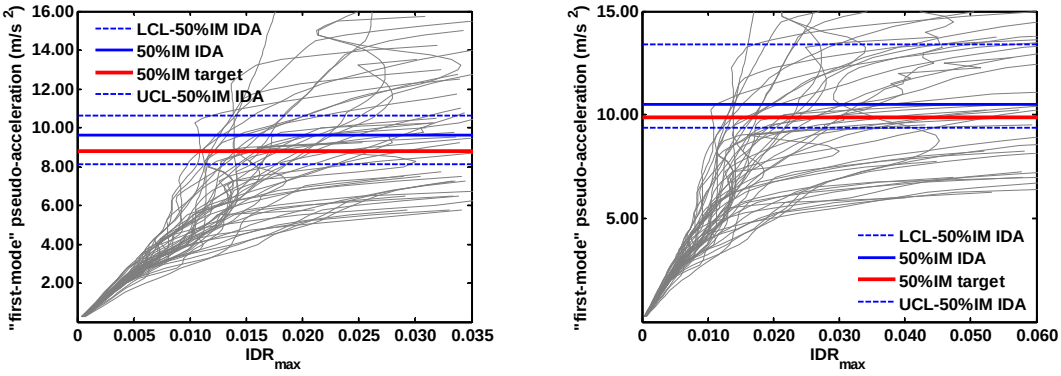

a) b)

Figure 4.90 IDA curves and 50% collapse intensities of 8-storey frame with T_1=1.10 s and θ_{AUX}-α=0.075 subjected to the FEMA-P695 set of records: a) near collapse μ=6; b) sidesway collapse $\mu=\mu_c$

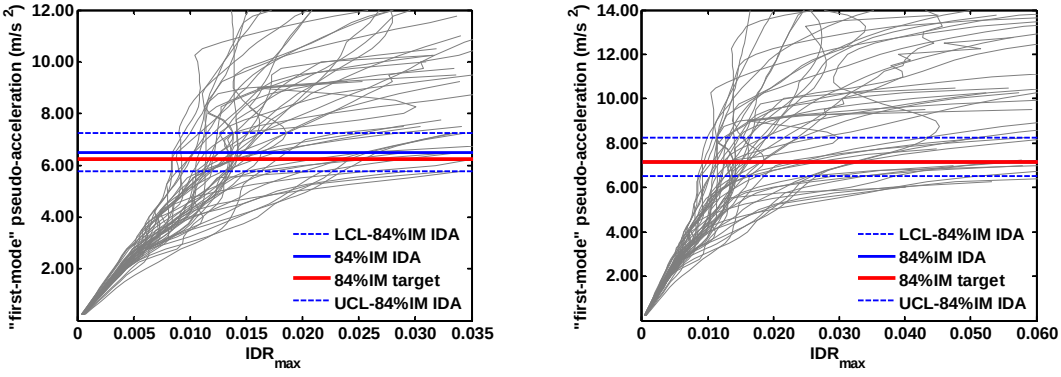

a) b)

Figure 4.91 IDA curves and 84% collapse intensities of 8-storey frame with T_1=1.10 s and θ_{AUX}-α=0.075 subjected to the FEMA-P695 set of records: a) near collapse μ=6; b) sidesway collapse $\mu=\mu_c$

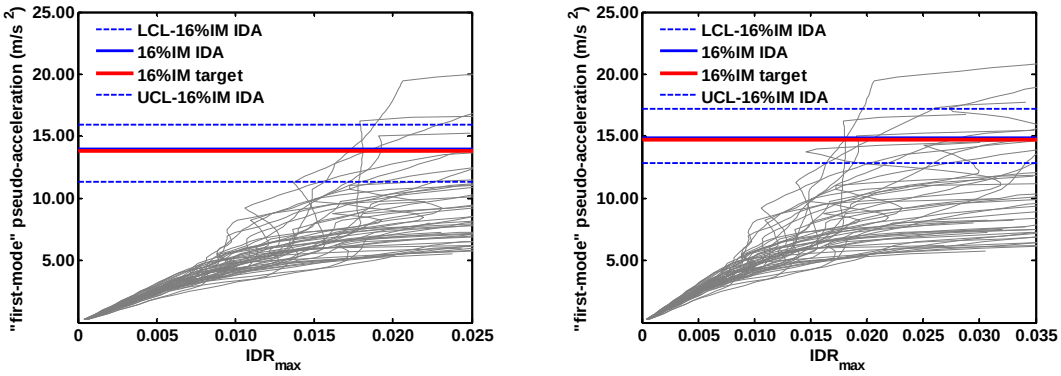

a) b)

Figure 4.92 IDA curves and 16% collapse intensities of 8-storey frame with T_1=1.10 s and θ_{AUX}-α=0.100 subjected to the FEMA-P695 set of records: a) near collapse μ=4; b) near collapse μ=5

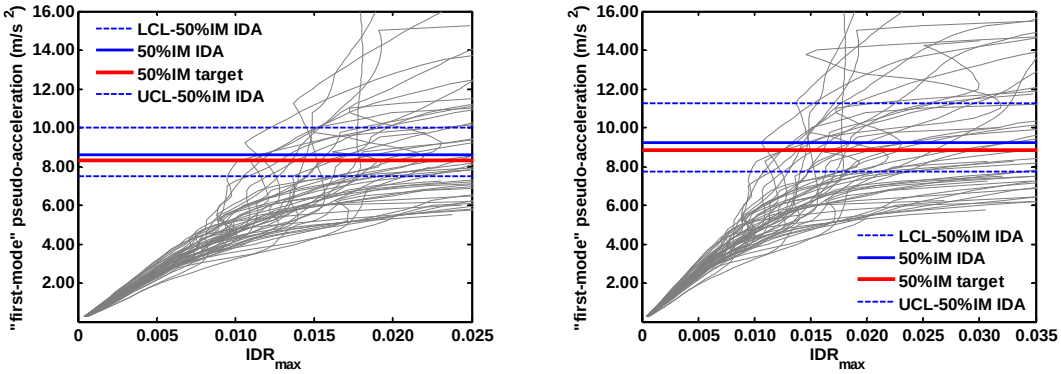

a) b)

Figure 4.93 IDA curves and 50% collapse intensities of 8-storey frame with T_1=1.10 s and θ_{AUX}-α=0.100 subjected to the FEMA-P695 set of records: a) near collapse μ=4; b) near collapse μ=5

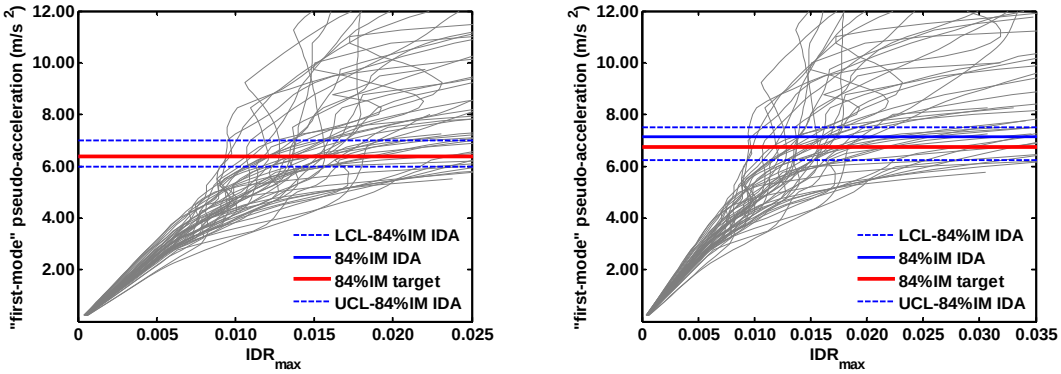

a) b)

Figure 4.94 IDA curves and 84% collapse intensities of 8-storey frame with T_1=1.10 s and θ_{AUX}-α=0.100 subjected to the FEMA-P695 set of records: a) near collapse μ=4; b) near collapse μ=5

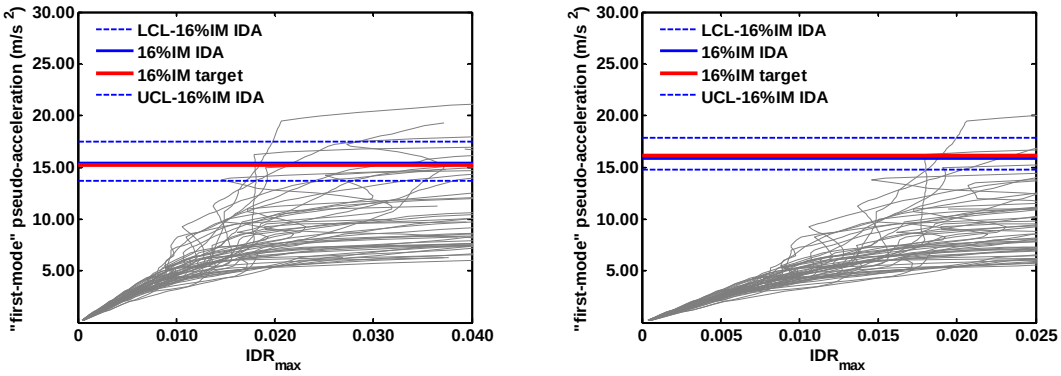

a) **b)**

Figure 4.95 IDA curves and 16% collapse intensities of 8-storey frame with T_1=1.10 s and θ_{AUX}-α=0.100 subjected to the FEMA-P695 set of records: a) near collapse μ=6; b) sidesway collapse $\mu=\mu_c$

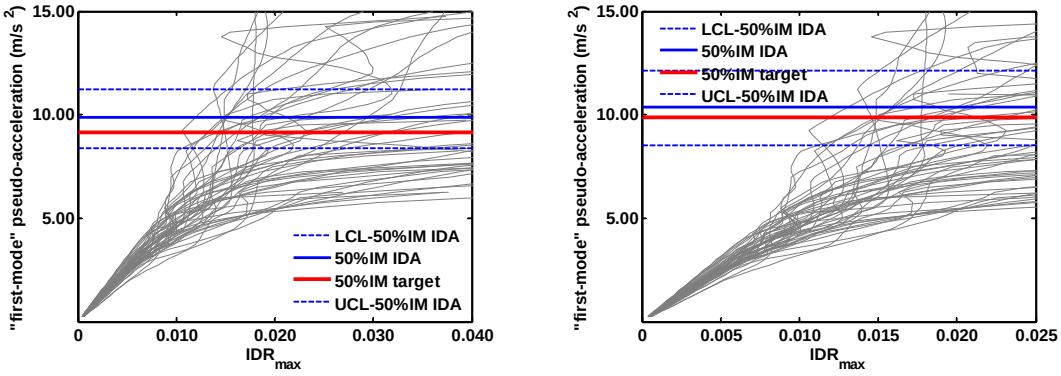

a) **b)**

Figure 4.96 IDA curves and 50% collapse intensities of 8-storey frame with T_1=1.10 s and θ_{AUX}-α=0.100 subjected to the FEMA-P695 set of records: a) near collapse μ=6; b) sidesway collapse $\mu=\mu_c$

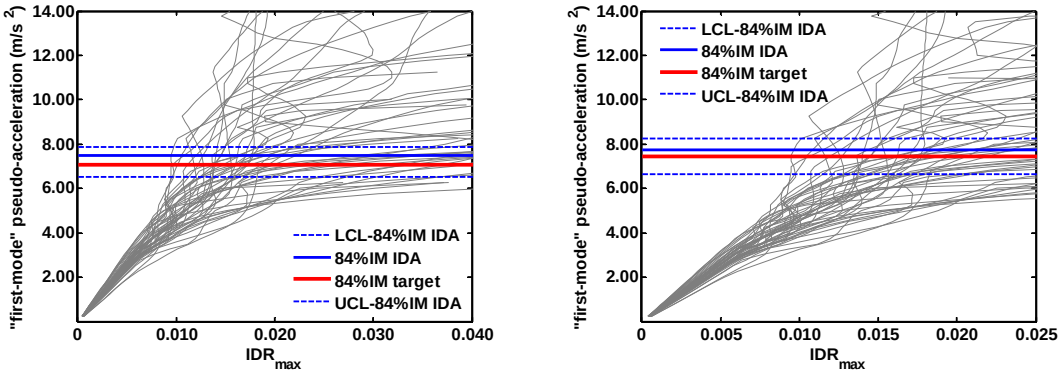

a) **b)**

Figure 4.97 IDA curves and 84% collapse intensities of 8-storey frame with T_1=1.10 s and θ_{AUX}-α=0.100 subjected to the FEMA-P695 set of records: a) near collapse μ=6; b) sidesway collapse $\mu=\mu_c$

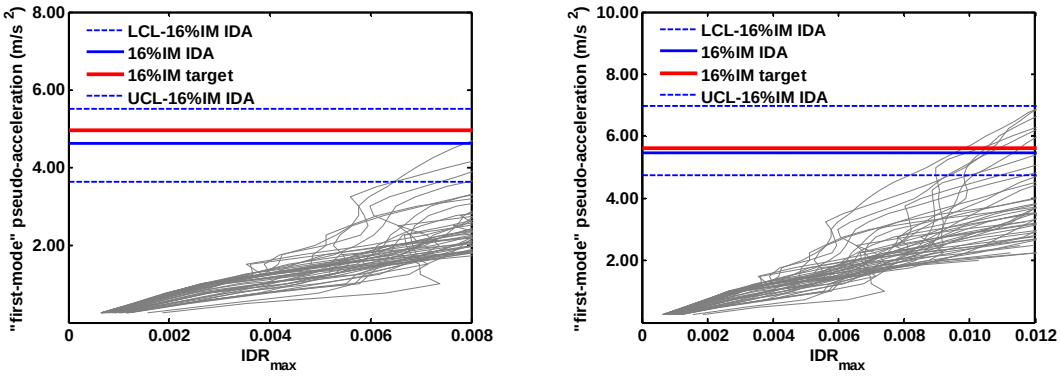

Figure 4.98 IDA curves and 16% collapse intensities of 12-storey frame with T_1=1.60 s and θ_{AUX}-α=0.025 subjected to the FEMA-P695 set of records: a) near collapse μ=4; b) near collapse μ=5

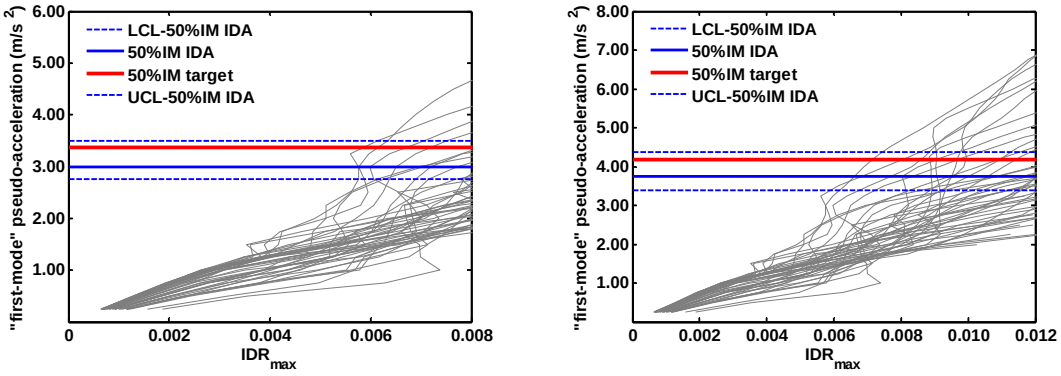

Figure 4.99 IDA curves and 50% collapse intensities of 12-storey frame with T_1=1.60 s and θ_{AUX}-α=0.025 subjected to the FEMA-P695 set of records: a) near collapse μ=4; b) near collapse μ=5

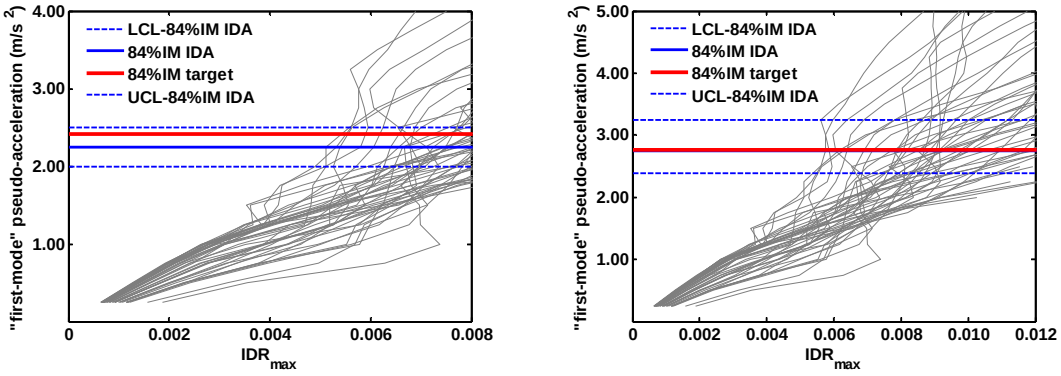

Figure 4.100 IDA curves and 84% collapse intensities of 12-storey frame with T_1=1.60 s and θ_{AUX}-α=0.025 subjected to the FEMA-P695 set of records: a) near collapse μ=4; b) near collapse μ=5

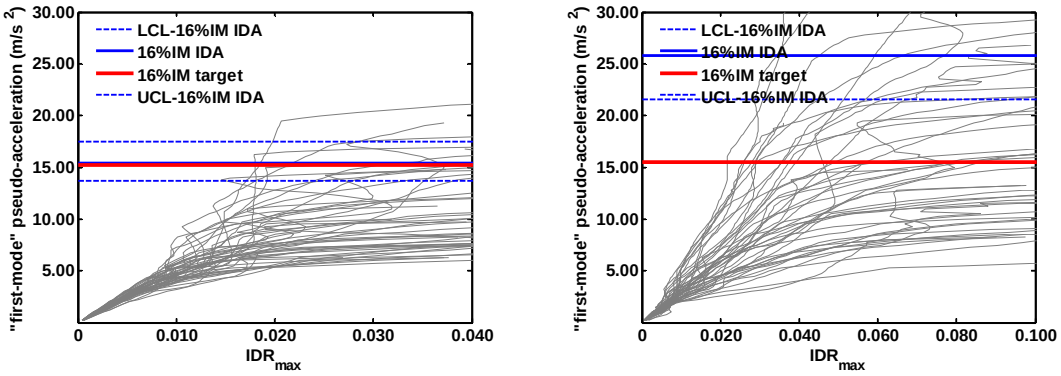

a) **b)**

Figure 4.101 IDA curves and 16% collapse intensities of 12-storey frame with T_1=1.60 s and θ_{AUX}-α=0.025 subjected to the FEMA-P695 set of records: a) near collapse μ=6; b) sidesway collapse $\mu=\mu_c$

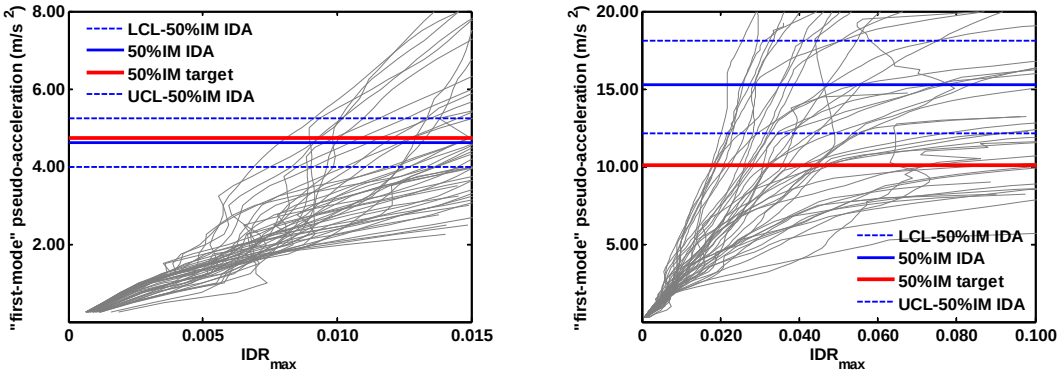

a) **b)**

Figure 4.102 IDA curves and 50% collapse intensities of 12-storey frame with T_1=1.60 s and θ_{AUX}-α=0.025 subjected to the FEMA-P695 set of records: a) near collapse μ=6; b) sidesway collapse $\mu=\mu_c$

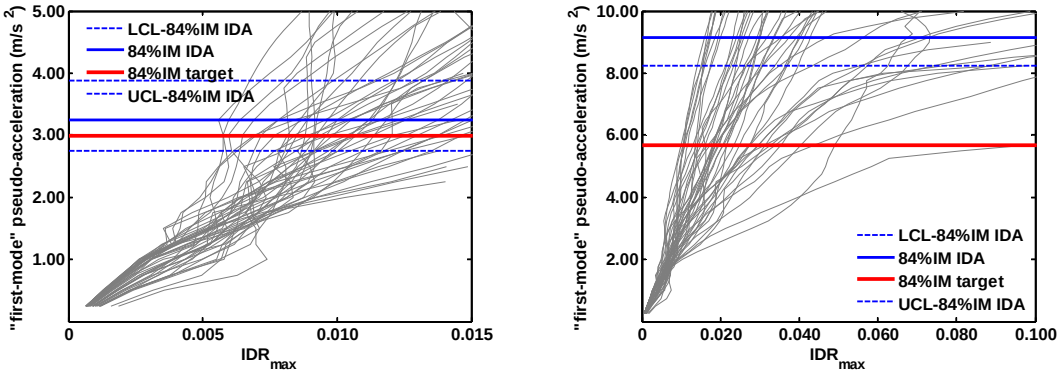

a) **b)**

Figure 4.103 IDA curves and 84% collapse intensities of 12-storey frame with T_1=1.60 s and θ_{AUX}-α=0.025 subjected to the FEMA-P695 set of records: a) near collapse μ=6; b) sidesway collapse $\mu=\mu_c$

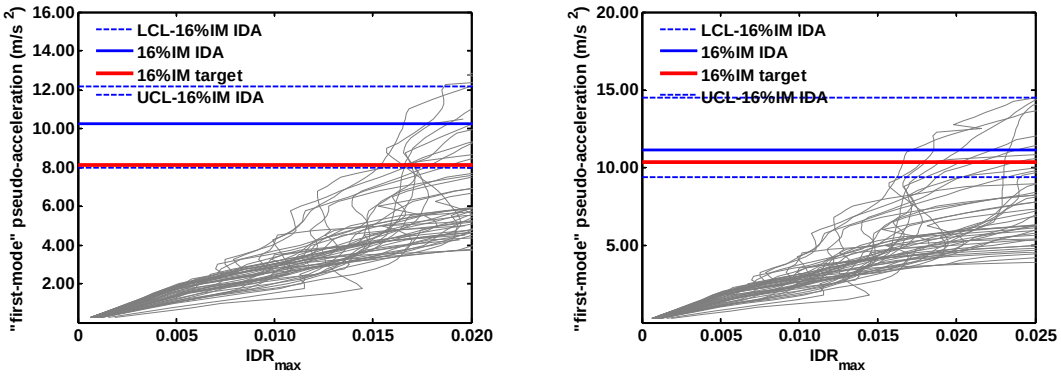

Figure 4.104 IDA curves and 16% collapse intensities of 12-storey frame with T_1=1.60 s and θ_{AUX}-α=0.05 subjected to the FEMA-P695 set of records: a) near collapse μ=4; b) near collapse μ=5

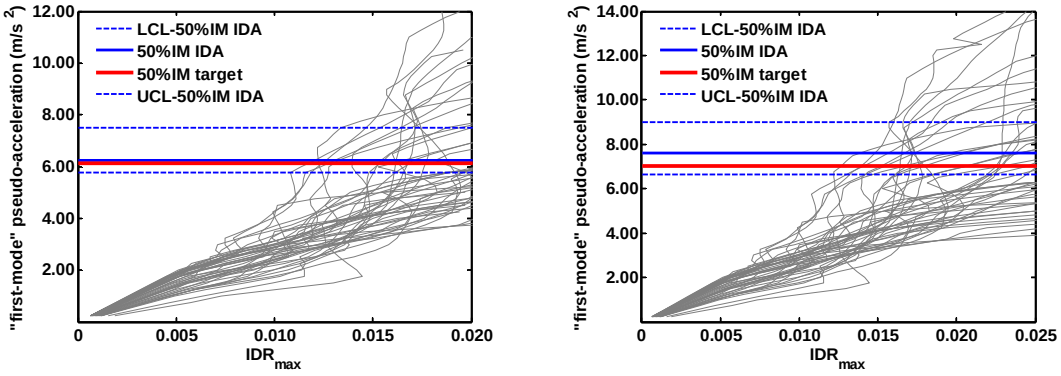

Figure 4.105 IDA curves and 50% collapse intensities of 12-storey frame with T_1=1.60 s and θ_{AUX}-α=0.05 subjected to the FEMA-P695 set of records: a) near collapse μ=4; b) near collapse μ=5

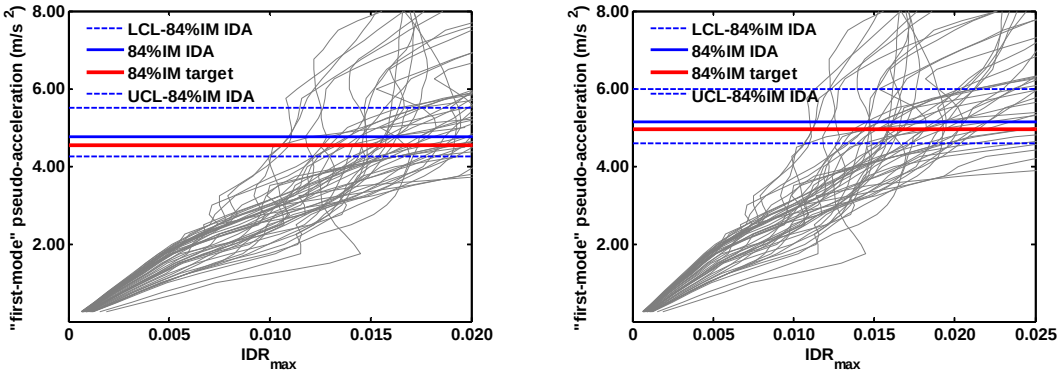

Figure 4.106 IDA curves and 84% collapse intensities of 12-storey frame with T_1=1.60 s and θ_{AUX}-α=0.05 subjected to the FEMA-P695 set of records: a) near collapse μ=4; b) near collapse μ=5

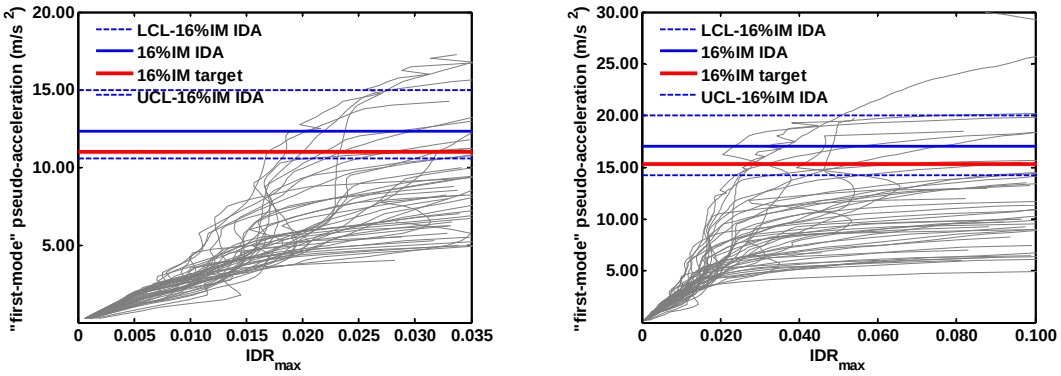

a) b)

Figure 4.107 IDA curves and 16% collapse intensities of 12-storey frame with T_1=1.60 s and θ_{AUX}-α=0.05 subjected to the FEMA-P695 set of records: a) near collapse μ=6; b) sidesway collapse $\mu=\mu_c$

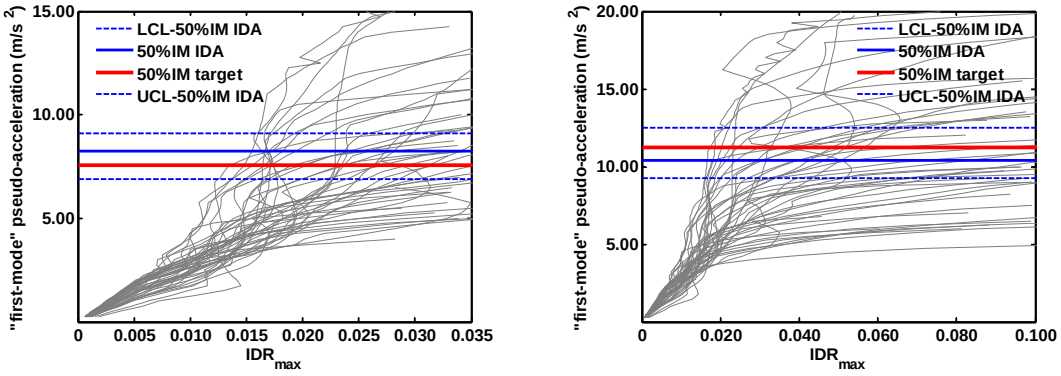

a) b)

Figure 4.108 IDA curves and 50% collapse intensities of 12-storey frame with T_1=1.60 s and θ_{AUX}-α=0.05 subjected to the FEMA-P695 set of records: a) near collapse μ=6; b) sidesway collapse $\mu=\mu_c$

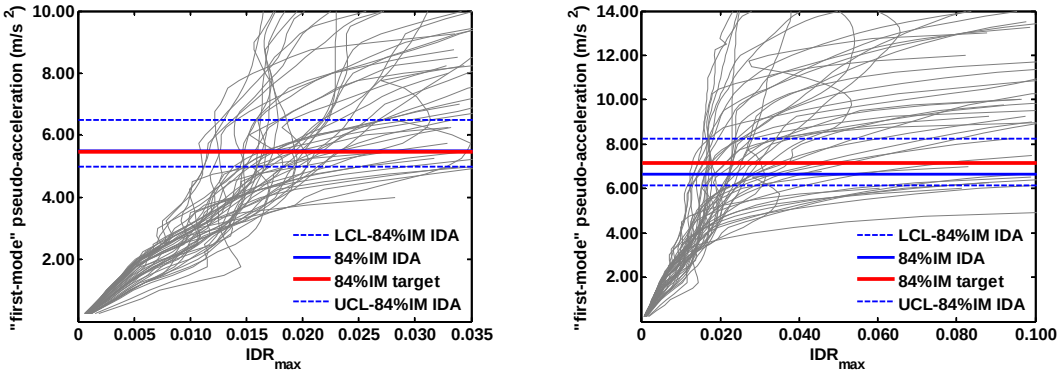

a) b)

Figure 4.109 IDA curves and 84% collapse intensities of 12-storey frame with T_1=1.60 s and θ_{AUX}-α=0.05 subjected to the FEMA-P695 set of records: a) near collapse μ=6; b) sidesway collapse $\mu=\mu_c$

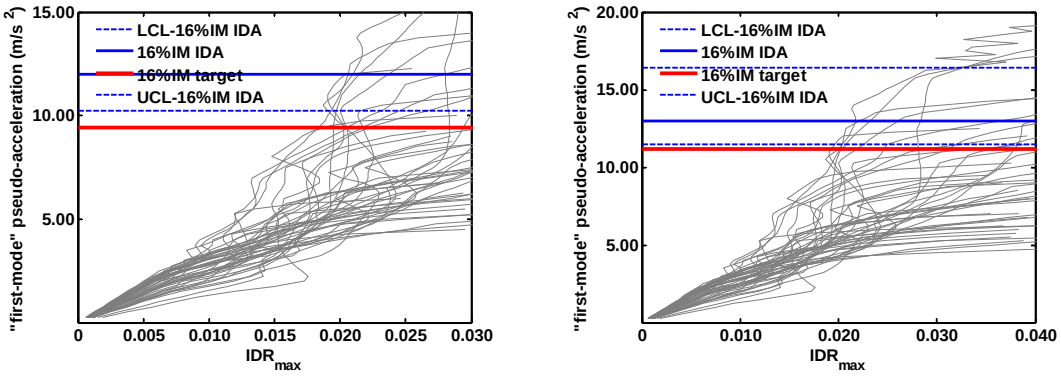

a) b)

Figure 4.110 IDA curves and 16% collapse intensities of 12-storey frame with T_1=1.60 s and θ_{AUX}-α=0.075 subjected to the FEMA-P695 set of records: a) near collapse μ=4; b) near collapse μ=5

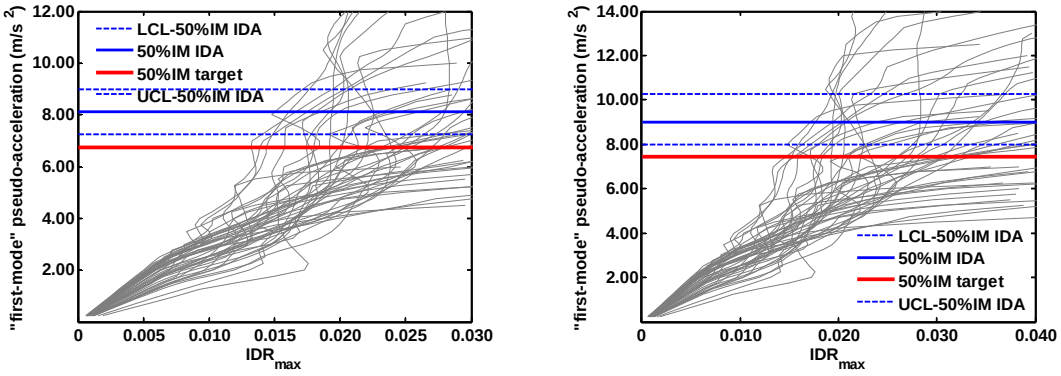

a) b)

Figure 4.111 IDA curves and 50% collapse intensities of 12-storey frame with T_1=1.60 s and θ_{AUX}-α=0.075 subjected to the FEMA-P695 set of records: a) near collapse μ=4; b) near collapse μ=5

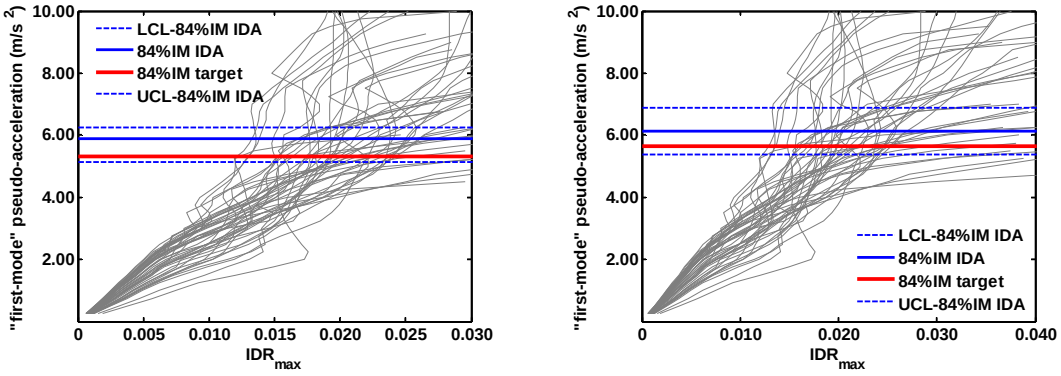

a) b)

Figure 4.112 IDA curves and 84% collapse intensities of 12-storey frame with T_1=1.60 s and θ_{AUX}-α=0.075 subjected to the FEMA-P695 set of records: a) near collapse μ=4; b) near collapse μ=5

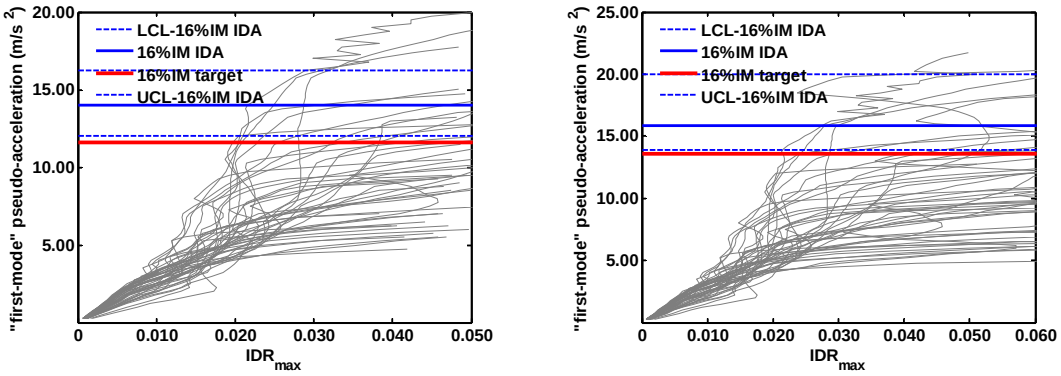

a) b)

Figure 4.113 IDA curves and 16% collapse intensities of 12-storey frame with T_1=1.60 s and θ_{AUX}-α=0.075 subjected to the FEMA-P695 set of records: a) near collapse μ=6; b) sidesway collapse $\mu=\mu_c$

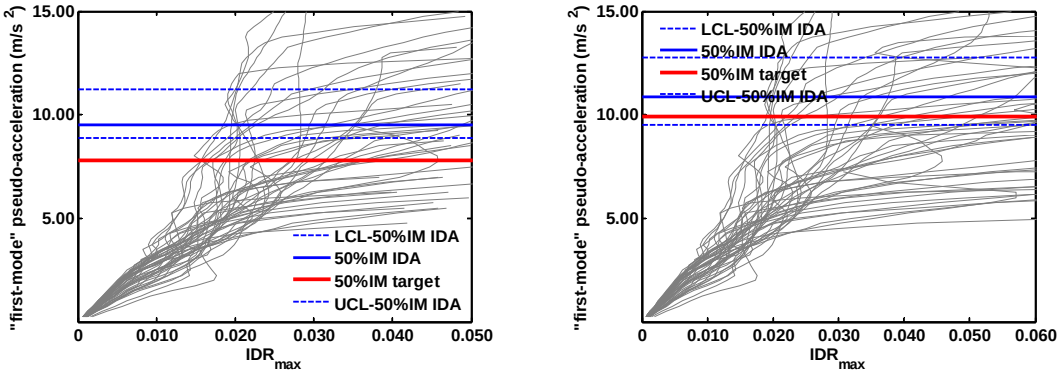

a) b)

Figure 4.114 IDA curves and 50% collapse intensities of 12-storey frame with T_1=1.60 s and θ_{AUX}-α=0.075 subjected to the FEMA-P695 set of records: a) near collapse μ=6; b) sidesway collapse $\mu=\mu_c$

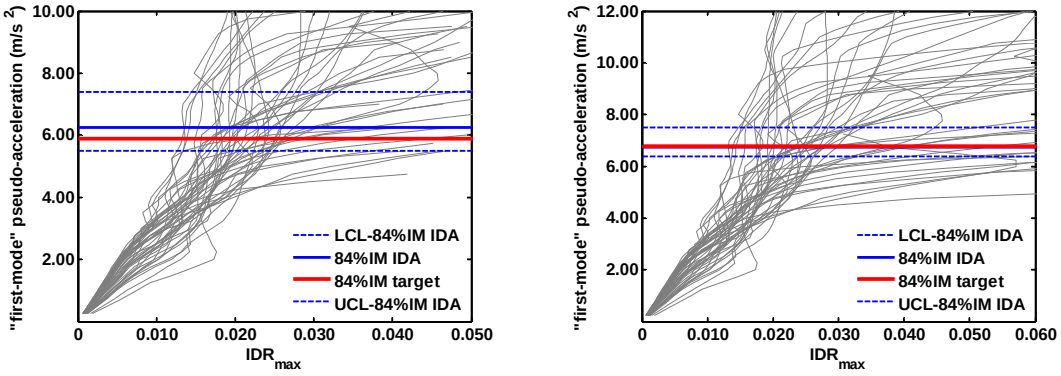

a) b)

Figure 4.115 IDA curves and 84% collapse intensities of 12-storey frame with T_1=1.60 s and θ_{AUX}-α=0.075 subjected to the FEMA-P695 set of records: a) near collapse μ=6; b) sidesway collapse $\mu=\mu_c$

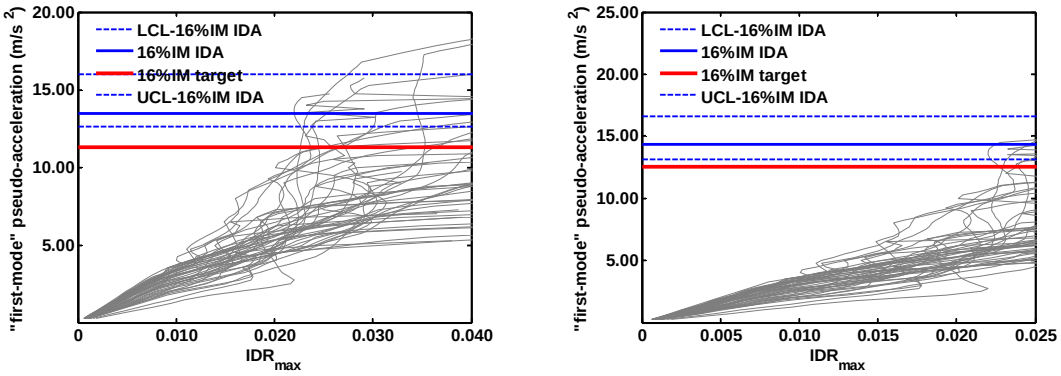

a) **b)**

Figure 4.116 IDA curves and 16% collapse intensities of 12-storey frame with T_1=1.60 s and θ_{AUX}-α=0.100 subjected to the FEMA-P695 set of records: a) near collapse μ=4; b) near collapse μ=5

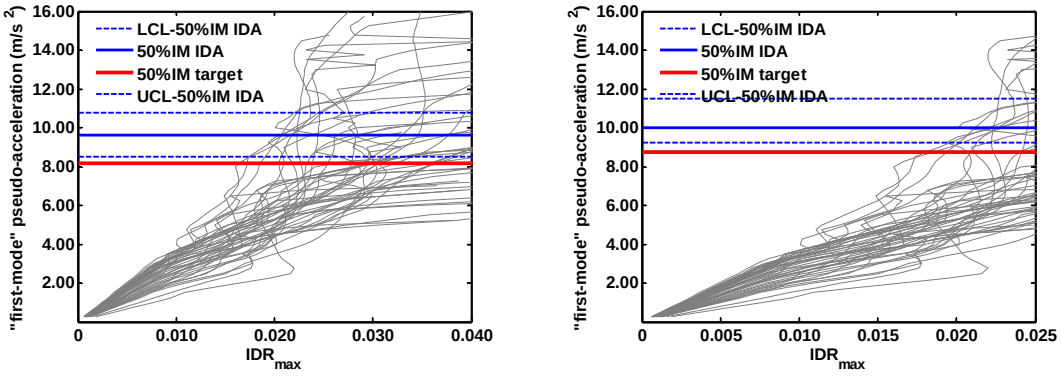

a) **b)**

Figure 4.117 IDA curves and 50% collapse intensities of 12-storey frame with T_1=1.60 s and θ_{AUX}-α=0.100 subjected to the FEMA-P695 set of records: a) near collapse μ=4; b) near collapse μ=5

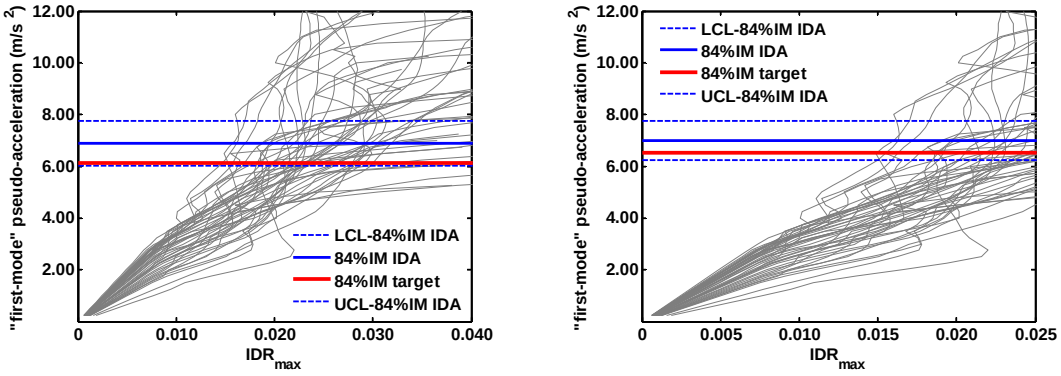

a) **b)**

Figure 4.118 IDA curves and 84% collapse intensities of 12-storey frame with T_1=1.60 s and θ_{AUX}-α=0.100 subjected to the FEMA-P695 set of records: a) near collapse μ=4; b) near collapse μ=5

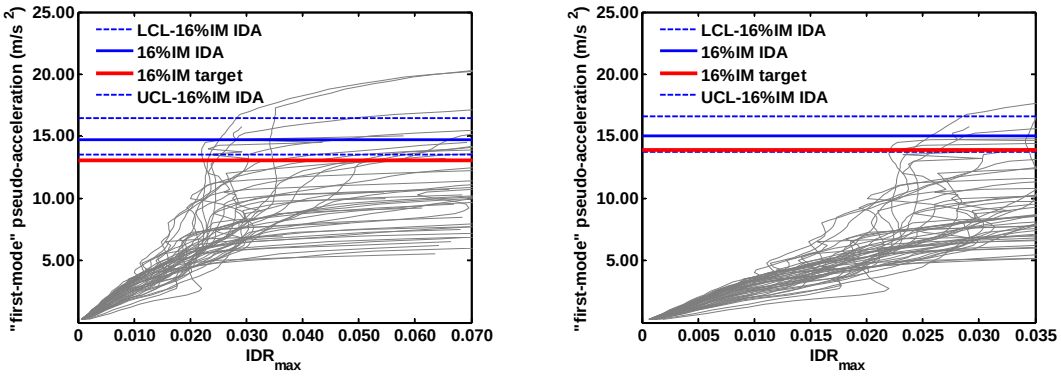

a) b)

Figure 4.119 IDA curves and 16% collapse intensities of 12-storey frame with T_1=1.60 s and θ_{AUX}-α=0.100 subjected to the FEMA-P695 set of records: a) near collapse μ=6; b) sidesway collapse $\mu=\mu_c$

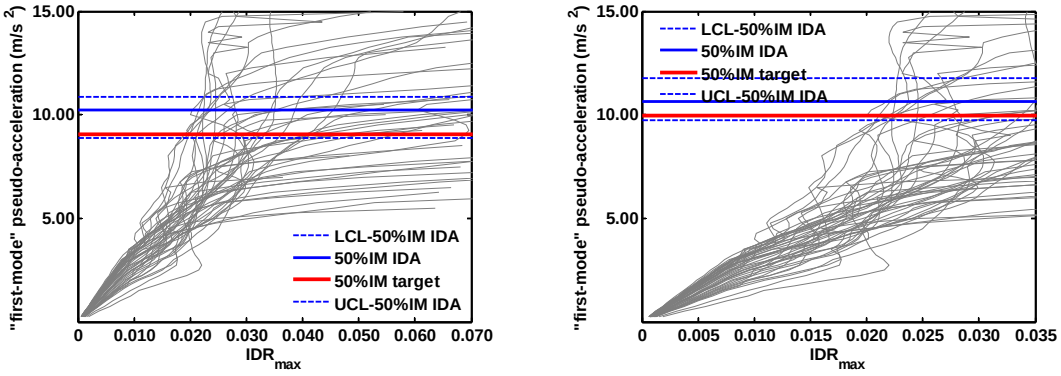

a) b)

Figure 4.120 IDA curves and 50% collapse intensities of 12-storey frame with T_1=1.60 s and θ_{AUX}-α=0.100 subjected to the FEMA-P695 set of records: a) near collapse μ=6; b) sidesway collapse $\mu=\mu_c$

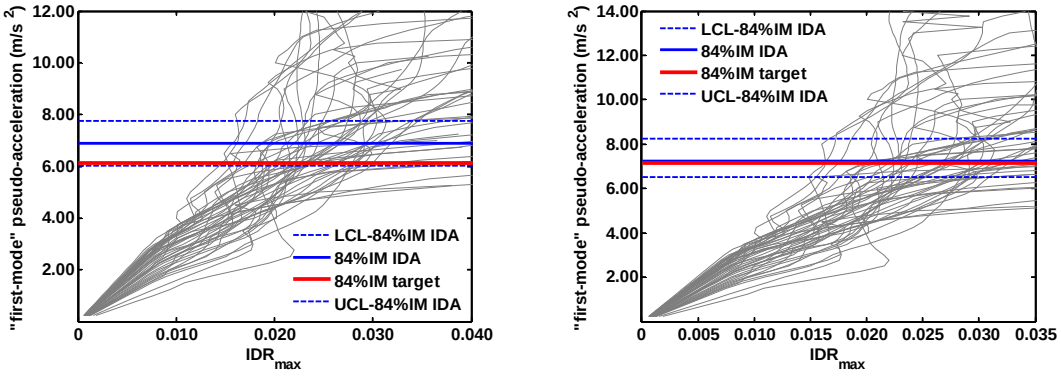

a) b)

Figure 4.121 IDA curves and 84% collapse intensities of 12-storey frame with T_1=1.60 s and θ_{AUX}-α=0.100 subjected to the FEMA-P695 set of records: a) near collapse μ=6; b) sidesway collapse $\mu=\mu_c$

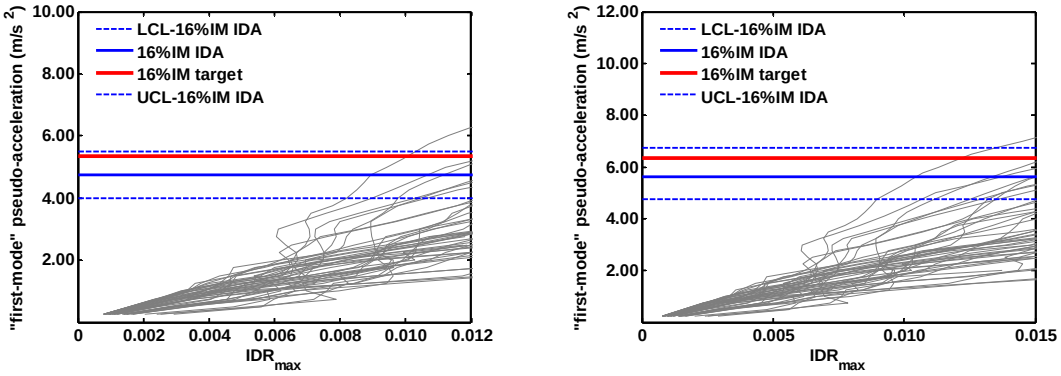

Figure 4.122 IDA curves and 16% collapse intensities of 16-storey frame with T_1=2.00 s and θ_{AUX}-α=0.025 subjected to the FEMA-P695 set of records: a) near collapse μ=4; b) near collapse μ=5

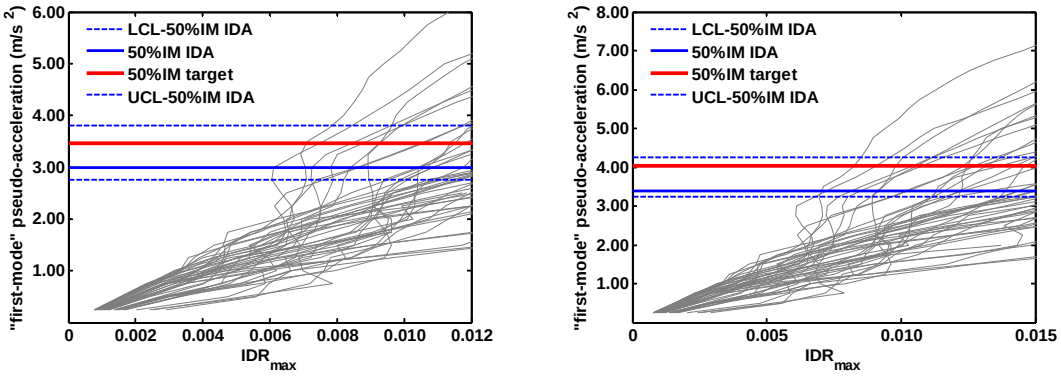

Figure 4.123 IDA curves and 50% collapse intensities of 16-storey frame with T_1=2.00 s and θ_{AUX}-α=0.025 subjected to the FEMA-P695 set of records: a) near collapse μ=4; b) near collapse μ=5

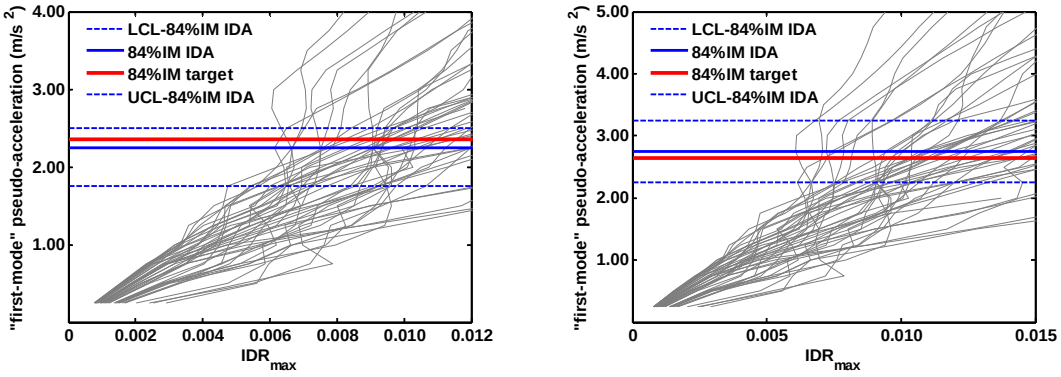

Figure 4.124 IDA curves and 84% collapse intensities of 16-storey frame with T_1=2.00 s and θ_{AUX}-α=0.025 subjected to the FEMA-P695 set of records: a) near collapse μ=4; b) near collapse μ=5

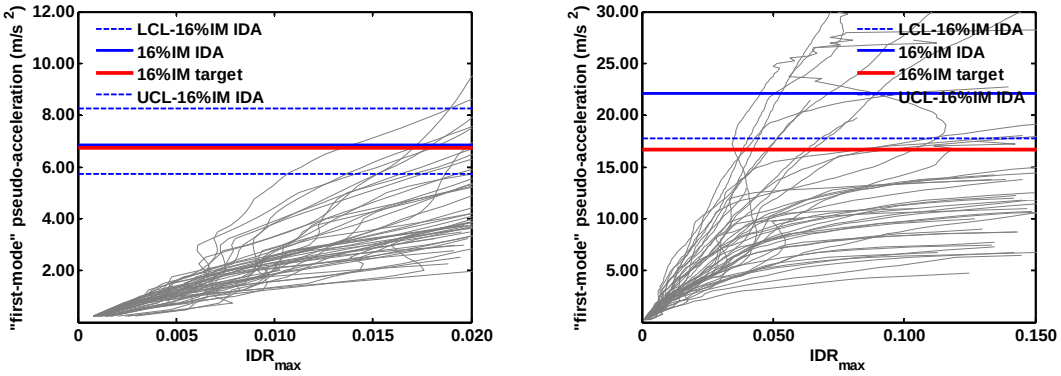

a) **b)**

Figure 4.125 IDA curves and 16% collapse intensities of 16-storey frame with T_1=2.00 s and θ_{AUX}-α=0.025 subjected to the FEMA-P695 set of records: a) near collapse μ=6; b) sidesway collapse $\mu=\mu_c$

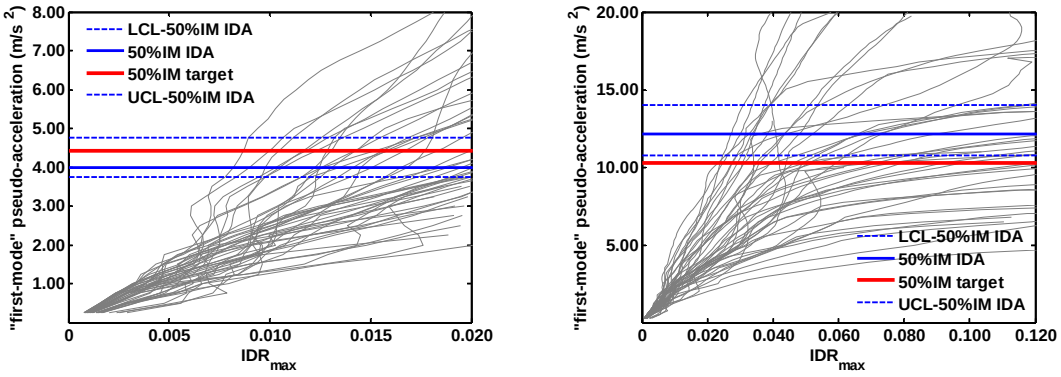

a) **b)**

Figure 4.126 IDA curves and 50% collapse intensities of 16-storey frame with T_1=2.00 s and θ_{AUX}-α=0.025 subjected to the FEMA-P695 set of records: a) near collapse μ=6; b) sidesway collapse $\mu=\mu_c$

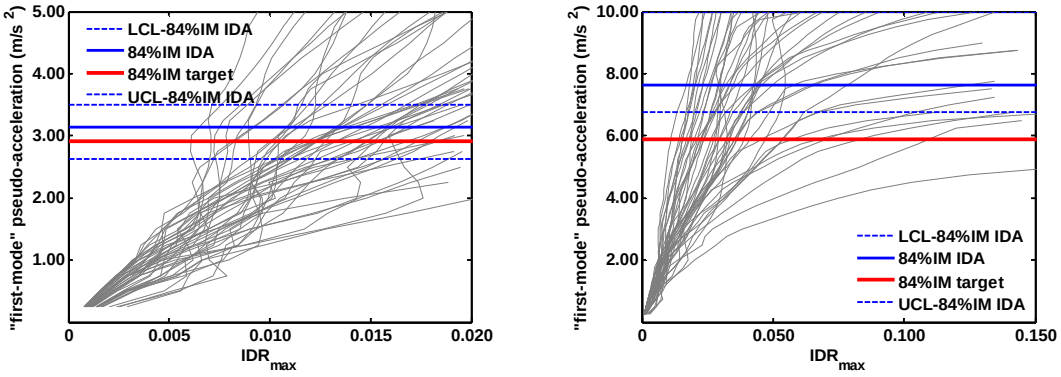

a) **b)**

Figure 4.127 IDA curves and 84% collapse intensities of 16-storey frame with T_1=2.00 s and θ_{AUX}-α=0.025 subjected to the FEMA-P695 set of records: a) near collapse μ=6; b) sidesway collapse $\mu=\mu_c$

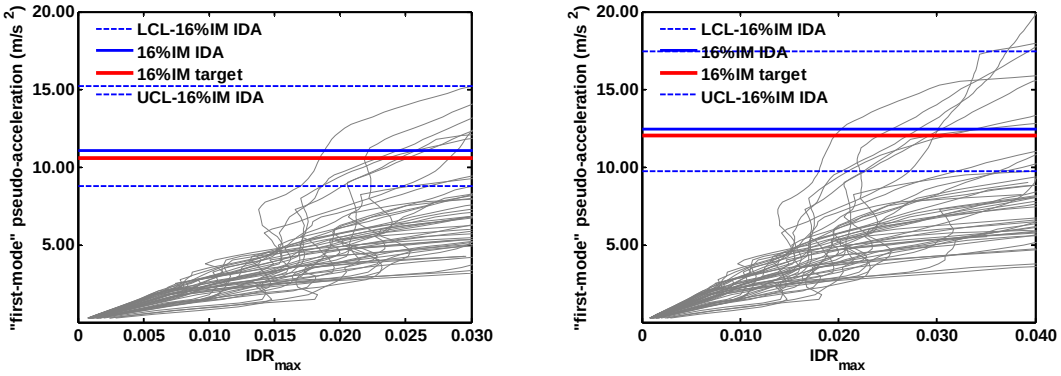

a) b)

Figure 4.128 IDA curves and 16% collapse intensities of 16-storey frame with T_1=2.00 s and θ_{AUX}-α=0.05 subjected to the FEMA-P695 set of records: a) near collapse μ=4; b) near collapse μ=5

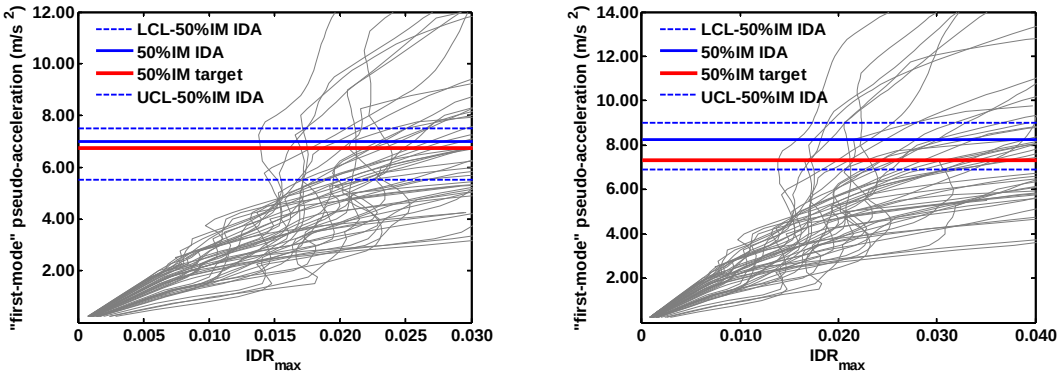

a) b)

Figure 4.129 IDA curves and 50% collapse intensities of 16-storey frame with T_1=2.00 s and θ_{AUX}-α=0.05 subjected to the FEMA-P695 set of records: a) near collapse μ=4; b) near collapse μ=5

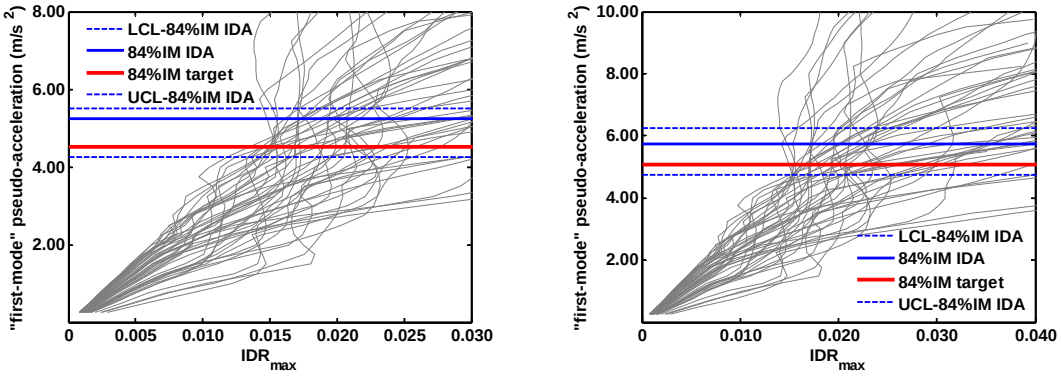

a) b)

Figure 4.130 IDA curves and 84% collapse intensities of 16-storey frame with T_1=2.00 s and θ_{AUX}-α=0.05 subjected to the FEMA-P695 set of records: a) near collapse μ=4; b) near collapse μ=5

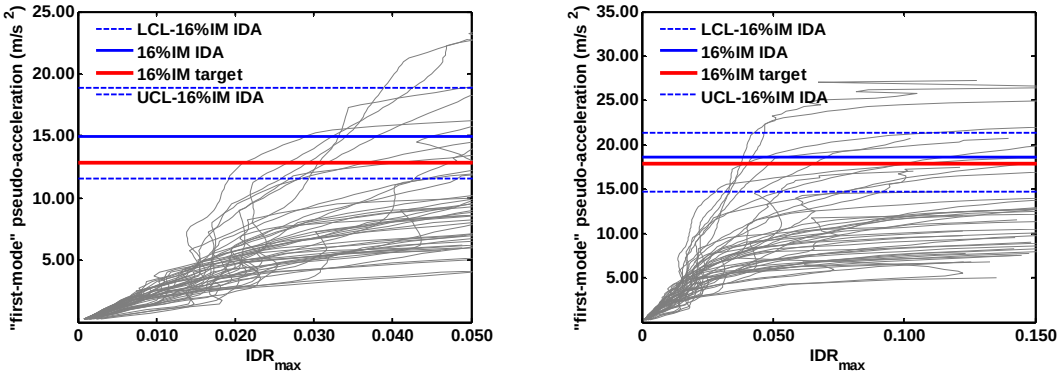

a) **b)**

Figure 4.131 IDA curves and 16% collapse intensities of 16-storey frame with T_1=2.00 s and θ_{AUX}-α=0.05 subjected to the FEMA-P695 set of records: a) near collapse μ=6; b) sidesway collapse $\mu=\mu_c$

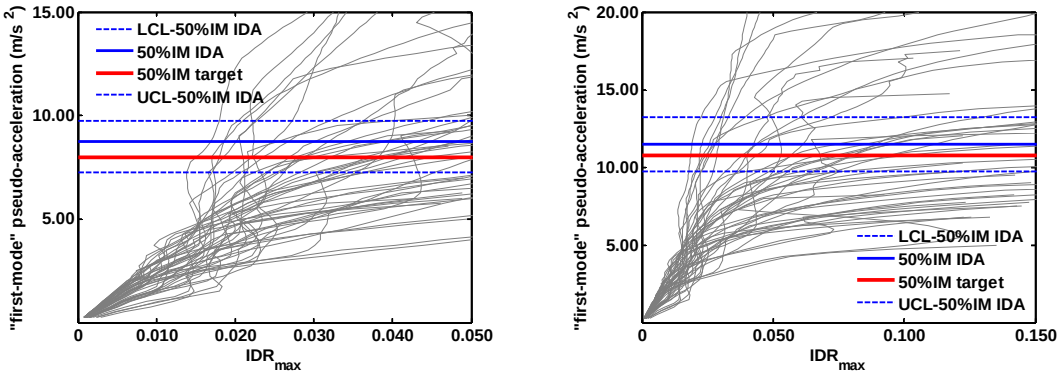

a) **b)**

Figure 4.132 IDA curves and 50% collapse intensities of 16-storey frame with T_1=2.00 s and θ_{AUX}-α=0.05 subjected to the FEMA-P695 set of records: a) near collapse μ=6; b) sidesway collapse $\mu=\mu_c$

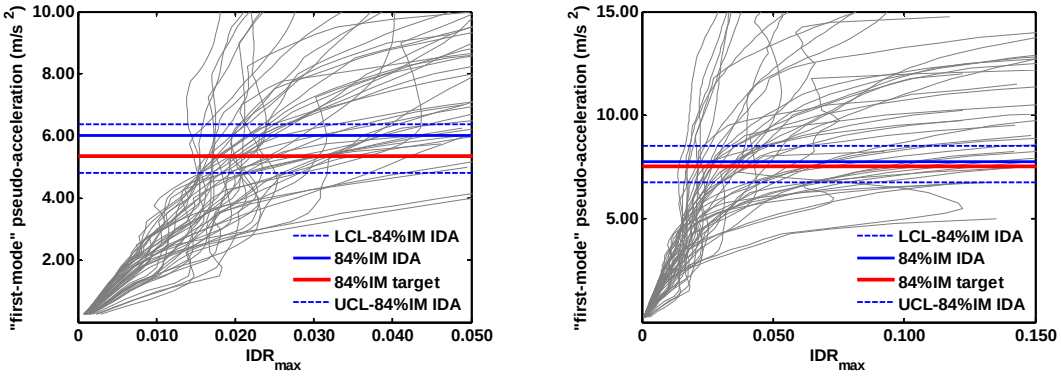

a) **b)**

Figure 4.133 IDA curves and 84% collapse intensities of 16-storey frame with T_1=2.00 s and θ_{AUX}-α=0.05 subjected to the FEMA-P695 set of records: a) near collapse μ=6; b) sidesway collapse $\mu=\mu_c$

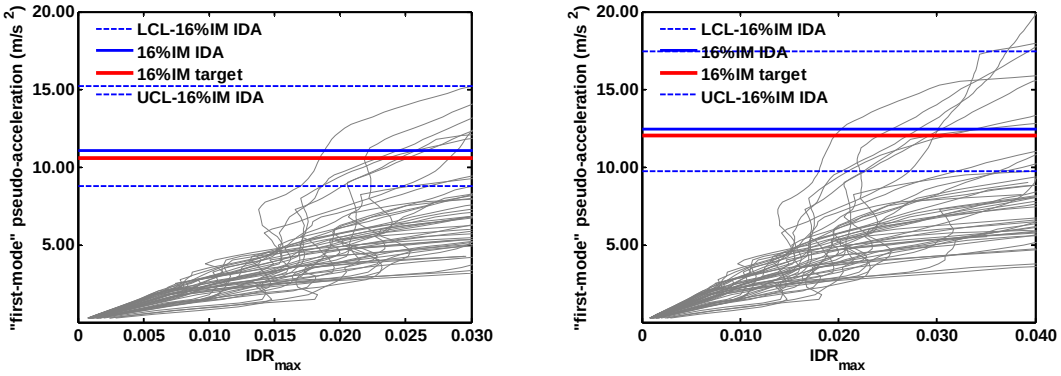

a) b)

Figure 4.134 IDA curves and 16% collapse intensities of 16-storey frame with T_1=2.00 s and θ_{AUX}-α=0.05 subjected to the FEMA-P695 set of records: a) near collapse μ=4; b) near collapse μ=5

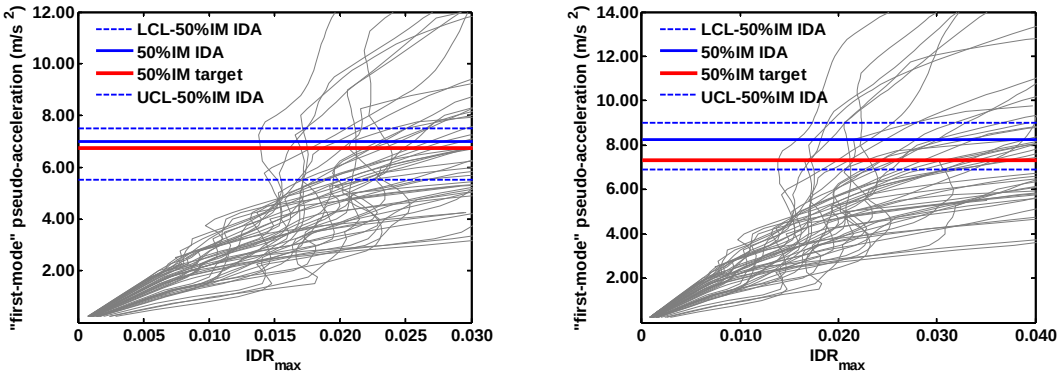

a) b)

Figure 4.135 IDA curves and 50% collapse intensities of 16-storey frame with T_1=2.00 s and θ_{AUX}-α=0.05 subjected to the FEMA-P695 set of records: a) near collapse μ=4; b) near collapse μ=5

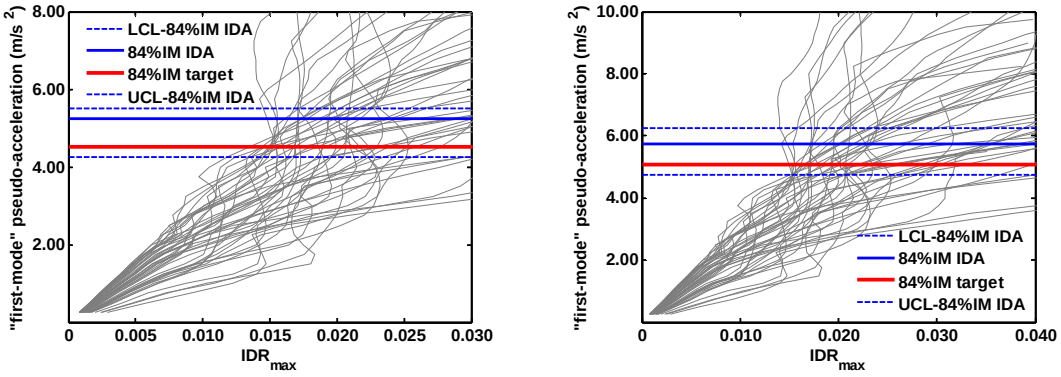

a) b)

Figure 4.136 IDA curves and 84% collapse intensities of 16-storey frame with T_1=2.00 s and θ_{AUX}-α=0.05 subjected to the FEMA-P695 set of records: a) near collapse μ=4; b) near collapse μ=5

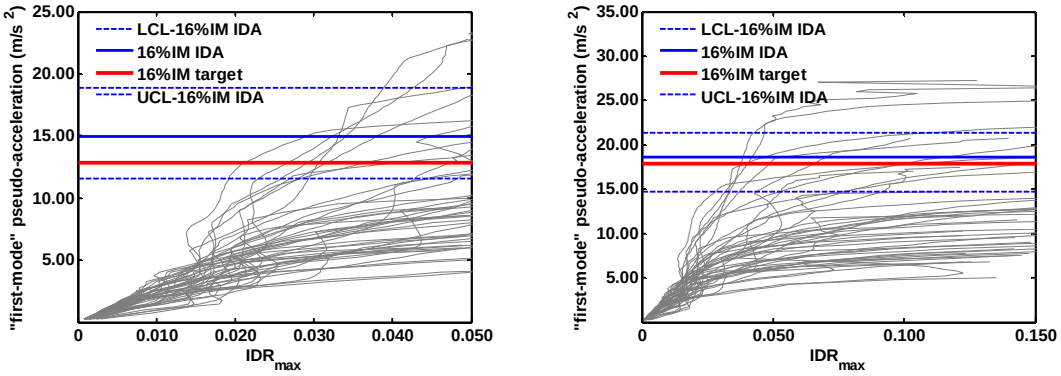

a) b)

Figure 4.137 IDA curves and 16% collapse intensities of 16-storey frame with T_1=2.00 s and θ_{AUX}-α=0.05 subjected to the FEMA-P695 set of records: a) near collapse μ=6; b) sidesway collapse $\mu=\mu_c$

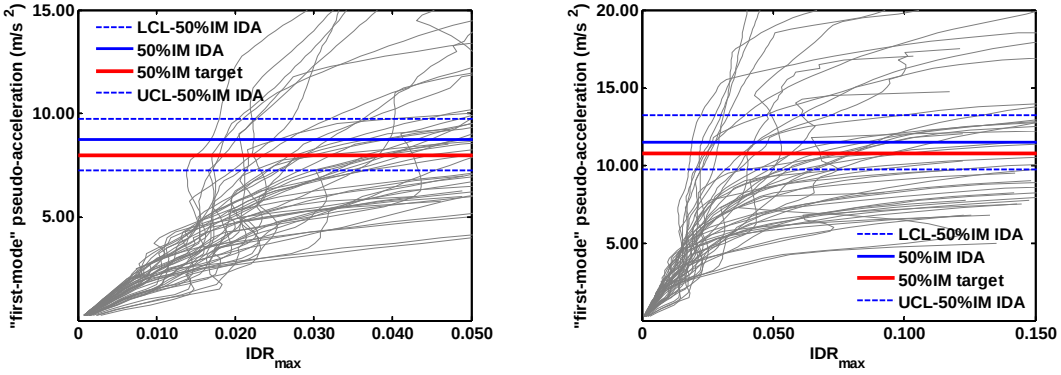

a) b)

Figure 4.138 IDA curves and 50% collapse intensities of 16-storey frame with T_1=2.00 s and θ_{AUX}-α=0.05 subjected to the FEMA-P695 set of records: a) near collapse μ=6; b) sidesway collapse $\mu=\mu_c$

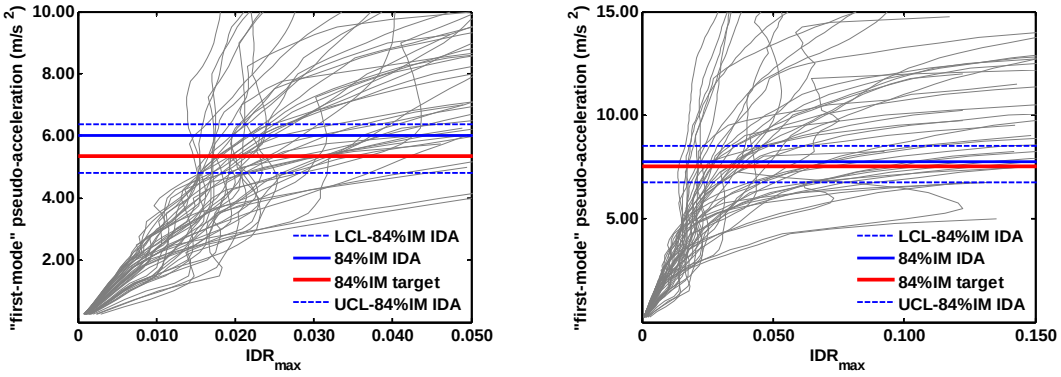

a) b)

Figure 4.139 IDA curves and 84% collapse intensities of 16-storey frame with T_1=2.00 s and θ_{AUX}-α=0.05 subjected to the FEMA-P695 set of records: a) near collapse μ=6; b) sidesway collapse $\mu=\mu_c$

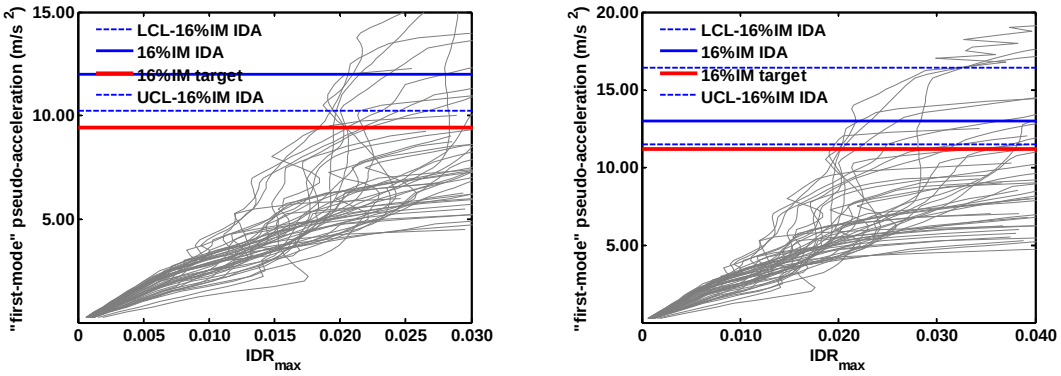

a) b)

Figure 4.140 IDA curves and 16% collapse intensities of 16-storey frame with T_1=2.00 s and θ_{AUX}-α=0.075 subjected to the FEMA-P695 set of records: a) near collapse μ=4; b) near collapse μ=5

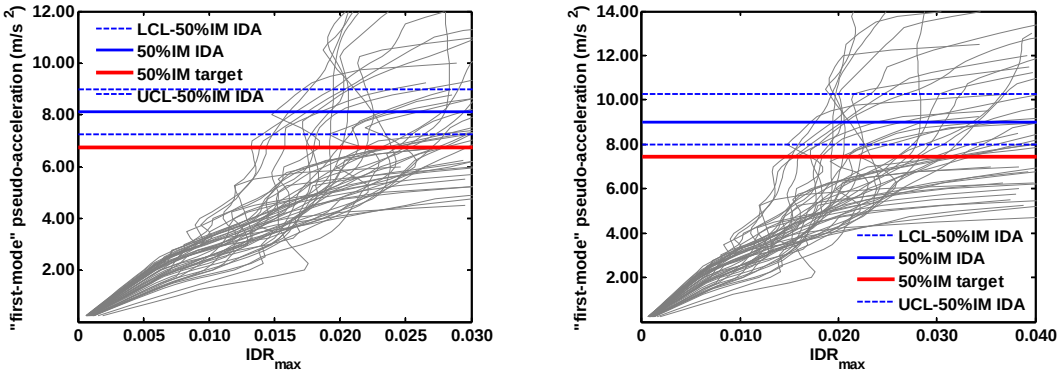

a) b)

Figure 4.141 IDA curves and 50% collapse intensities of 16-storey frame with T_1=2.00 s and θ_{AUX}-α=0.075 subjected to the FEMA-P695 set of records: a) near collapse μ=4; b) near collapse μ=5

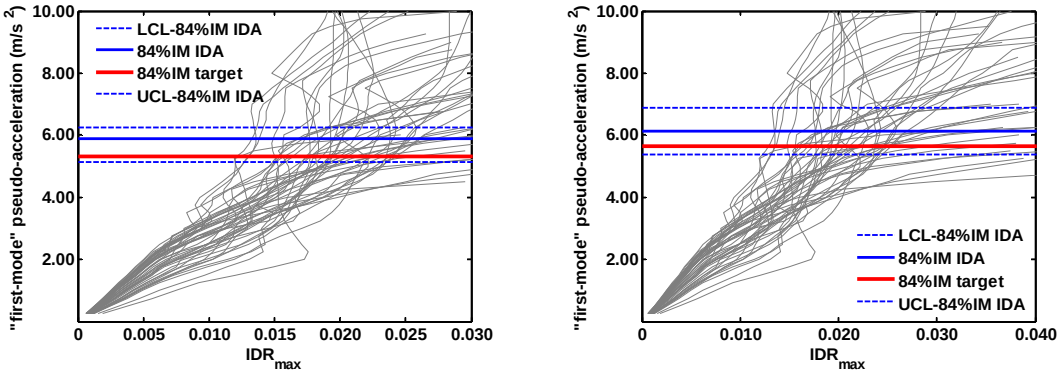

a) b)

Figure 4.142 IDA curves and 84% collapse intensities of 16-storey frame with T_1=2.00 s and θ_{AUX}-α=0.075 subjected to the FEMA-P695 set of records: a) near collapse μ=4; b) near collapse μ=5

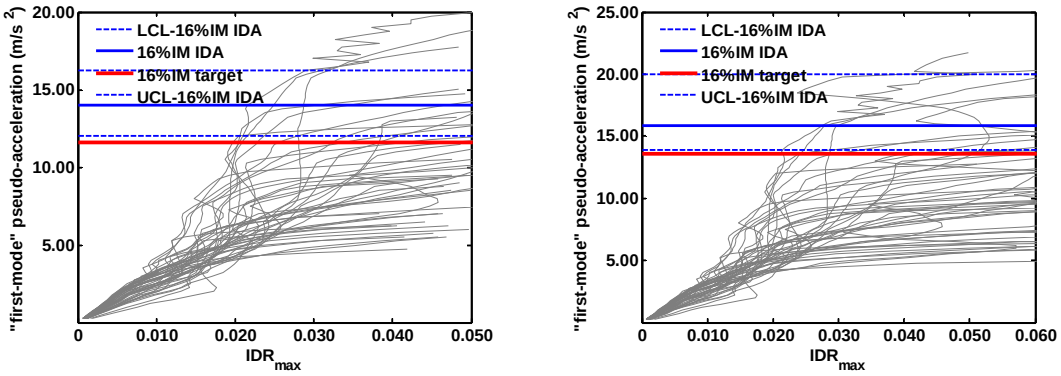

a) **b)**

Figure 4.143 IDA curves and 16% collapse intensities of 16-storey frame with T_1=2.00 s and θ_{AUX}-α=0.075 subjected to the FEMA-P695 set of records: a) near collapse μ=6; b) sidesway collapse $\mu=\mu_c$

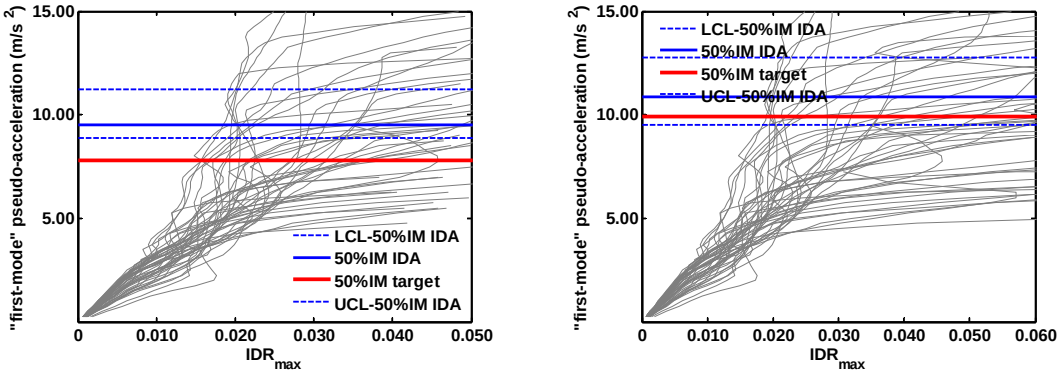

a) **b)**

Figure 4.144 IDA curves and 50% collapse intensities of 16-storey frame with T_1=2.00 s and θ_{AUX}-α=0.075 subjected to the FEMA-P695 set of records: a) near collapse μ=6; b) sidesway collapse $\mu=\mu_c$

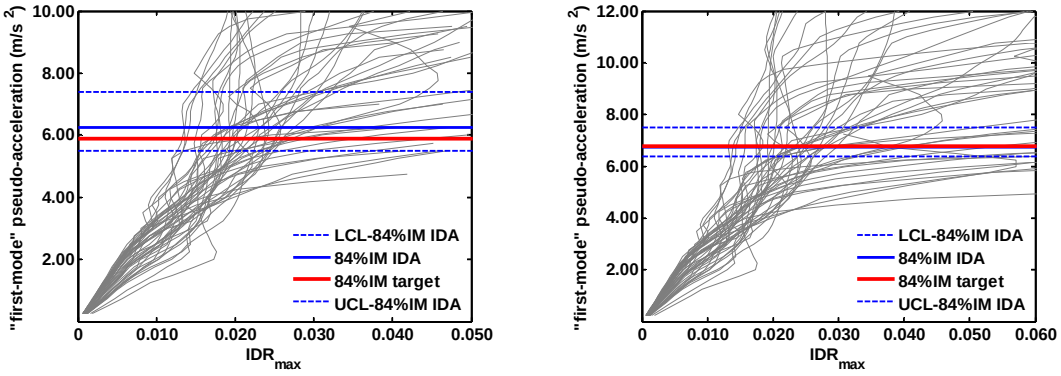

a) **b)**

Figure 4.145 IDA curves and 84% collapse intensities of 16-storey frame with T_1=2.00 s and θ_{AUX}-α=0.075 subjected to the FEMA-P695 set of records: a) near collapse μ=6; b) sidesway collapse $\mu=\mu_c$

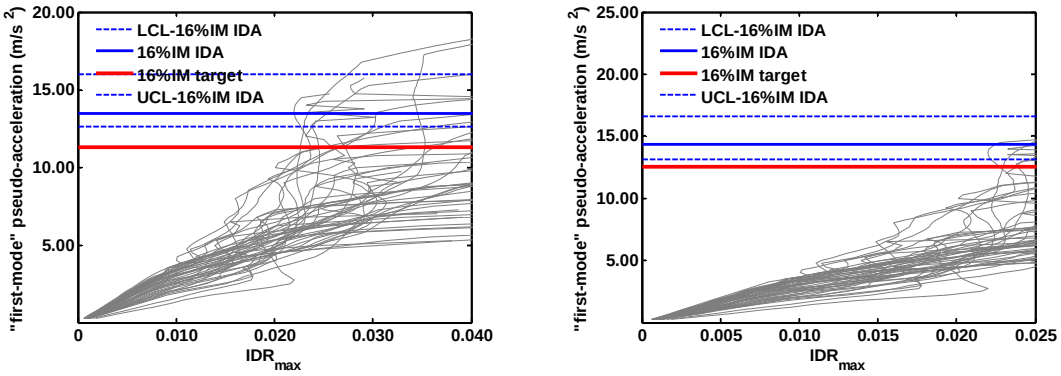

a) b)

Figure 4.146 IDA curves and 16% collapse intensities of 16-storey frame with T_1=2.00 s and θ_{AUX}-α=0.100 subjected to the FEMA-P695 set of records: a) near collapse μ=4; b) near collapse μ=5

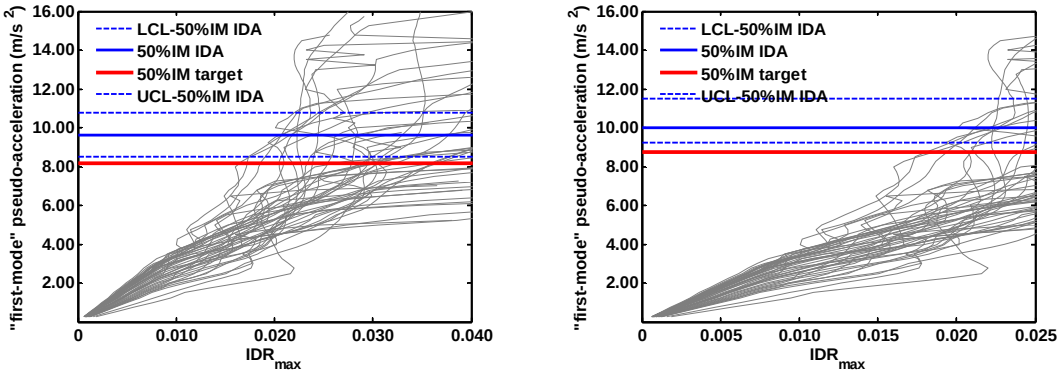

a) b)

Figure 4.147 IDA curves and 50% collapse intensities of 16-storey frame with T_1=2.00 s and θ_{AUX}-α=0.100 subjected to the FEMA-P695 set of records: a) near collapse μ=4; b) near collapse μ=5

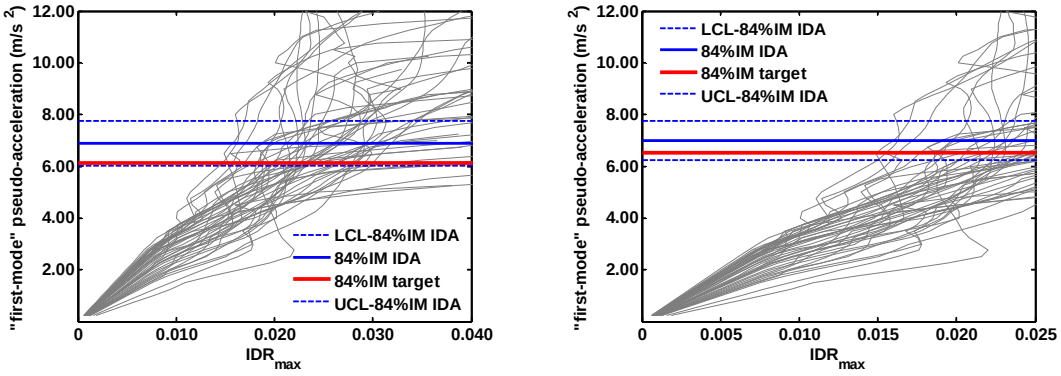

a) b)

Figure 4.148 IDA curves and 84% collapse intensities of 16-storey frame with T_1=2.00 s and θ_{AUX}-α=0.100 subjected to the FEMA-P695 set of records: a) near collapse μ=4; b) near collapse μ=5

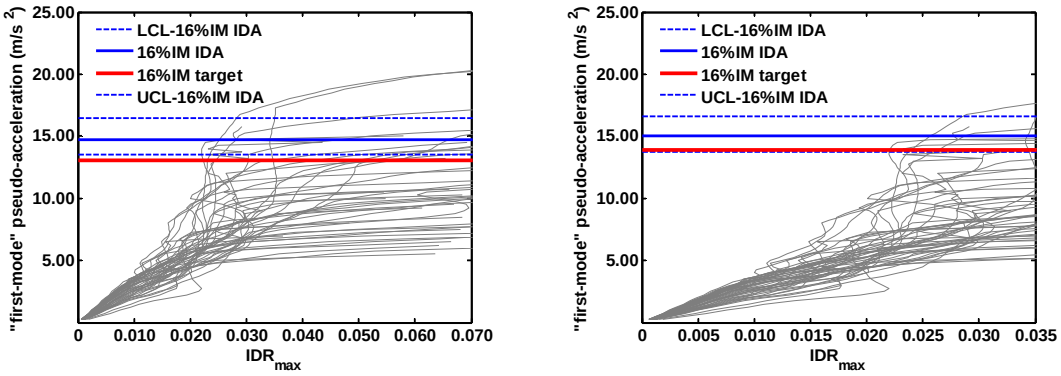

a) b)

Figure 4.149 IDA curves and 16% collapse intensities of 16-storey frame with T_1=2.00 s and θ_{AUX}-α=0.100 subjected to the FEMA-P695 set of records: a) near collapse μ=6; b) sidesway collapse $\mu=\mu_c$

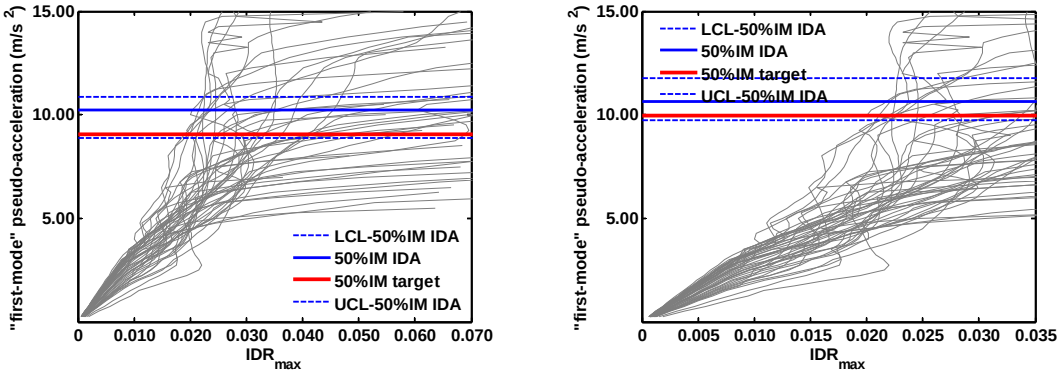

a) b)

Figure 4.150 IDA curves and 50% collapse intensities of 16-storey frame with T_1=2.00 s and θ_{AUX}-α=0.100 subjected to the FEMA-P695 set of records: a) near collapse μ=6; b) sidesway collapse $\mu=\mu_c$

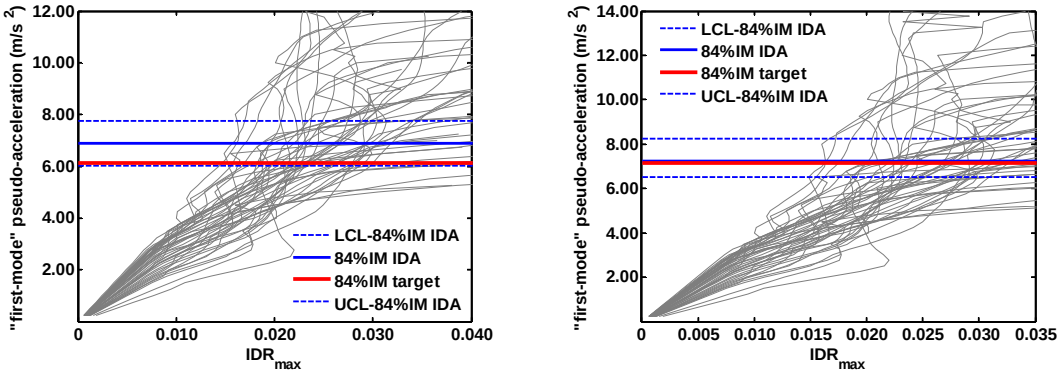

a) b)

Figure 4.151 IDA curves and 84% collapse intensities of 16-storey frame with T_1=2.00 s and θ_{AUX}-α=0.100 subjected to the FEMA-P695 set of records: a) near collapse μ=6; b) sidesway collapse $\mu=\mu_c$

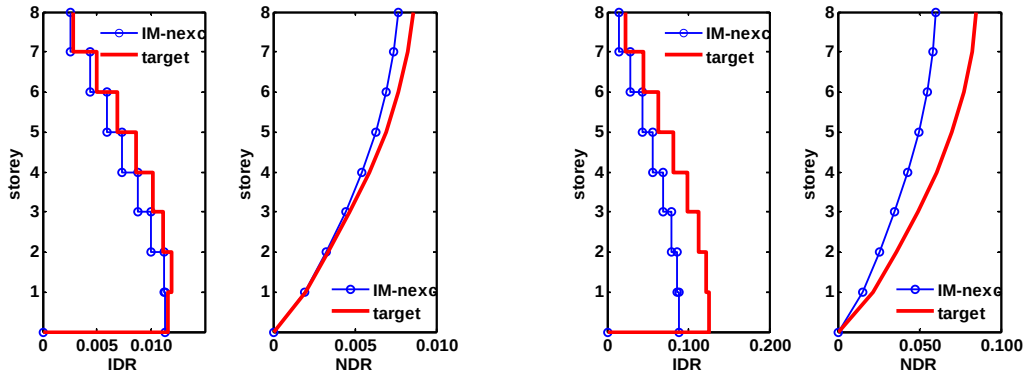

Figure 4.152 Displacement and interstorey drift profiles (median) of 8-storey frame with T_1=1.40 s and θ_{AUX}-α=0.025 subjected to the VM set of records: a) near collapse μ=4; b) sidesway collapse $\mu=\mu_c$

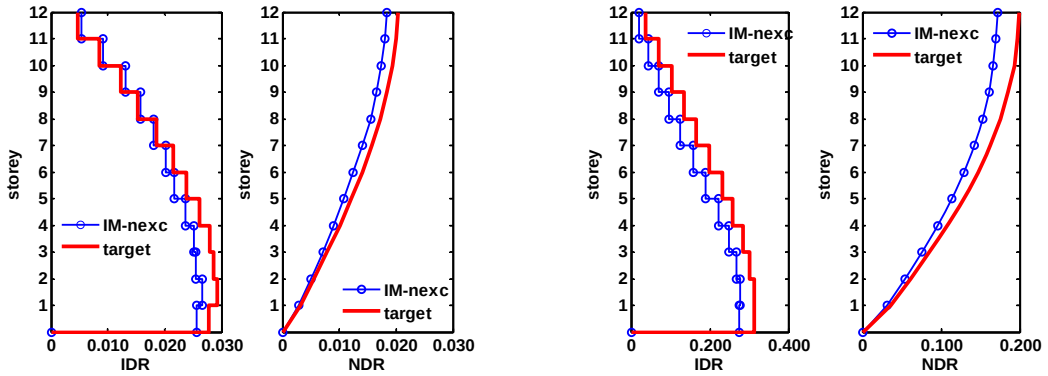

Figure 4.153 Displacement and interstorey drift profiles (median) of 12-storey frame with T_1=1.90 s and θ_{AUX}-α=0.025 subjected to the VM set of records: a) near collapse μ=4; b) sidesway collapse $\mu=\mu_c$

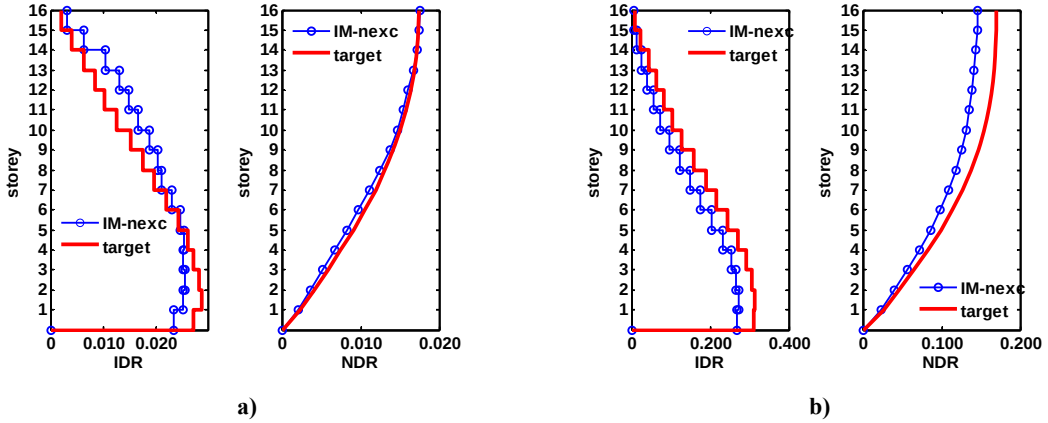

Figure 4.154 Displacement and interstorey drift profiles (median) of 16-storey frame with T_1=2.30 s and θ_{AUX}-α=0.025 subjected to the VM set of records: a) near collapse μ=4; b) sidesway collapse $\mu=\mu_c$

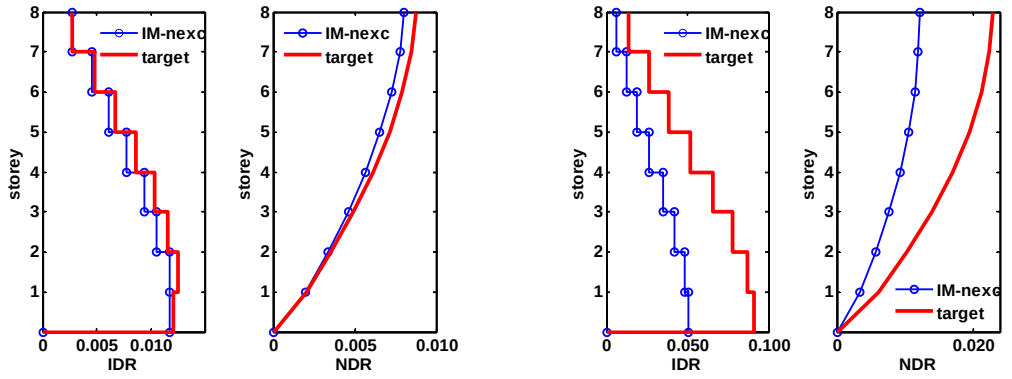

Figure 4.155 Displacement and interstorey drift profiles (median) of 8-storey frame with T_1=1.40 s and θ_{AUX}-α=0.05 subjected to the VM set of records: a) near collapse μ=4; b) sidesway collapse $\mu=\mu_c$

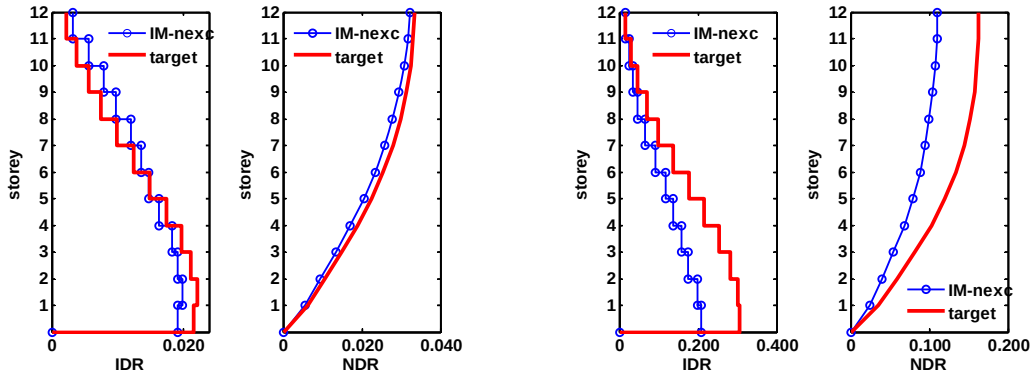

Figure 4.156 Displacement and interstorey drift profiles (median) of 12-storey frame with T_1=1.90 s and θ_{AUX}-α=0.05 subjected to the VM set of records: a) near collapse μ=4; b) sidesway collapse $\mu=\mu_c$

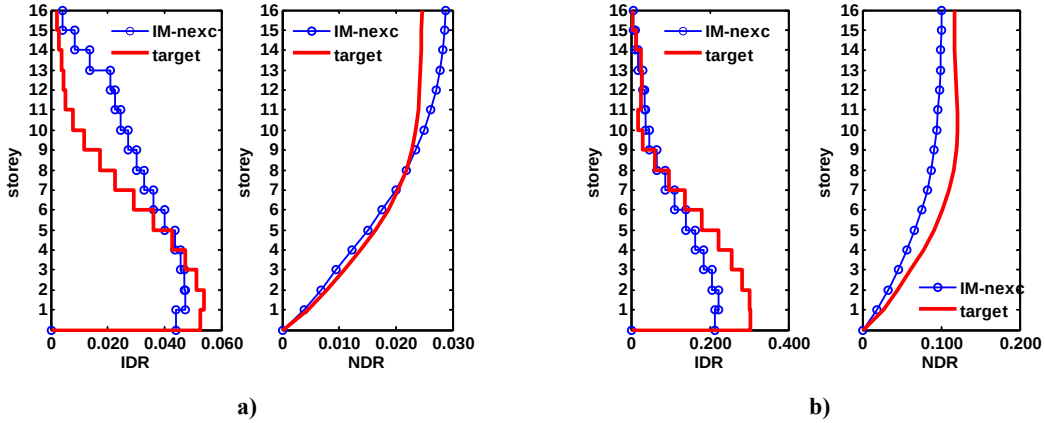

Figure 4.157 Displacement and interstorey drift profiles (median) of 16-storey frame with T_1=2.30 s and θ_{AUX}-α=0.05 subjected to the VM set of records: a) near collapse μ=4; b) sidesway collapse $\mu=\mu_c$

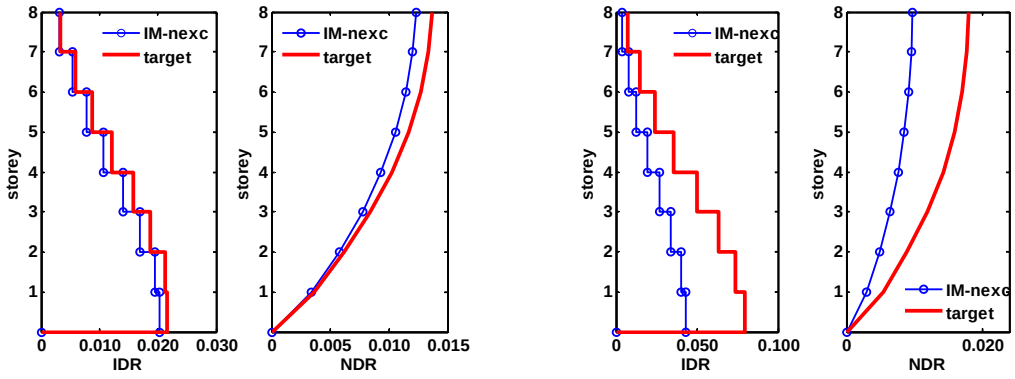

Figure 4.158 Displacement and interstorey drift profiles (median) of 8-storey frame with T_1=1.40 s and θ_{AUX}-α=0.075 subjected to the VM set of records: a) near collapse μ=4; b) sidesway collapse $\mu=\mu_c$

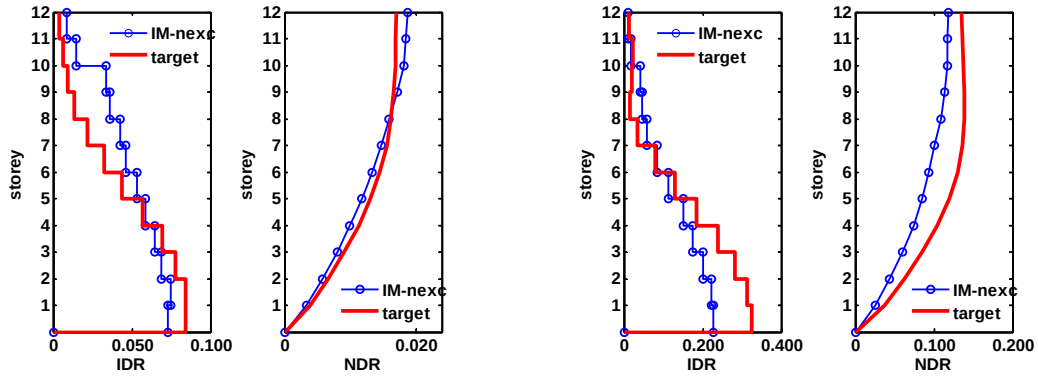

Figure 4.159 Displacement and interstorey drift profiles (median) of 12-storey frame with T_1=1.90 s and θ_{AUX}-α=0.075 subjected to the VM set of records: a) near collapse μ=4; b) sidesway collapse $\mu=\mu_c$

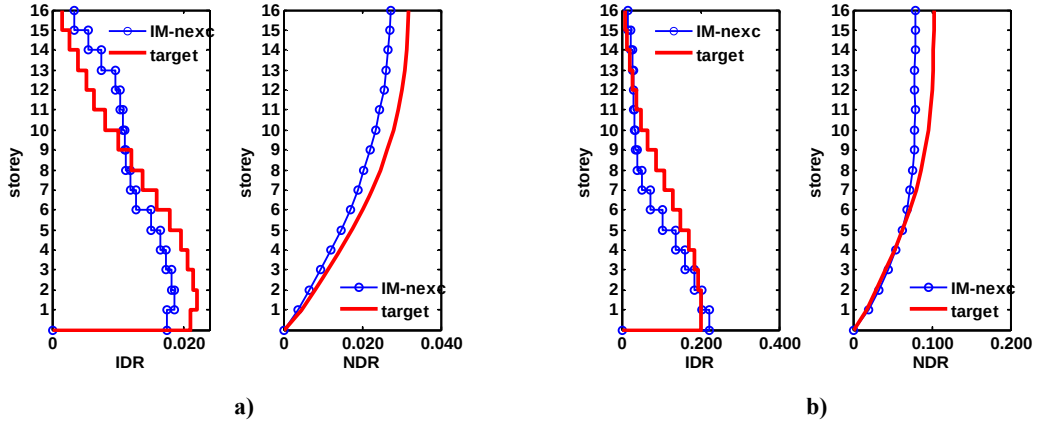

Figure 4.160 Displacement and interstorey drift profiles (median) of 16-storey frame with T_1=2.30 s and θ_{AUX}-α=0.075 subjected to the VM set of records: a) near collapse μ=4; b) sidesway collapse $\mu=\mu_c$

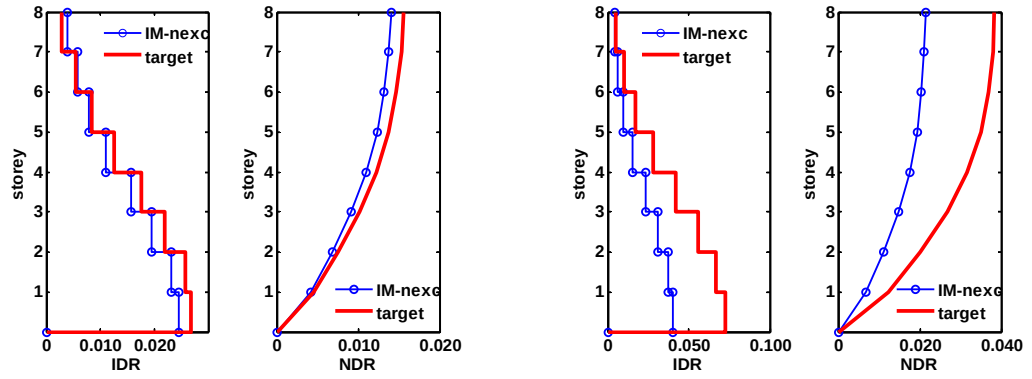

Figure 4.161 Displacement and interstorey drift profiles (median) of 8-storey frame with T_1=1.40 s and θ_{AUX}-α=0.100 subjected to the VM set of records: a) near collapse μ=4; b) sidesway collapse $\mu=\mu_c$

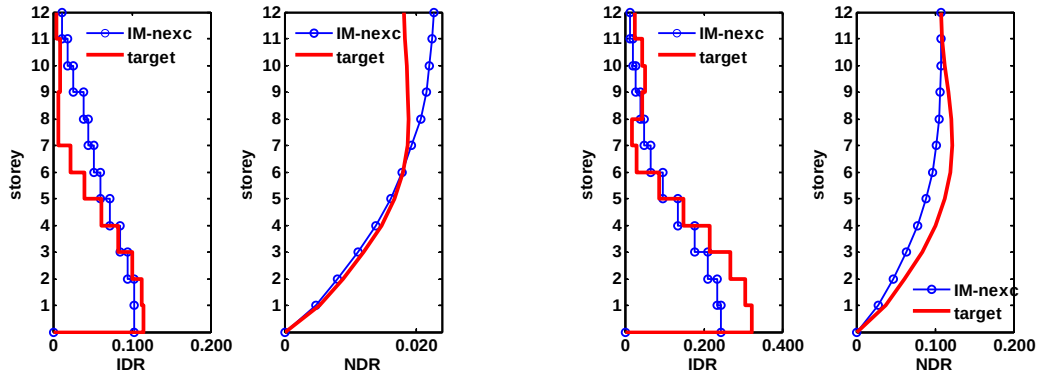

Figure 4.162 Displacement and interstorey drift profiles (median) of 12-storey frame with T_1=1.90 s and θ_{AUX}-α=0.100 subjected to the VM set of records: a) near collapse μ=4; b) sidesway collapse $\mu=\mu_c$

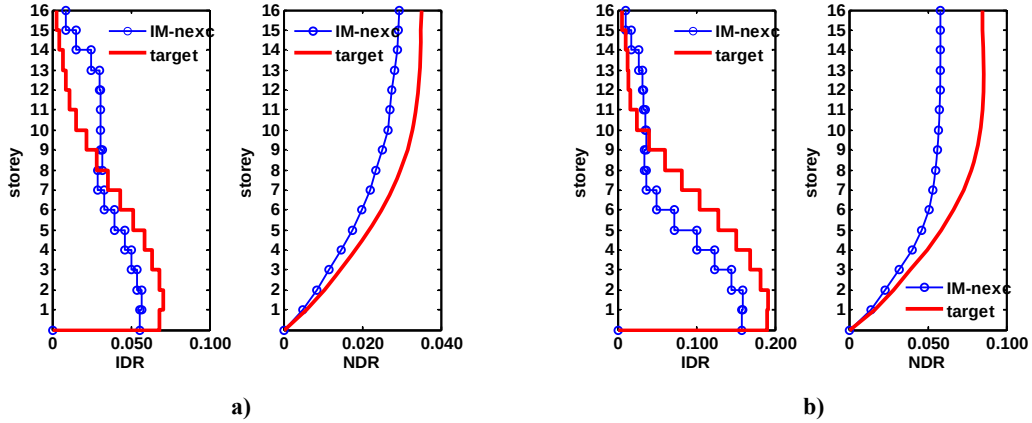

Figure 4.163 Displacement and interstorey drift profiles (median) of 16-storey frame with T_1=2.30 s and θ_{AUX}-α=0.100 subjected to the VM set of records: a) near collapse μ=4; b) sidesway collapse $\mu=\mu_c$

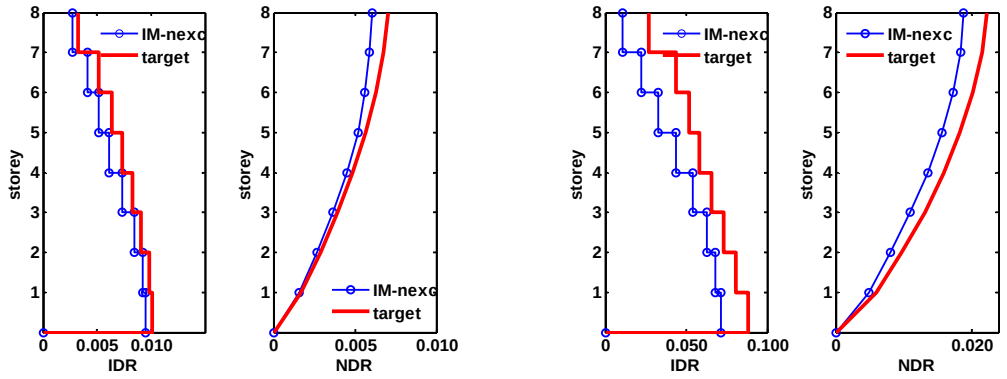

a) b)

Figure 4.164 Displacement and interstorey drift profiles (median) of 8-storey frame with T_1=1.10 s and θ_{AUX}-α=0.025 subjected to the FEMA-P695 set of records: a) near collapse μ=5; b) sidesway collapse $\mu=\mu_c$

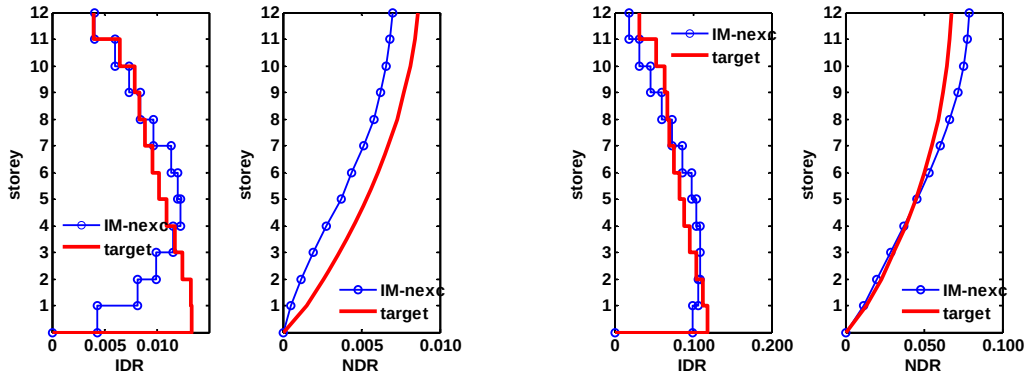

a) b)

Figure 4.165 Displacement and interstorey drift profiles (median) of 12-storey frame with T_1=1.60 s and θ_{AUX}-α=0.025 subjected to the FEMA-P695 set of records: a) near collapse μ=5; b) sidesway collapse $\mu=\mu_c$

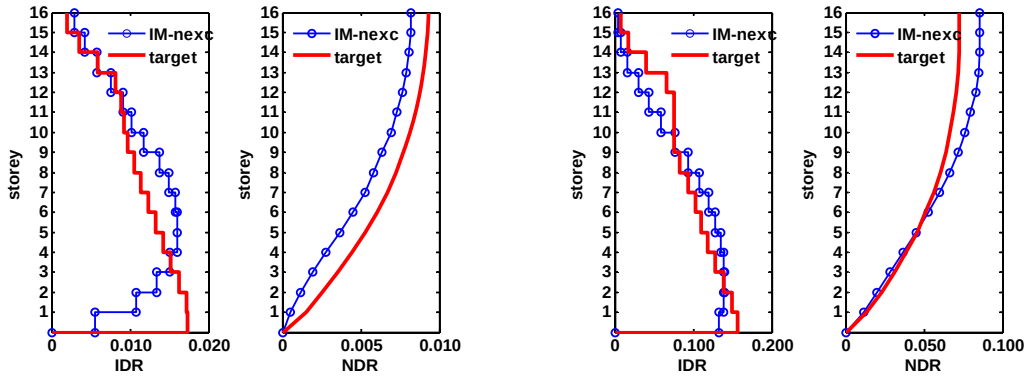

a) b)

Figure 4.166 Displacement and interstorey drift profiles (median) of 16-storey frame with T_1=2.00 s and θ_{AUX}-α=0.025 subjected to the FEMA-P695 set of records: a) near collapse μ=5; b) sidesway collapse $\mu=\mu_c$

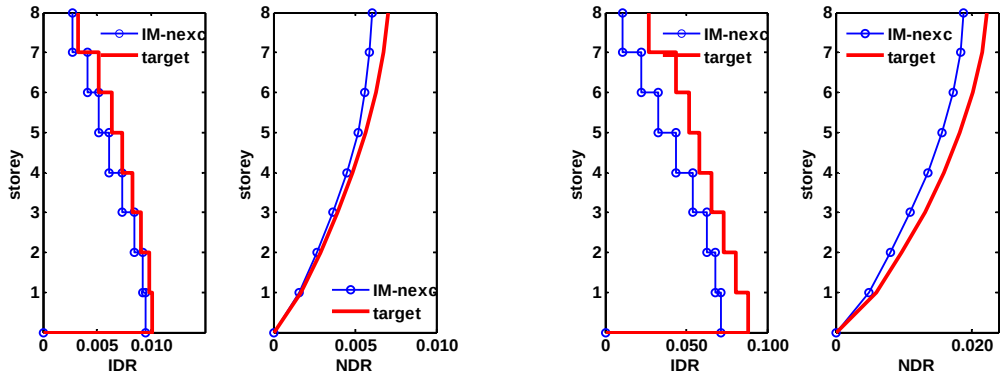

a) b)

Figure 4.167 Displacement and interstorey drift profiles (median) of 8-storey frame with T_1=1.10 s and θ_{AUX}-α=0.05 subjected to the FEMA-P695 set of records: a) near collapse μ=5; b) sidesway collapse $\mu=\mu_c$

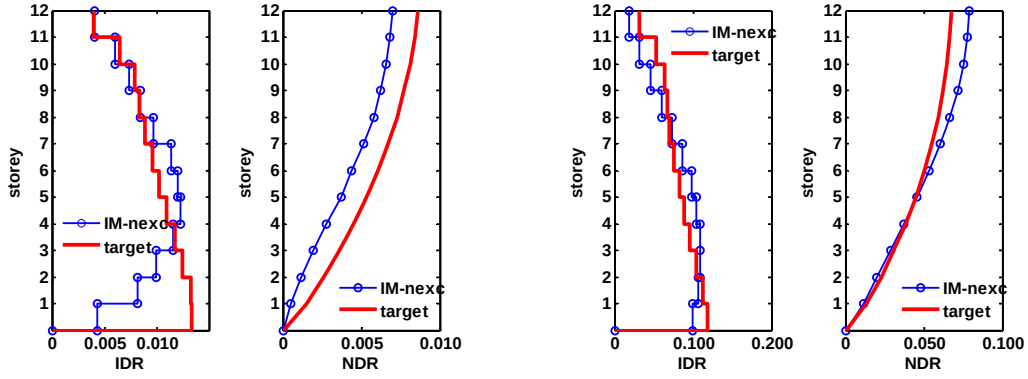

a) b)

Figure 4.168 Displacement and interstorey drift profiles (median) of 12-storey frame with T_1=1.60 s and θ_{AUX}-α=0.05 subjected to the FEMA-P695 set of records: a) near collapse μ=5; b) sidesway collapse $\mu=\mu_c$

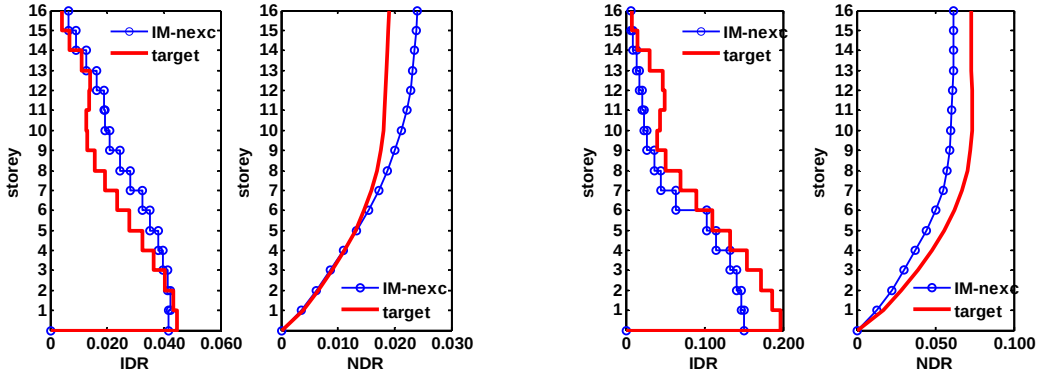

a) b)

Figure 4.169 Displacement and interstorey drift profiles (median) of 16-storey frame with T_1=2.00 s and θ_{AUX}-α=0.05 subjected to the FEMA-P695 set of records: a) near collapse μ=5; b) sidesway collapse $\mu=\mu_c$

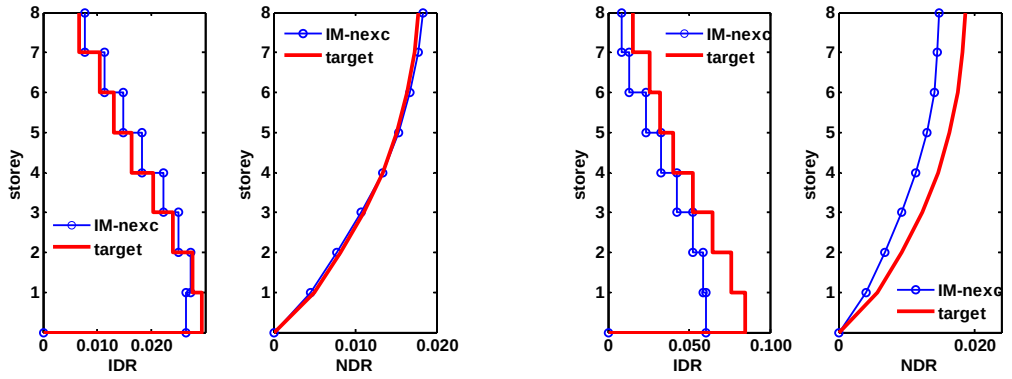

a) b)

Figure 4.170 Displacement and interstorey drift profiles (median) of 8-storey frame with T_1=1.10 s and θ_{AUX}-α=0.075 subjected to the FEMA-P695 set of records: a) near collapse μ=5; b) sidesway collapse $\mu=\mu_c$

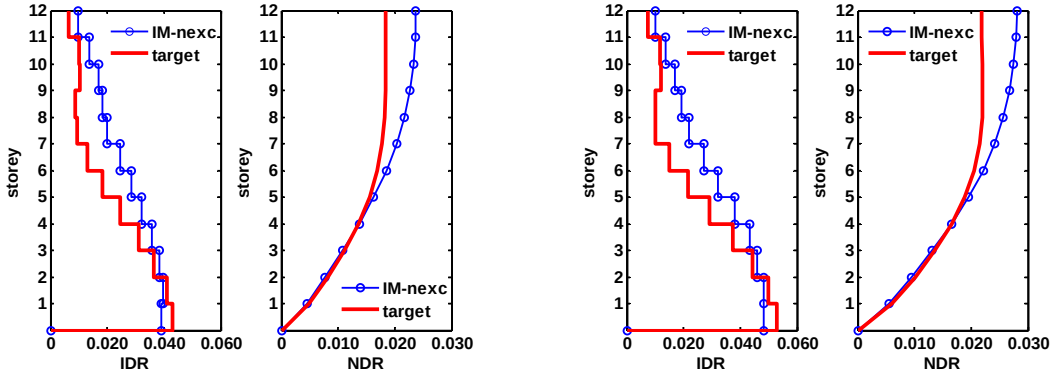

a) b)

Figure 4.171 Displacement and interstorey drift profiles (median) of 12-storey frame with T_1=1.60 s and θ_{AUX}-α=0.075 subjected to the FEMA-P695 set of records: a) near collapse μ=5; b) sidesway collapse $\mu=\mu_c$

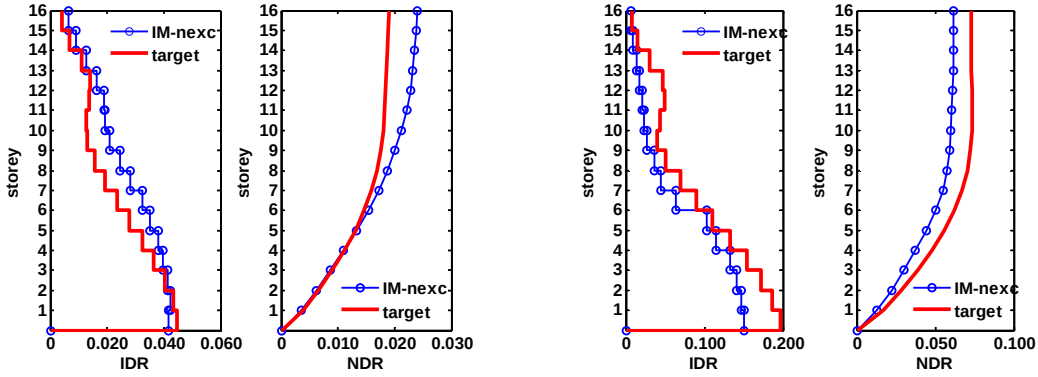

a) b)

Figure 4.172 Displacement and interstorey drift profiles (median) of 16-storey frame with T_1=2.00 s and θ_{AUX}-α=0.075 subjected to the FEMA-P695 set of records: a) near collapse μ=5; b) sidesway collapse $\mu=\mu_c$

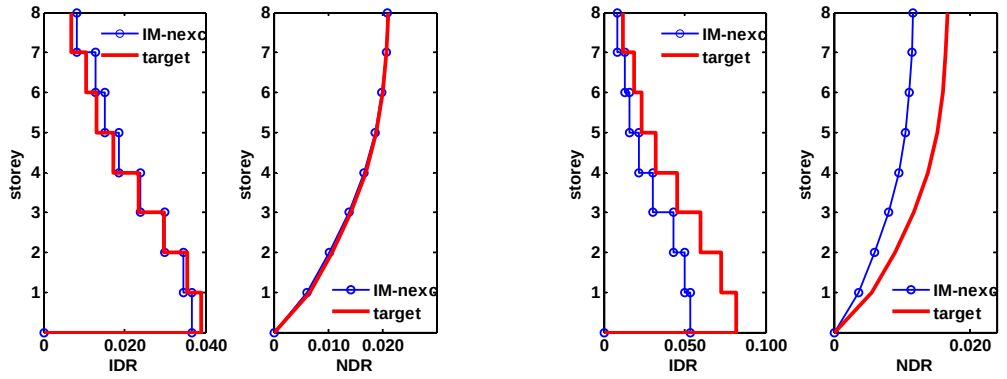

a) b)

Figure 4.173 Displacement and interstorey drift profiles (median) of 8-storey frame with T_1=1.10 s and θ_{AUX}-α=0.100 subjected to the FEMA-P695 set of records: a) near collapse μ=5; b) sidesway collapse $\mu=\mu_c$

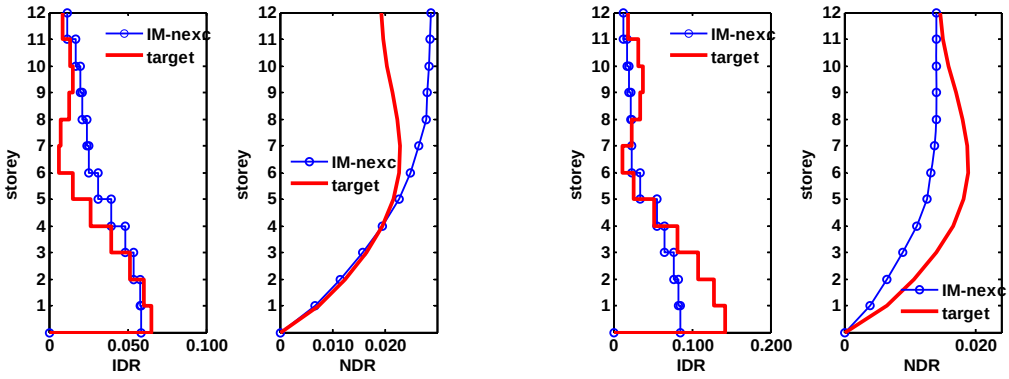

a) b)

Figure 4.174 Displacement and interstorey drift profiles (median) of 12-storey frame with T_1=1.60 s and θ_{AUX}-α=0.100 subjected to the FEMA-P695 set of records: a) near collapse μ=5; b) sidesway collapse $\mu=\mu_c$

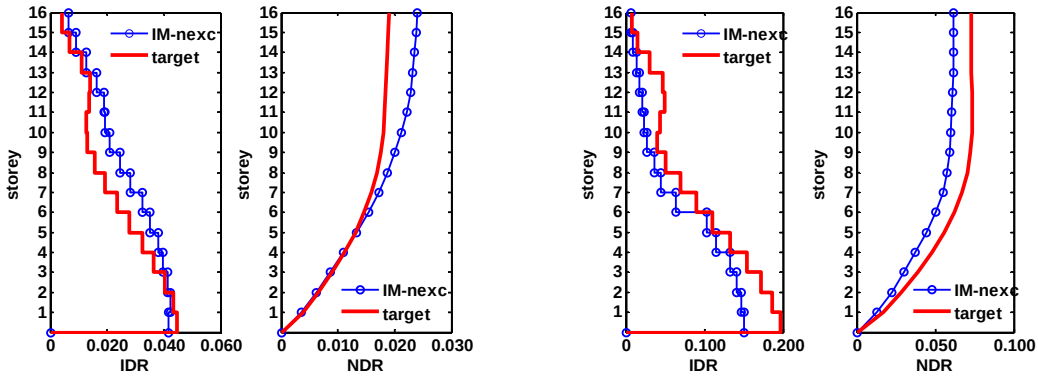

a) b)

Figure 4.175 Displacement and interstorey drift profiles (median) of 16-storey frame with T_1=2.00 s and θ_{AUX}-α=0.100 subjected to the FEMA-P695 set of records: a) near collapse μ=5; b) sidesway collapse $\mu=\mu_c$

CHAPTER 5

CONCLUSIONS

In this thesis, a displacement-based seismic design method considering sidesway collapse prevention for instability prone multi-storey frames has been presented. The framework of the method proposed is based on the characterization of a MDOF structure via a RSDOF system whose properties are consistent with the fundamental mode and modal spectral analysis involving a simplified criterion regarding the contribution of higher modes to seismic performance. The properties of the RSDOF system are obtained from modal analysis of two elastic models that are representative of the elastic and inelastic stages of behaviour; the latter being defined in accordance with a design damage state which is also, to a certain extent, a design target.

The validation of the method proposed was carried out using as illustrative examples the design of three regular plane frame types under four different levels of axial load and comparing the statistics of its performance under a set of standardized and particular interest earthquake records with the corresponding results obtained through the application of IDA. The results obtained show that the method proposed allows the design of instability-prone structures due to P-Delta effects that exhibit adequate performance when subjected to seismic loading, for both near-collapse and actual collapse. Therefore, it is generally concluded that the goal of this investigation was fulfilled and, consequently, an important step towards the development of a robust design and assessment method that can be employed in engineering practice in the near future was achieved. In particular, the conclusions regarding specific issues dealt in this investigation are the following.

5.1 RSDOF system approach

The method is able to approximate to a sufficient degree the seismic performance of framed structures subjected to seismic loading that exhibit P-Delta induced negative stiffness since the design RSDOF is defined directly from the dynamic properties of the structure. These properties are obtained from modal analysis (first and second order) of models that are representative of the elastic and damage stages and, thus, providing a rational definition of first mode design demands and a consistent design displacement shape. The results are congruent with those obtained from assessment approaches proposed by Bernal (1998) or Adam (2012a) where actual collapse capacity due to P-Delta effects was sufficiently approximated using the ESDOF approach by means of a capacity curve obtained via pushover analysis. However, in this work,

the method was validated not only for actual sidesway-collapse, but for several target interstorey drifts associated with given ductility values.

Even though displacement response of regular framed structures is governed by the first mode of vibration, higher modes may contribute significantly to the seismic design forces. For the purpose of ensuring a desirable damage state and, thus, providing displacement control in the designed structure, the estimation of design forces considering higher mode effects is necessary. The criterion employed in this investigation to account for the contribution of higher modes to design demands is, to a certain extent, the same as that followed for the definition of the RSDOF system in the sense that the stiffnesses of higher modes are consistent with the design damage state of the structure. However, it is important to emphasize that the actual contribution of higher modes varies from record to record, information that is not rigorously characterized in design spectra. Moreover, modal spectral analysis is employed to estimate design demands of an inelastic structure, which is not theoretically valid. Notwithstanding, the results obtained from the application of the method proposed show that the use of such criterion provides a good approximation of structural response for various deformation and seismic demand intensity levels.

5.2 Special spectra for P-Delta induced instability prone systems

Two set of records were considered in this investigation: the FEMA-P695 far field set, comprised of 44 records of hard and stiff rock soils, which is recommended by such provision for collapse assessment in the USA, and a suite of 100 records from earthquakes recorded in soft soils sites in Mexico City used by Miranda and Ruiz-Garcia (2002). For such sets, 16^{th}, 50^{th}, 84^{th} percentile spectra were calculated, from which trends of behaviour of instability prone frames were withdrawn and allowed to validate the method proposed with an appropriate representation of record-to-record variability for distinct soil site types.

As shown in this investigation, the use of particular design spectra for systems with P-Delta induced instability, is necessary to appropriately design or assess instability prone framed structures since the design demands of such structures are fundamentally different than those of stable systems. The results obtained from applications of the method proposed for both record sets were sufficiently accurate, thus, it is concluded that this method can be employed for the design of structures at both hard and soft soil sites. However, for the latter, it is necessary to carry out an investigation regarding the development of a criterion to consider soil-structure interaction, as, in soft soils sites, such issue is deemed relevant.

5.3 Applicability of the method proposed

The method proposed requires the use of elastic analyses and a set of constant ductility spectra corresponding to SDOF systems with a P-Delta induced negative post-yield stiffness, hence, non-linear dynamic analysis is not required. The relative complexity of its application is a consequence of the definition of the design auxiliary SDOF system for which first and second order modal analyses of two elastic models are performed. Nonetheless, the application may be carried out using commercial software that performs elastic analysis only, in conjunction with conventional data processing software. Moreover, an implementation of the method proposed can be readily carried out in structural analysis software.

5.4 Future studies

In order to apply this method to the design of real structures it is necessary to extended to more general structures such as buildings with walls and with in-plan and/or in-height irregularities; the results obtained in this investigation encourage the continued development of this displacement based design approach.

Furthermore, the author of this study suggests the development of design demands for unstable systems due to P-Delta effects for specific soil sites in the form of uniform hazard spectra which includes not only the uncertainties in the seismic records but also in the structural properties and even in the definition of the performance indices used for the design of the considered limit state.

REFERENCES

Adam C, Jäger C (2012a) Seismic collapse capacity of basic inelastic structures vulnerable to the P-delta effect. Earthquake Eng Struct Dyn 41: 775-793.

Adam C, Jäger C (2012b) Simplified collapse capacity assessment of earthquake excited regular frame structures vulnerable to P-delta. Eng Struct 44: 159-173.

ASCE/SEI (2006) Minimum design loads for buildings and other structures. ASCE Standard ASCE/SEI 7-05, including Supplement No. 1, American Society of Civil Engineers, Reston, Virginia.

Asimakopoulos AV, Karabalis DL, Beskos, DE (2007) Inclusion of P-effect in displacement-based seismic design of steel moment resisting frames. Earthquake Eng Struct Dyn 36:2171–2188.

Ayala AG (2001). Evaluation of seismic performance of structures, a new approach (in Spanish). Revista Internacional de Métodos Numéricos para Cálculo y Diseño en Ingeniería 17(3): 285-303.

Ayala AG, Castellanos H, López S (2012) A displacement-based seismic design method with damage control for RC buildings. Earthquakes and Structures 3(3): 414-434.

Baradaran Shoraka M (2013) Collapse assessment of concrete buildings: an application to non-ductile reinforced concrete moment frames. PhD thesis, The University of British Columbia, Vancouver.

Bernal D (1998) Instability of buildings during seismic response. Eng Struct 20(4-6): 496-502.

Chopra AK, Goel RK (2002) A modal pushover analysis procedure for estimating seismic demands for buildings. Earthquake Eng Struct Dyn 31(3): 561-582.

Chopra AK, Goel RK (2000) Building period formulas for estimating seismic displacements. Eng Struct 16(2): 553-536.

CEN (2001) EC 8 (Eurocode 8) Design of structures for earthquake resistance-Part 1: General Rules, Seismic Actions and Rules for Buildings. European Committee for Standardization (CEN), Brussels, 2001.

DiCiccio TJ, Efron B (1996) Bootstrap confidence intervals. Statistical Science 11(3):189-228

FEMA (2009a) Effects of strength and stiffness degradation on Seismic Response. FEMA P-440A, Federal Emergency Management Agency, Washington, D.C.

FEMA (2009b) Quantification of building seismic performance factors. FEMA-P695, Federal Emergency Management Agency, Washington D.C.

Fenwick RC, Davidson BJ, Chung BT (1992) P-Delta actions in seismic resistant structures. Bulletin of the NZ National Society for Earthquake Engineering 25(1):56-69.

Gupta A, Krawinkler H (2000) Dynamic P-delta effects for flexible inelastic steel structures. J Struct Eng126:145–154

Haselton CB, Liel AB, Deierlein GG (2009) Simulating structural collapse due to earthquakes: Model idealization, model calibration, and numerical simulation algorithms. In: Proceedings of the 2nd International Conference on Computational, CD-ROM paper, Paper no. CD 497, Methods in Structural Dynamics and Earthquake Engineering (COMPDYN 2009), eds, M. Papadrakakis, N. D. Lagaros, M. Fragiadakis, Rhodes, Greece.

Haselton CB, Liel AB, Deierlein GG, Dean BS, Chou, JH (2011) Seismic collapse assessment of reinforced concrete buildings. I: Assessment of ductile moment frames. ASCE J Struct Eng 137(4): 481-491.

Ibarra LF, Krawinkler H (2005) Global collapse of frame structures under seismic excitations. Report No. PEER 2005/06. Pacific Earthquake Engineering Research Center, University of California, Berkeley CA.

Iervolino I, Manfredi G (2008) A review of ground motion record selection strategies for dynamic structural analysis. Modern Testing Techniques for Structural Systems, CISM International Centre for Mechanical Sciences 502/2008(131-163).

Jäger C, Adam, C (2013) Influence of collapse definition and near field effects on collapse capacity spectra. J Earthq Eng 17: 859-878.

Krawinkler H, Zareian F, Lignos D, Ibarra LF (2009) Prediction of collapse of structures under earthquake excitations. In: 2nd International Conference on Computational Methods in Structural Dynamics and Earthquake Engineering (COMPDYN 2009). Ed. by M. Papadrakakis, N.D. Lagaros and M. Fragiadakis. June 22-24. Rhodes, Greece: CD–ROM paper, Paper No. CD449, 19 pp.

Lignos D, Krawinkler H (2008) Sidesway collapse of deteriorating structural systems under seismic excitations. Rep. No. TB 177, The John A. Blume Earthquake Engineering Research Center, Stanford University, Stanford, CA.

Lopez SE, Ayala AG, Adam C (2015) A novel displacement-based seismic design method for framed structures considering P-Delta induced dynamic instability. Bulletin Earthquake Eng 13:1227-1247

MacRae GA (1993) P-Delta design in seismic regions. Report SSRP-93/05, Department of Applied Mechanics and Engineering Sciences, University of California at San Diego, La Jolla, CA.

MacRae GA (1994) P-Delta effects on single-degree-of-freedom structures in earthquakes. Earthquake Spectra 10: 539–568.

McKenna F, Fenves GL, Scott MH (2004) OpenSees: open system for earthquake engineering simulation. Pacific Earthquake Engineering Research Center, University of California, Berkeley, CA. <http://opensees.berkeley.edu>.

Medina R, Krawinkler H (2003) Seismic demands for nondeteriorating frame structures and their dependence on ground motions. Rep. No. TR 144, The John A. Blume Earthquake Engineering Research Center, Stanford University, Stanford, CA.

Miranda E, Akkar SD (2003) Dynamic instability of simple structural systems. ASCE J Struct Eng 129(12): 1722-1726.

Miranda E, Ruiz-García J (2002). Influence of stiffness degradation on strength demands of structures built on soft soil sites. Eng Struct 24(10): 1271-1281.

Paulay T (1978) A consideration of P-Delta effects in ductile reinforced concrete frames. Bulletin of the New Zealand National Society for Earthquake Engineering 11(3):151-160.

PEER/ATC (2010) Modeling and acceptance criteria for seismic design and analysis of tall buildings. PEER/ATC-72-1, Applied Technology Council, Redwood City CA.

Pettinga JD, Priestley MJN (2007) Accounting for P-Delta effects in structures when using direct-displacement based design of structures. Research Report No. 2007/02 ROSE (European School for Advanced Studies in Reduction of Seismic Risk), 2007/02.

Priestley MJN, Calvi GM, Kowalsky MJ (2007) Displacement-based seismic design of structures. IUSS Press, Pavia, Italy.

Rahnama M, Krawinkler H (1993) Effects of soils and hysteresis model on seismic demands. Rep. No. TB 108, The John A. Blume Earthquake Engineering Research Center, Stanford University, Stanford, CA.

Sasaki F, Freeman S, Paret T (1998) Multi-mode pushover procedure (MMP)—a method to identify the effect of higher modes in a pushover analysis. In: Proceedings of the 6th US National Conference on Earthquake Engineering.

Shafei B, Zareian F, Lignos DG (2011) A simplified collapse capacity assessment of moment-resisting frame and shear wall systems. Eng Struct 33(4):1107-1116.

Sullivan TJ, Priestley MJN, Calvi GM (2008). Estimating the higher-mode response of ductile structures. J Earthq Eng 12(3): 456-472.

Takizawa H, Jennings PC (1980) Collapse of a model for ductile reinforced concrete frames under extreme earthquake motions. Earthquake Eng Struct Dyn 8: 117-144.

Vamvatsikos D, Cornell CA (2002). Incremental dynamic analysis. Earthquake Eng Struct Dyn 31(3): 491-514.

ACKNOWLEDGMENTS

Foremost, the author would like to thank Dr. A. G. Ayala for his guidance and continuous support in the development of this study.

The author also acknowledges the National Council of Science and Technology (CONACyT) for his graduate scholarship and the Institute of Engineering for giving him the opportunity of being part of it and granting him the additional support that made reality the completion of his graduate work.